UQAC

Université du Québec à Chicoutimi

Studies of surface preparation and structural adhesive bonding of aluminum and other materials

By

Mani Mohan Tiwari

Under supervision of Prof. Dilip Sarkar and co-supervision of Prof. X.-Grant Chen

Thesis Presented to Université du Québec à Chicoutimi in Partial Fulfillment of the Requirements for the Degree of Doctor of Philosophy (Ph. D.) in Engineering.

Submitted on November 2023

BOARD OF EXAMINERS:

Prof. Zhan Zhang, President, Université du Québec à Chicoutimi (UQAC), Canada

Prof. Santanu Das, External Member, Indian Institute of Technology (BHU), India

Dr. Kun Liu, External Member, CanmetENERGY-Ottawa, Canada

Prof. Dilip Kumar Sarkar, Internal Member, Université du Québec à Chicoutimi (UQAC), Canada

Prof. X.-Grant Chen, Internal Member, Université du Québec à Chicoutimi (UQAC), Canada

Québec, Canada

Études de préparation de surface et d'assemblage structural par adhésif d'aluminium et d'autres matériaux

Résumé

Le besoin croissant de structures légères et performantes a stimulé des recherches approfondies visant à améliorer l'assemblage des matériaux par le biais de liaisons à l'aide d'adhésifs structuraux. Contrairement aux méthodes conventionnelles (par exemple, soudage, rivetage et boulonnage), le collage adhésif structural excelle en intégrant des techniques avancées de traitement de surface. Ces techniques jouent un rôle crucial dans la détermination de la stabilité et des performances des joints collés. Les traitements de surface électrochimiques traditionnels (par exemple, l'anodisation acide) impliquent l'utilisation d'acides et soulèvent d'importantes préoccupations environnementales et de sécurité. Ainsi, le présent travail vise à utiliser des techniques de traitement de surface respectueuses de l'environnement, rentables et moins complexes pour préparer les surfaces métalliques et polymères, facilitant ainsi des applications de collage adhésif similaires et dissemblables.

Ce travail de thèse a été développé en deux sections. La première section aborde la préparation de surface et le collage adhésif des substrats métal/métal, tandis que la deuxième section traite de la même chose sur des substrats métal/polymère. L'aluminium (Al) a été sélectionné pour le système métal/métal, tandis que l'Al et le chlorure de polyvinyle (PVC) ont été choisis comme substrats pour le système métal/polymère. Un processus d'abrasion mécanique utilisant du carbure de silicium (SiC) et une technique d'anodisation électrochimique ont été utilisés pour traiter la surface de l'Al afin d'ajuster ses propriétés de mouillage. L'érection de microstructures rugueuses sur l'Al en raison de l'abrasion mécanique a amélioré sa nature hydrophile en fournissant un angle de contact avec l'eau d'environ ~53°. Les surfaces traitées, lorsqu'elles étaient collées avec l'adhésif n #1 et l'adhésif n #2. Cela a entraîné un gain relatif de 46 % dans leur résistance au cisaillement simple (SLS) par rapport à celles collées sans aucun traitement de surface à l'aide de l'adhésif n #2. De plus, l'effet de divers environnements (eau déionisée, solutions aqueuses de NaCl à 3,5 et 7% en poids) sur le vieillissement a été exploré, et un modèle approprié a été proposé pour expliquer la résistance SLS résiduelle dans ces échantillons.

D'autre part, la croissance d'une couche d'oxyde poreuse a été observée sur le substrat en Al lorsqu'il était électro chimiquement anodisé dans une solution aqueuse de phosphate de sodium dihydrogène (Na_2HPO_4). La rugosité moyenne de ces surfaces était d'environ ~1,4 μm, fournissant un angle de contact avec l'eau d'environ ~42°. Ces surfaces ont été collées à l'aide d'un adhésif n #3, et le gain relatif de la résistance SLS obtenue était de 133% par rapport aux joints Al/Al d'origine. Ces résultats indiquent que la technique d'anodisation a conduit à une performance supérieure par rapport à l'abrasion mécanique lorsqu'elle est collée adhésivement.

De plus, l'influence d'un organosilane, à savoir le [3-glycidoxypropyl] triméthoxysilane (GPS), sur la rugosité et les propriétés morphologiques de l'aluminium anodisé a été étudiée pour investiguer leur influence sur les résistances au cisaillement simple (SLS) lorsqu'elles sont collées avec l'adhésif n #4. Dans cette étude, l'anodisation a été réalisée dans des électrolytes aqueux du GPS organique et d'un sel inorganique de nitrate de zinc ($Zn(NO_3)_2$). L'insertion de molécules de GPS pendant l'anodisation a produit un effet de rugosité à deux

niveaux avec une microrugosité d'environ ~8 μm sur l'aluminium anodisé. Ces surfaces ont été collées à l'aide d'un adhésif organique à base biologique, et la résistance mesurée au cisaillement simple (SLS) a été améliorée de 160% par rapport aux joints d'aluminium d'origine. En comparaison avec l'abrasion et l'anodisation, cette technique offre un gain relatif plus élevé dans les résistances SLS lorsqu'elle est utilisée pour le collage adhésif.

La deuxième partie de ce travail implique le collage du PVC avec de l'aluminium, le PVC étant, par nature, un matériau hydrophobe présentant une réactivité de surface très faible et une faible affinité envers les adhésifs. Par conséquent, afin de traiter le PVC moins réactif, une méthode de traitement de surface par décharge corona a été utilisée pour activer leurs surfaces en faveur du collage adhésif. Les analyses de spectroscopie infrarouge à transformée de Fourier (FTIR) ont présenté des preuves de l'incorporation de groupes fonctionnels polaires –OH à 3390 cm^{-1}, entraînant une réduction de l'angle de contact avec l'eau à environ ~36° par rapport aux ~98° de la surface de PVC non traitée, ce qui est favorable à l'amélioration de la résistance de liaison entre le PVC et l'adhésif. En conséquence, la résistance au cisaillement simple (SLS) des joints Al/PVC collés adhésivement a montré un gain relatif de 300% par rapport à leurs homologues d'origine. En plus de modifier les substrats en PVC pour améliorer la résistance SLS, une tentative supplémentaire a été faite pour mélanger deux adhésifs chimiquement différents (époxy et silicone) pour coller deux substrats chimiquement différents (Al et PVC). Les spectres FTIR de l'adhésif mélangé ont révélé la présence de pics superposés avec le PVC, notamment $–CH_2$, $–CH_3$ autour de 2800–3000 cm^{-1} et $Si–CH_3$ à 1260 cm^{-1}, confirmant la signature des deux chimies adhésives. La résistance SLS des joints Al/PVC collés avec l'adhésif mixte a montré que le gain relatif était 447% plus élevé que celui des joints Al/PVC fabriqués uniquement avec de l'adhésif silicone.

Dans les deux cas étudiés, à savoir les joints collés adhésivement Al/Al et Al/PVC, un traitement de surface était nécessaire pour améliorer le gain relatif des résistances des joints. Dans le cas des joints adhésifs Al/Al, les techniques d'anodisation ont fourni un gain relatif plus élevé dans les résistances des joints que le traitement par abrasion mécanique. Dans le cas du Al/PVC, un traitement par décharge corona était nécessaire pour augmenter l'affinité de la surface du PVC envers l'adhésif, ce qui a conduit à des résistances de liaison améliorées. Lorsque des joints adhésifs Al/PVC ont été réalisés à l'aide d'un adhésif mixte époxy/silicone, le gain relatif des résistances adhésives a encore augmenté à des valeurs plus élevées. Les résultats indiquent la faisabilité d'ajuster les caractéristiques de surface de métaux tels que l'aluminium et même de matériaux légers difficiles à coller comme le PVC, ce qui améliore les résistances des liaisons adhésives, démontrant ainsi un potentiel d'utilisation dans des structures où la légèreté est de plus en plus recherchée.

Studies of surface preparation and structural adhesive bonding of aluminum and other materials

Abstract

The growing need for lightweight and high-performance structures has fueled extensive research into refining the assembling of materials to bonding using structural adhesives. Unlike conventional methods (e.g., welding, riveting, and bolting), structural adhesive bonding excels by integrating advanced surface treatment techniques. These techniques play a crucial role in determining the stability and performance of the bonded joints. Traditional electrochemical surface treatments (e.g., acid anodization) involves use of acids and raise serious environmental and safety concerns. Hence, the present work aims to utilize eco-friendly, cost-effective, and less complex surface treatment techniques for preparing metal and polymer surfaces, facilitating similar and dissimilar adhesive bonding applications.

This thesis work has been developed into two sections. The first section addresses surface preparation and adhesive bonding of metal/metal substrates, and the second section deals with the same on metal/polymer substrates. Aluminum (Al) was selected for the metal/metal system, while Al and polyvinyl chloride (PVC) were chosen as substrates for the metal/polymer system. A mechanical abrasion process using silicon carbide (SiC) and an electrochemical anodization technique were used to surface treat Al to tune it's wetting properties. The erection of micro-rough structures on Al due to mechanical abrasion enhanced the hydrophilic nature providing a water contact angle of ~53°. The treated surfaces, were bonded using Adhesive #1 and Adhesive #2. This resulted in a relative gain of 46% in their single lap shear (SLS) strength compared to those bonded without any surface treatment using Adhesive #2. Furthermore, the effect of various environments (DI water, 3.5 and 7 wt.% aqueous NaCl solutions) on aging was explored, and a suitable model was proposed to explain the residual SLS strength in these samples. On the other hand, the growth of a porous oxide layer was observed on the Al substrate when it was electrochemically anodized into an aqueous salt solution of disodium hydrogen phosphate (Na_2HPO_4). The average roughness of these surfaces was found to be ~ 1.4 μm providing a water contact angle of ~42°. These surfaces were bonded using an Adhesive #3, and the relative gain in the obtained SLS strength was 133% compared to as-received Al/Al joints. These results indicated that the anodization technique resulted in a superior performance as compared to the mechanical abrasion when bonded adhesively.

Furthermore, the influence of an organosilane, namely [3-glycidoxypropyl] trimethoxysilane (GPS), on the roughness and morphological properties of anodized Al was performed to investigate their influence on the SLS strengths when bonded with Adhesive #4. In this study, the anodization was conducted in aqueous electrolytes of the organic GPS and an inorganic salt of zinc nitrate ($Zn(NO_3)_2$. The insertion of GPS molecules during anodization has provided a two-tire roughness effect with microroughness of ~ 8 μm on the anodized Al. These surfaces were bonded using a bio-based organic adhesive, and the measured SLS strength was enhanced by 160% compared to as-received Al/Al joints. As compared to the abrasion and anodization, this technique provides a higher relative gain in the SLS strengths when bonded adhesively.

The second part of this work involves bonding PVC with Al, where PVC, by nature, is a hydrophobic material and presents very low surface reactivity and low affinity towards

adhesives. Therefore, in order to treat the less reactive PVC, a corona discharge surface treatment method was used to activate their surfaces to favor adhesive bonding. Fourier transform infrared spectroscopy (FTIR) analyses presented evidence of incorporation of –OH polar functional groups at 3390 cm^{-1} leading to a lowering of water contact angle to ~36° from ~98° on untreated PVC surface, which is favorable to improving the bond strength between PVC and the adhesive. As a result, the SLS strength of adhesively bonded Al/PVC joints demonstrated a relative gain of 300% compared to its as-received counterparts. Apart from modifying the PVC substrates to improve the SLS strength, an additional attempt was made to mix two chemically dissimilar adhesives (epoxy and silicone) to bond two chemically dissimilar substrates (Al and PVC). FTIR spectra of the mixed adhesive revealed the presence of overlapping peaks with PVC, namely $–CH_2$, $–CH_3$ around 2800–3000 cm^{-1} and $Si–CH_3$ at 1260 cm^{-1} confirming the signature of both adhesive chemistries. The SLS strength of Al/PVC joints bonded using mixed adhesive showed that the relative gain was 447% higher than that of Al/PVC joints made with only silicone adhesive.

In both cases studied, namely, adhesively bonded Al/Al joints and Al/PVC joints, a surface treatment was required to improve the relative gain in the joint strengths. In the case of Al/Al adhesive joints, anodization techniques provided higher relative gain in the joint strengths than the mechanical abrasion treatment. In the case of Al/PVC, corona discharge treatment was required to increase the PVC surface affinity towards adhesive resulting in improved bond strengths. When Al/PVC adhesive joints were made using a mixed epoxy/silicone adhesive, the relative gain in adhesive strengths further increased to higher values. The results indicate the feasibility of tuning the surface characteristics of metals such as aluminum and even the most difficult-to-bond light weight material such as PVC in enhancing the adhesive bond strengths, hence demonstrating potentials to be used in structures where light-weight is increasingly sought.

Table of Contents

List of Tables

List of Figures

List of Abbreviations

ASTM	American Society for Testing and Materials
A F	Adhesive Failure
at %	Atomic percent
ATR-FTIR	Attenuated total reflectance- Fourier transform infrared
C F	Cohesive Failure
EDS	Energy-Dispersive X-ray Spectrometer
El	Elongation
eq	Equations
HV	Hardness Vickers
j	Current density
OES	Optical Emission Spectrometer
OM	Optical Microscope
rms	Root-mean square
RT	Room Temperature
SEM	Scanning Electron Microscope
SLS	Single-Lap shear
S F	Substrate Failure
Wt%	Weight percent
XRD	X-Ray diffraction
YS	Yield strength

List of Symbols

Al	Aluminum
Cl	Chlorine
Cr	Chromium
Cu	Copper
Fe	Iron
h	Hours
H	Hydrogen
kV	Kilovolt
m	Milli
Mg	Magnesium
Mn	Manganese
MPa	Mega Pascal
N	Nitrogen
Na	Sodium
nm	Nanometer
O	Oxygen
^{o}C	Centigrade degree
P	Phosphorous
s	Second
Si	Silicon
Ti	Titanium

Zn	Zinc
μm	Micrometer
Π	Mathematical constant (3.14159)

DEDICATION

With deep gratitude and profound love, I dedicate this thesis to my parents, Dr. Rajendra Tiwari and Smt. Nisha Tiwari. Their boundless support, selfless sacrifices, and unwavering belief in my abilities have been the guiding forces throughout my academic journey.

I also pay tribute to my late grandfather, Shri Laxmi Narayan Tiwari, whose wisdom and values continue to inspire me. In loving memory of my late grandmother, Smt. Shanti Tiwari, whose enduring spirit and kindness have left an indelible mark on my heart. This work is a reflection of the values instilled in me by my family, and I am grateful for their constant belief in my abilities.

ACKNOWLEDGMENT

After years of extensive research, this thesis has finally come to fruition. It is a great pleasure to convey my sincere gratitude to all individuals involved in the development of this thesis.

In the first place, I would like to express my deep sense of gratitude and indebtedness to Prof. Dilip Kumar Sarkar, the director of my thesis project, for his valuable suggestions and encouragement. Working with Prof. Sarkar has been a great pleasure. His truly scientific intuition exceptionally inspired and helped me grow as a student, a researcher and a scientist. His originality, experience and contributions in this field nourished the value of this thesis. An extremely busy professional, Prof. Sarkar has always been available and kind in need. It is an honor for me to earn my graduation under his direction.

I am extremely grateful to my co-director, Prof. X.-G.Chen, for his supervision, advice, firm guidance, suggestions, scientific and technical criticisms and constant encouragement. Prof. Chen had thoroughly guided and provided his feedback on my all writing tasks. Thanks Prof. Chen. I am grateful in every possible way and hope to keep up our collaboration in the future.

I would like to express my sincere gratitude and immense respect to Dr. Saleema Noormohammed, with whom I had the privilege to work closely. Her guidance and training, both in academic and non-academic tasks, have been invaluable. Words fall short in capturing the depth of my appreciation. Upon joining Prof. Sarkar's research group at UQAC, Dr. Noormohammed became more than a mentor; she was the first person I shared special and joyful moments with, from working in the laboratory to hiking national parks in

Canada. Throughout my thesis work, she consistently supported and assisted me in various writing tasks. I am truly indebted to her for her unwavering guidance and kind support; this thesis would not have been possible without her influence.

I would also like to thank all the sponsors of this research project, namely, the Natural Sciences and Engineering Research Council of Canada (NSERC) and Centre de recherche sur l'aluminium (REGAL).

I am deeply grateful to my committee members, for their valuable comments, guidance, and support.

Special thanks to Mr. Dany Racine, Mr. Samuel Dessureault, and Mr. Felix Tremblay for their innumerable technical support during my PhD journey.

Then, I would like to express my thankfulness to Dr. Zhan Zhang and Dr. Kun Liu for their help in characterization analysis in SEM and MTS system, respectively. My gratitude goes to Prof. Emad Elgallad and Mr. Zhixing Chen for being the laboratory in charge during the COVID phase.

Meanwhile, I am also intensely indebted to all my colleagues for their collaboration, insightful and fruitful scientific and experimental discussions, and for sharing their experiences with me: Dr. Angshuman Sarkar, Dr. Abhishek Ghosh, Dr. Redouane Farid, Henry Agbe, Rania Afia Numah, Berti Chilton Takoufack, Charlie Girard, Ahmed Algendy, Mohamed Qassem, Siamak Nikzad Khangholi, Ali Elashery, Mohammadreza Mofarrehi, Chaima Hajji, Mohamed Ahmed, Mohamed Attia, Amara Belkacem, Peng Hu, Liying Cui.

My dearest friends, Dr. Siddhartha Khare, Teena Sharma, Suyash Khare, Dr. U. Mohan Rao, Jayasree Thota, Dr. Rama Vara Prasad Chavali, Vineeth Reddy, never made me feel

the distance between Chicoutimi (where I live) and India (where my parents live). I must mention that we all had a great time in badminton court. A special thanks to you Siddhartha bhaiya and Teena bhabhi for making me feel like family.

My family back in India deserves a special mention for their immense moral support, encouragement and prayers for the completion of my thesis. As the only child of my parents, my father and mother never lost their patience, despite not being able to see me at home for the past four years.

Finally, I would like to thank everybody who was important to the successful realization of this thesis; I apologize that I could not thank them personally one by one.

Chapter 1: Introduction

Climate change policies focus more on energy efficiency as a central strategy for greenhouse-gas emissions reduction. To mitigate the impact of the materials on greenhouse gases emissions is to improve material efficiency (light-weighting); reducing yield losses in the manufacturing processes; minimizing the by-products; and using products more intensely or at a higher capacity. In the course of the current socio-political changes, the "European Green Deal" in particular will bring additional requirements and thus new challenges across the globe [1, 2].

The design spaces in industry and trade are also subject to a continuous process of change due to constantly changing technical, social and legal conditions. Continuous inventions and innovations of the players in the development of raw materials, adhesives and adhesively bonded products have enabled a dynamic development in the past decades. Adhesive technology has the potential to answer these new requirements with technical innovations. A recent study suggests that, the value-added chains of adhesively bonded products must be viewed holistically in the product life cycles "production", "utilization" and "disposal" [2-12].

Especially for lightweight construction, adhesive bonding is a key technology. In the automotive sector, the use of adhesive bonding technology (e. g. adhesive bonding of car windshields, bonding of stiffening profiles, bonding in the car body) supports the use of thinner sheets to save material and energy during the use phase in addition to encouraging reduced number of mechanical weights such as rivets and bolts. In rail vehicle construction, the product life cycle phase "utilization", i.e. the driving operation compared to the product

life cycle phases “production” and “disposal”, represents the determining factor with regard to energy and emission reduction: The use of lightweight construction materials in adhesive bonding technology reduces energy consumption and thus the specific CO_2 equivalent emissions per passenger or ton-kilometer. The long-term stability of adhesively bonded joints also supports the service life of adhesively bonded products. Traditional joining techniques (soldering, welding and etc.) hinder the designs by unavoidable changes in size, shape and weight of the object, hence to remove such obstacles, a monotonic development of adhesive bonding for better performance by reducing the weight and strengthening the joints are desirable, especially in the aeronautic and automobile industries [13-26]. One of the main benefits with adhesives bonds compared to mechanical joints, like screws, bolts and rivets, is that the stresses are distributed evenly across the adherends [27-34]. The strength for mechanical joints is limited to the area where the joints are located. Adhesives are also useful for application where temperature variations are present. Using adhesives to bond metal to metal instead of welding can reduce production time by up to 30% to 40%. The use of quality jigs and a streamlined work flow (e.g. having the assembler work on additional parts while adhesive is curing) will further increase productivity and drive down the cost/part [35-57]. Additionally, when we consider labor and material costs, adhesives can reduce the cost to assembly by 10% to 40% compared to welding [58-61]. This doesn’t even factor in defects and rework that can arise due to the variation in welder skill. The adhesive itself can also contribute to more sustainable recycling by using alternative components. For example, those components based on recycled materials can be suitable raw materials for adhesives. In addition, bio-based adhesives are already being used today in certain mass applications. However, many of the necessary property profiles of synthetic adhesives cannot yet be fully

represented by bio-based adhesives, which currently limit their applicability. Adhesives are an ideal product group especially for the use of alternative or renewable raw materials [62].

Even though adhesive bonds could be used to replace mechanical joints for many applications, certain challenges still exist. In order to create durable bonds, thorough surface preparation is required. It is also crucial to clean all the contaminants, that are left from the surface preparation, which could be detrimental to the strength of the bond. Furthermore, the cure times could be long, especially for adhesives that require high curing temperatures. Ovens, fixtures and presses are essential, which is not necessary for most other mechanical joining methods.

Among different factors, surface roughness places crucial role as it is the foundation factor for bonding at the interface between the surface and the adhesive. Despite having an excellent adhesive, the joint will fail prematurely if the surface fails due to poor preparation. When the surface of the adherend, whether metal or plastic, is treated appropriately, a combination of chemical and mechanical links is created to bond strongly with the adhesive. For example, creation of rough surface features can help in mechanical anchoring of the adhesive within the rough structure. On the other hand, enriching the chemistry of the adherend surface can enhance the chemical bonds favorable to adhesion with the adhesives. [13-15, 39-52]

Therefore, this research project addresses the advances in the similar and dissimilar structural adhesive joints by altering the surface properties of adhering material via chemical, mechanical and physical surface treatments. More emphasis has been placed on the surface treatment technique as it has been found to provide enhancement in the bonding strength at the interface of adhesive and adhering surface.

1.1 Problem statement

Adhesive bonding between two similar and dissimilar materials is still a challenge at the upfront of the next generation of structures of vehicle, marine technology, medical device, and in the field of aerospace as well as in electronic devices. Traditional joining techniques (soldering, welding and etc.) hinder the designs by unavoidable changes in size, shape and weight of the object, hence to remove such obstacles, a monotonic development of adhesive bonding for better performance by reducing the weight and strengthening the joints are desirable, especially in the aeronautic and automobile industries.

The main problem in the field is, surface roughness that is the foundation factor for bonding at the interface between the surface and the adhesive. Even with its superior adhesive properties, inappropriate surface preparation can still lead to premature failure of the joint.. When the surface of the adherend, whether metal or plastic, is treated appropriately, a combination of chemical and mechanical links is created to bond strongly with the adhesive. On the other hand, enriching the chemistry of the adherend surface can enhance the chemical bonds favorable to adhesion with the adhesives.

To address these issues of adhesive bonding, combining the mechanical and chemical properties of the surface of adherend can harness the advantages of mechanical interlocking along with heightened chemical bonding, facilitated by the increased surface area resulting from roughness. Based on the current state of the art of the structural adhesive bonding, this research work intends to focus on addressing the current challenges mentioned above with the objective as described in the following section.

1.2 Objectives

By careful engineering through optimization of surface treatment parameters, surfaces with desirable properties can be achieved. The global objective of this thesis is to perform systematic study on surface treatment for structural adhesive bonding between two similar (aluminum-aluminum) and dissimilar (aluminum-polymer) materials. The specific objectives to attain the global objective are as follows:

I. To study the parametric influence of roughness due to mechanical abrasion on the structural adhesive bonding of Al/Al. (Chapter 4)

a) Investigate the topographical and morphological changes due to the mechanical abrasion using SiC abrasive.
b) Evaluate the effect of various size of grit and mode of operation on the SLS strength of Al/Al adhesive joints.
c) Explore the effect of environmental aging on the adhesive joints.

II To synthesize the porous oxide layer on Al substrates by anodization in a salt electrolyte of sodium phosphate (Na_2HPO_4) for the application of structural adhesive bonding of Al/Al. (Chapter 5)

a) Perform the electrochemical anodization for various time durations ranging from 0 min to 60 min.
b) Investigate the pattern of roughness and evolution of porous oxide layer.
c) Discuss the SLS strengths vs anodization time of adhesively bonded SLS specimens.

III. To incorporate the organosilane of GPS by in-situ silanization and anodization using inorganic salt electrolyte of zinc nitrate ($Zn(NO_3)_2$) for the application of structural adhesive bonding of Al/Al. (Chapter 6)

a) Perform the electrochemical anodization into a salt electrolyte with an added volume fraction of an organosilane of GPS.
b) optimize the roughness parameter and investigate the evolution of modified porous oxide layer.
c) Discuss the SLS strengths and improved bonding performance.

IV. Joining of aluminum-polymer lightweight multi-material (Chapter 7 and Chapter 8)

a) Investigate the effect of corona discharge on PVC for structural adhesive bonding applications.
b) Investigate the effect of chemistry of mixed adhesive.

1.3 Originality statement

An existing global concern regarding the reduction of greenhouse gas is keeping the human inquisitiveness persistent regarding material efficiency. Where a significant contribution occurs from the transportation industry, which puts a constant pressure over redesigning and advancing the efficiency of system by reducing the overall weight. Adhesive bonding is one of the fields of research having capability to provide bonding of large area with uniform stress distribution, bonding of dissimilar materials of any thickness, eliminate corrosion, cost-effectiveness and aesthetic. One of the main benefits with adhesives bonds,

which addresses the existing challenges of material efficiency, compared to mechanical joints, like screws, bolts and rivets, is that the stresses are distributed evenly across the adherends. The strength for mechanical joints is limited to the area where the joints are located. Adhesives are also useful for application where temperature variations are present. In this research work, novel surface preparation techniques have been applied to achieve high bonding strength at the interface of adhesive and adherent for metal-metal and metal-polymer adhesive joints.

a. Typically, highly corrosive inorganic acids are utilized in practice to modify the surfaces of Al for the structural adhesive bonding applications. In this project, as the originality, we have utilized self-degradable and environment friendly salt electrolytes $Zn(NO_3)_2$ and Na_2HPO_4, to anodize Al to achieve porous AAO layers on the aluminium surfaces with varied surface features.

b. Additionally, one novel approach to enhance the strength of SLS specimens involves the simultaneous anodization and silane impregnation. This approach explored as a potential alternate, also provides highly textured, as well as chemically rich surfaces, in addition to the increased SLS strength obtained.

c. Further, we have performed a novel investigation on the optimization of mixed adhesives, *i.e.* epoxy and silicone, to bond the two dissimilar materials as PVC and Al. This investigation leads to understand the compatibility of an optimized ratio of adhesive mixture with mechanically abraded PVC surfaces, which, in turn, enhances the mechanical interlocking on PVC and AAO surfaces.

The detailed description of each experimental procedures is provided in their respective chapters. The remainder of the thesis is structured as follows:

1.4 Thesis outline

The current PhD thesis comprises nine chapters:

The Chapter 1 presents a brief introduction to the current project, followed by defining the problem statement and the originality of this study.

In the Chapter 2, I focused the literature review and the identified research gaps. This Chapter provides a brief overview of literature on adhesive bonding between similar and dissimilar materials. Furthermore, the detailed description of the experimental procedures is provided in Chapter 3. The rest of the thesis is structured as follows:

Chapter 4 will discuss the effect of parametric influence of mechanical abrasion using SiC abrasives for application of Al/Al adhesive joints. This chapter mainly address the relationship of roughness of mechanically created microrough structures with the SLS strength of adhesively bonded joints. In addition to that when these joints were ages into various environments, a model has been proposed for observed residual SLS strength.

Chapter 5 will provide a detailed discussion on the synthesize porous oxide layer on Al substrates by anodization in an aqueous salt solution of disodium hydrogen phosphate (Na_2HPO_4).

Chapter 6 will detail the influence of an organosilane, namely [3-glycidoxypropyl] trimethoxysilane (GPS), on the roughness and morphological properties of anodized Al was performed to investigate their influence on the SLS strengths. In this study, the in-situ

silanization and anodization was conducted in aqueous electrolytes of the organic GPS and an inorganic salt of zinc nitrate ($Zn(NO_3)_2$.

Chapter 7 will discuss the effect of effect of atmospheric plasma ionization of PVC for structural adhesive bonding applications at Al/PVC interface. Furthermore, Chapter 8 will provide the optimization of the mixing proportions of two most different adhesives, namely, epoxy and silicone, to bond the dissimilar materials (Al and PVC).

Finally, Chapter 9 will provide the overall conclusion of the thesis, though each contributing chapter and recommendations for future work. Besides the main chapters, appendix I is also listed at the end of this thesis, providing the general description of the sample preparation before any surface treatment. In addition, Appendix II, III, and IV present the supplementary data for Chapters 5, 6, and 8, respectively.

Chapter 2: Background and Literature review

The available literature on adhesive bonding between similar and dissimilar materials will be reviewed in the following sections of this chapter.

2.1 Adhesive bonding

Adhesive bonding is a process in which two or more materials are joined together using adhesive substances to create a strong and durable bond. This versatile technique transcends traditional mechanical fastening methods by enabling the creation of robust and durable connections between a wide array of substrates, ranging from metals (Al) and plastics (e.g., PVC) to composites and ceramics. The inherent advantages of adhesive bonding, such as even stress distribution, enhanced structural integrity, and the ability to join dissimilar materials, have driven its integration into diverse sectors, including automotive, aerospace, electronics, construction, and medicine. Its development accelerated acutely over the last century, especially in the aeronautic industry, as it is a key technology in assembling lightweight structures. The research area has recently received massive attention of researchers due to their potential to be able to contribute for a global challenge of greenhouse gas reduction as well. Fig. 2.1 illustrates the number of published documents over the last few decades, in the field of adhesive bonding technology. This bar diagram has been plotted using the number of published data at web of science [53].

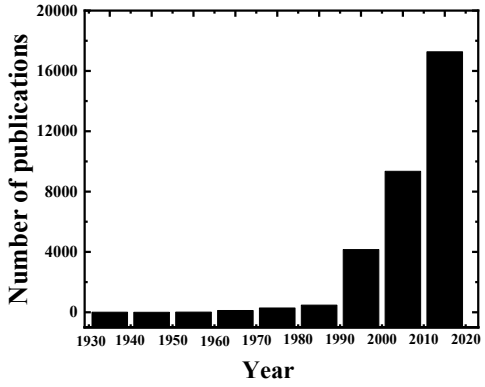

Figure 2.1. Statistical representation of number of publications in adhesive bonding between 1930-2020. © Mani Mohan Tiwari, 2023.

During the early 1940s, the first aluminum components were bonded by means of a hot-setting phenolic resin plastified with polyvinyl formal, called Redux [54]. Moreover, as time advanced into the 1960s, the aircraft manufacturing sector underwent a significant transformation. The previously utilized brittle phenolic adhesives, which exhibited limited resistance to peel forces, were progressively substituted with epoxide-based adhesives that were enhanced with nitrile rubber. This modification resulted in heightened heat resistance, with capabilities extending up to 80°C. The future of adhesive bonding is promising, with the ever-present need for better performance keeping demand high for the technology, and generating new applications with their concurrent challenges.

A theoretical background on adhesion principles is presented in the following section along with a literature review. It must be noted that the literature in the field of adhesive bonding is sparse and an effort has been made to provide a review based on the few important literature sources available.

2.2 Theoretical background

The most challenging aspect of writing about the history of adhesive bonding lies in determining where to commence, as it remains impossible to definitively ascertain when and where adhesive materials were initially utilized [55]. Despite substantial written records and archaeological findings suggesting that humans have employed adhesive substances for millennia in their quest to enhance the attractiveness, strength, utility, or affordability of objects, there doesn't appear to be a singular 'Eureka' moment that marked the initial discovery of their utility [55]. Instead, the incorporation of adhesives likely unfolded gradually, starting with the application of naturally adhesive materials and then progressing to the development of simple adhesives, potentially derived from cooking by-products.

Commencing with the proposition presented by the Roman author and scientist Pliny the Elder provides an alluring starting point. Pliny suggested that adhesive was invented by Daedalus [56]. Nevertheless, beyond this straightforward assertion, scant details regarding his invention are available. According to various renditions of the legend, Daedalus is credited with inventing an array of other innovations, encompassing ship sails, various techniques used in sculpture, art, and construction, as well as a multitude of tools utilized in carpentry [56]. Therefore, incorporating adhesive into this catalogue of accomplishments seems logical and fitting.

Conclusive proof of adhesive utilization by the Egyptians is evident in a wall carving originating from approximately 2000 BC, discovered within the tomb of Rekhmara []. This depiction portrays the process of adhering a delicate wood veneer onto a more substantial plank using adhesive. In the initial phases of adhesive history, it's probable that these materials were crafted on a notably small scale, potentially within the confines of individual

users' kitchens. However, by approximately 1700, the adhesive production landscape embarked on a significant transformation, transitioning into a prominent industry. According to suggestions [56], the earliest known practical instance of adhesive manufacturing dates back to around 1690 in Holland. Soon after, the industry made its way to England and was solidified as a "permanent industry" around 1700. The first reference to adhesive in patent literature can be traced back to a British patent for a substance termed "fish glue" in 1754 [56]. In the subsequent century, this marked the commencement of a series of patents focused on the formulation of diverse types of animal glues [56].

2.2.1 Theories of adhesion

There are four main theories that have been proposed to explain the phenomenon of adhesion. Although the most widely accepted is the adsorption theory, each of the others is appropriate in certain circumstances, and may contribute to some extent to intrinsic adhesion [57]. The adhesion mechanisms are explained in detail by a number of authors and are briefly described in the following subsections. The four main theories are: (i) Mechanical interlocking. (ii) Diffusion theory. (iii) Electrostatic theory. (iv) Adsorption theory.

(i) **Mechanical interlocking:** This theory proposes that the major source of intrinsic adhesion is a result of mechanical interlocking of the adhesive into the irregularities of the adherend surface. However, adhesion has been attained on perfectly smooth surfaces and optically smooth surfaces, which would suggest that mechanical interlocking is only responsible at macroscopic level, at least not on a molecular level [58]. There is no doubt that mechanical interlocking is the

appropriate mechanism in certain circumstances, for example, it is responsible for securing the mercury amalgam in tooth cavities.

Another example is the bonding of leather, where the outer layer of leather is removed to free the ends of the corium fibers so that they can embed in the adhesive and the adhesive penetrate between them [58]. Roughening the substrate surface prior to bonding, either by physical or chemical means, is often carried out to improve joint strength, although the enhanced performance is more likely to be due to the more rigorous cleaning afforded by these techniques or because of the increased surface area available for surface adsorption which results from surface roughening, rather than the increase in strength being as a consequence of mechanical interlocking.

(ii) **Diffusion theory:** Voyutskii first proposed that diffusion is the major driving force for polymer autohesion i.e. adhesion of polymers to themselves and to each other [59]. Autohesion involves the mutual diffusion of polymer molecules across the interface, and it requires that molecules, or chain segments, of the polymers (adhesive and adherend) possess sufficient mobility and are mutually soluble [59]. The concept is quite simple; one end of the polymer molecule chain from one surface diffuses into the structure of the second surface so that the molecule forms a bridge or bond across the interface [59]. This theory however, is only relevant in the adhesion of a material to itself or a similar material, and therefore, is not an appropriate model for polymer-metal (metal oxide) adhesion.

(iii) **The electrostatic theory:** If the adhesive and the adherend have different electronic band structures there will probably be some transfer of electrons on

contact in order to balance Fermi levels, which will result in the formation of a double layer of electrical charge at the interface [60]. This theory was primarily proposed by Deryaguin et al [60], and suggests that the electrostatic forces for such contact or junction potentials may contribute significantly to intrinsic adhesion [60]. The adhesive and the adherend are likened to the two plates of a capacitor, and the work of separation is equated to that required to separate the two charged capacitor plates [60].

(iv) **The adsorption theory:** The adsorption theory is the most widely accepted theory, and adequately explains metal (metal oxide) - polymer adhesion. This mechanism proposes that materials will adhere because of the inter-atomic and intermolecular forces which are established between the atoms and the molecules in the surface of the adhesive and adherend [61]. The most common forces are Lifshitz - van der Waals forces. These forces give rise to secondary bonds and are subdivided into: permanent dipole - dipole interactions; dipole - induced dipole interactions; and London dispersion forces [61]. Hydrogen bonds can also be formed across the adhesive / adherend interface, and these are similarly classed as secondary bonds. Primary bonds across the adhesive / adherend interface are possible (chemisorption), which incorporates ionic, covalent, and metallic interfacial bonds [61]. Donor acceptor bonds may also occur and they have a bond strength intermediate between primary and secondary bonds. These bonds are subdivided into Bronsted acid - base interactions and Lewis acid - base interactions [61].

Adsorption is believed to be one of the most important mechanisms in achieving polymer-metal adhesion. Thus, surface free energies and surface wettability are important factors to consider; since the extent of atomic or molecular interaction will increase as the degree of intimacy between adhesive and adherend increases.

2.2.2 Interfacial contact

Interfacial contact and surface wetting are an important part for adhesion. Before explaining wettability, it is necessary to define surface tension and surface free energy.

(i) **Surface tension and surface free energy:** Within the bulk of a liquid the attractive forces exerted on molecules by adjacent molecules are balanced in all directions [62]. However, at the liquid surface there is an imbalance of attractive forces which results in the surface molecules experiencing a net inward attraction towards the bulk liquid.

(ii) **Wetting of a solid surface:** In 1805, Young showed that the surface tensions acting at the surface of the three-phase contact point of the liquid drop resting at equilibrium on a solid surface may be resolved in a direction parallel to the surface [63].

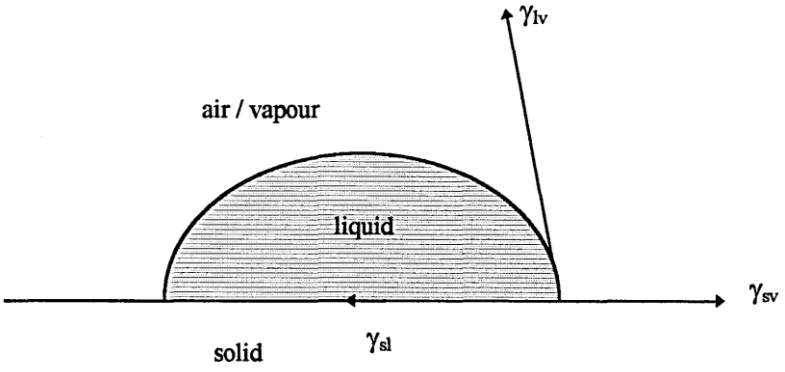

Figure 2.2 A liquid drop resting at equilibrium on a solid surface.

$$\gamma_{sv} = \gamma_{sl} + \gamma_{lv} \cos\theta \quad \textit{The young equation} \tag{2.1.}$$

Where, γ_{sv} = surface tension or surface free energy of solid,

γ_{sl} = surface tension of the liquid,

γ_{lv} = interfacial tension.

As shown in Fig. 2.2, the term γ_{sv} is the surface tension or the surface free energy of the solid surface resulting from adsorption of vapour from the liquid, and will be lower than the surface energy of the solid surface in a vacuum, γ_s by an amount known as the equilibrium spreading pressure, π_s

$$\gamma_{sv} = \gamma_{lv} - \pi_s \tag{2.2.}$$

Substituting into equation (2.1.)

$$\gamma_s = \gamma_{sl} + \gamma_{lv} \cos\theta + \pi_s \tag{2.3.}$$

When $\theta > 0°$, the liquid is non-spreading. But the liquid will spread spontaneously over the surface when, $\theta = 0°$. Thus, for complete wetting to occur,

$$\gamma_{sv} \geq \gamma_{sl} + \gamma_{lv} \tag{2.4.}$$

$$\gamma_{sv} \geq \gamma_{sl} + \gamma_{lv} + \pi_s \tag{2.5.}$$

(iii) Effect of surface roughness on contact angle: Contact angle hysteresis occurs because solid surfaces are seldom smooth or chemically homogenous, and thus different values of the equilibrium contact angle, θ, may be obtained depending upon whether the liquid drop is advanced or withdrawn across the solid surface [63]. It can

be shown that surface roughness can change the apparent advancing contact angle, as shown in Fig. 2.3.

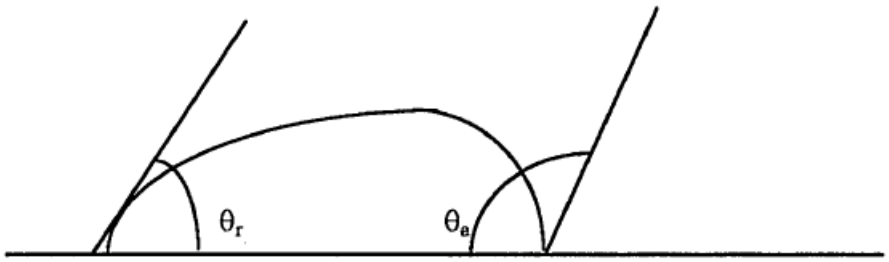

Figure 2.3. A liquid drop showing advancing and receding contact angles, where θ_a is the advancing contact angle and θ_r is the receding contact angle.

Contact angle hysteresis occurs because solid surfaces are chemically homogenous, and thus different values of the equilibrium contact angle, θ, may be obtained depending upon whether the liquid drop is advanced or withdrawn across the solid surface. It can be shown that surface roughness can change the apparent advancing contact angle and may be expressed by,

$$\cos \theta_f = r_f \cos \theta_s \qquad (2.6.)$$

where, θ_s is the contact angle of a liquid drop on a smooth surface,

θ_f is the contact angle of a liquid drop on a rough surface,

r_f is a surface roughness parameter; = actual area / projected area.

If on a smooth surface θ_s is less than 90°, then roughening the surface will further decrease the contact angle to 0f and thereby increase the wettability. However, if on a smooth surface

θ_s is greater than 90°, roughening the surface will only increase the contact angle to 0 f and thereby decrease the wettability [63].

The strength of an adhesive joint depends not only on the cohesive strength of the adhesive, but also on the bond strength at the adherend/adhesive interface [63]. The key component in the adhesive bonding and technology is the surface preparation, as it decides the nature of failure in the bonded joint.

2.3 Surface treatment

Any method of treating a material (e.g., metal, polymer, and wood) so as to alter the surface, rendering it receptive to inks, paints, lacquers, adhesives, and various other treatments, or resistant to weather or chemical attack. It can be divided into three major categories-

2.3.1 Surface treatment by chemical process

It is a process, which involves altering a surface through the implementation of chemical processes. Such process provides the formation of a stable linkage by the reaction between a chemical group on the adherend surface and a compatible group in the adhesive [64]. Adherend surfaces are usually given surface treatments involving chemicals (e.g. cleaning, degreasing, chemical etching, electrochemical anodization, conversion coatings, etc.) to create compatible groups. These treatments serve to increase the concentration of oxygen and any other desirable chemical component on the adherend surface since these species are considered to enhance adhesion by encouraging the formation of strong covalent or hydrogen bonds.

2.3.2 Surface treatment by mechanical methods

Surface treatment by mechanical methods involves altering the topography, composition, or properties of a material's surface through mechanical actions such as abrasion, polishing, grinding, machining, or shot peening [64]. Related to the degree of roughness and, subsequently, the friction of the adherend, a certain level of bonding can be anticipated solely through mechanical interlocking. This interlocking is achieved by creating an augmented overall surface area suitable for mechanical interlocking through techniques, such as, like grit blasting, abrasion, and sandblasting, etc., when applied to the surface of adherent. While the strength of the bond can be influenced by various factors on the surface of adherent, the SLS strength experiences a notable enhancement with increased roughness.

2.3.3 Surface treatment by physical process

Physical surface treatment refers to a set of techniques and processes that alter the properties, composition, or structure of a material's surface through non-chemical means []. These processes typically involve applying various forms of energy, such as heat, mechanical forces, or electromagnetic radiation, to modify the surface characteristics without introducing additional substances. Physical surface treatment methods include processes like ion implantation, sputtering, vapor deposition, thermal spraying, shot peening, and laser surface treatment [64]. The formation of a physical bond originates from highly localized intermolecular forces. Adhesives with surface energies lower than that of the adherend surface will easily spread across the surface and establish strong bonds. If sufficiently interaction between a functional group present on the adherend surface and the adhesive, a physical connection emerges between the atoms of both materials, resulting in wetting. Such

wetting phenomenon can be developed by surface treatment using plasma process, laser ablation methods, corona discharge, etc. The extent of wetting is contingent upon the variations in surface free energies among the solid, liquid, and the ensuing interface. A short-detailed literature reviews will be presented in the later sections, discussing the values of SLS strengths, obtained by various investigation with the aforementioned surface treatments.

Nevertheless, the selection of adhesive materials is indeed equally important and critical as surface treatment when it comes to achieving successful and reliable adhesive bonding. Both factors play pivotal roles in determining the SLS strength, and durability of adhesive joints.

2.4 Selection of adhesive materials

Commonly, substrates are selected to provide the engineering and aesthetic properties required by the product. Although the selection of an adhesive is a critical factor in the bonding process. There are many different types of adhesives are available to cover a myriad of structural joining needs [65]. Within the wide range of classes, there are many possible material chemistries and curing mechanisms. The most important are:

(i) Single-part: A one-part adhesive contains a polymer resin system that cures directly on exposure to moisture, oxygen, UV light, or elevated temperature. Mainly, single-part adhesive can be divided into two sub categories, heat cured and moisture cured.

a) Single-part, heat-cured: The adhesive is formulated with resin and hardening agent present together but inhibited from reacting unless exposed to high temperatures. Single part adhesives include epoxy, acrylic, silicone, phenolic, polyimide and elastomer (butadiene) chemistries. Single part adhesives are commonly used for

structural applications and surface component mounting in electronics. They are typically supplied as thick liquids and pastes although some are in the form of films.

b) Single-part, moisture-cured: Adhesives, such as single-part polyurethanes and silicones, that cure in the presence of moisture.

(ii) Two-part: The adhesive is formulated with separate resin and hardener. Once these are mixed, the cure reaction starts. Normally the formulations will cure at room temperature although cure rates can be increased by raising the temperature. Two-component adhesive types include epoxies, acrylics, silicones and polyurethanes.

(iii) Anaerobic: Enclosed cure adhesive that cures in thin gaps through the catalytic action of surface moisture in the absence of oxygen, which inhibits the reaction.

(iv) Cyanoacrylate: Enclosed cure adhesive, based on acrylic monomer, that polymerizes into an acrylic polymer in contact with alkaline surfaces. The presence of surface moisture helps neutralize acidic stabilizers in the adhesive and promotes the hardening reaction.

(v) UV Curing: Adhesive where the cure reaction is initiated by ultra-violet light. Acrylic monomer polymerizes into acrylic polymer.

(vi) Solvent-based: Adhesive material is carried in a solvent (either an organic solvent or water). Water dispersed adhesives are commonly known as water-based adhesives. The solvent must evaporate (dry), depositing the adhesive film, before bonding. Owing to health and environmental concerns organic solvent-based systems are being replaced by water-based systems. An activation stage (e.g. heating) may be required before bonding. Rubbery polymers such as natural rubber, urea formaldehyde, polyvinyl acetate, polyurethane, polychloroprene or acrylics are used in these formulations.

(vii) Pressure sensitive: PSAs are semi-solid adhesive, permanently tacky due to their viscoelastic characteristics, often used on tapes and labels. PSAs may be made from film-forming elastomeric materials, such as styrene-butadiene rubber, butyl rubber, silicone rubber, nitrile rubber and acrylic rubber, or block-copolymers with the addition of small quantities of tackifiers, plasticizers, waxes or oils.

(viii) Hot melt: Thermo-plastic, solvent-free materials, characteristically solid at low temperatures, which are low viscosity fluids above 80 °C and rapidly set upon cooling. Hot melt adhesives are used in a variety of manufacturing processes, including bookbinding, product assembly, and box and carton heat sealing. There are a number of hot melt adhesives in use, with the most common being those used for hot melt pressure sensitive adhesive applications, such as, ethylene vinyl acetate (EVA) copolymers, styrene-isoprene-styrene (SIS) copolymers, styrene-butadiene-styrene (SBS) copolymers, polyimides, polyesters, ethylene ethyl acrylate copolymers (EEA) and polyurethane reactive (PUR).

Whereas, the aforementioned section provides a short-detailed information related to the different types of adhesives, in order to make a compatible choice with the desirable surface treatment. During the investigation of proposed objectives in this thesis, room temperature cured and RH cured adhesives are utilized under their respective recommended curing conditions.

2.5 A brief literature review on treatment of surfaces for the application in adhesive bonding

Adhesive bonding has attracted a lot of interest both in academia and industry due to their high SLS strength and least complexity. To date, a literature search in "web of science" alone provides enormous numbers of articles on adhesive bonding written in the last decade.

2.5.1 Adhesives and adhesion properties in nature

The ingenuity of humankind is frequently ignited by the wonders of nature, leading to remarkable technological advancements. Adhesives conform to this rule without exception. The earliest adhesives at our disposal were sourced directly from the natural world. Presently, nature continues to unveil novel compounds that have the potential to enhance our adhesive technologies. Presented below is a concise compendium exploring intriguing natural adhesive sources.

To start with, in the realm of adhesives, honeybees exhibit the same level of industriousness as they do in honey production. They create their own adhesive that is called propolis. This adhesive is crafted from a combination of their saliva and a botanical oil known as pollenkitt, produced by flowers. Bees employ this adhesive to safeguard their nectar during their return journey to the hive [66]. Even today, this adhesive maintains its renowned for its remarkable capacity to retain its stickiness under wet or humid circumstances. It is still a challenge to design a synthetic glue that can meet these challenges.

Figure 2.4 A friendly bee standing on some grass. © Mani Mohan Tiwari, 2023.

There exist many other examples which demonstrate inheriting unique adhering nature for their survival and existence. The remarkable climbing abilities of geckos are attributed to their adhesive-coated feet [67]. Surprisingly, geckos possess the capability to toggle the adhesive properties of their feet on and off at will. This unique attribute is due to the presence of minuscule bristles that further subdivide into even smaller hairs, generating an electromagnetic attraction that aids geckos in adhering to an extensive variety of surfaces [67].

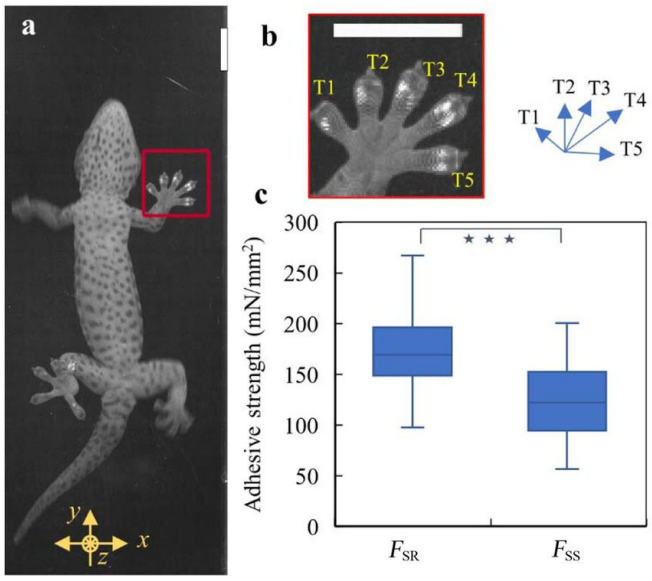

Figure 2.5 Estimation of real contact area and reaction force at the feet of climbing geckos. (a) The measurement of contact area at the feet of a gecko when climbing an acrylic board; (b) distributed toes functioning as vectors; and (c) the frictional adhesion strength calculated using resultant contact area (FSR) and overall contact area (FSS). Adapted from [67] with authorization from Springer Nature.

In 2014, Ditsche *et al.* investigated that the effect of biofilms on the underwater adhesion of mayfly larvae, as shown in Fig. 2.5. The results indicate biofilms enhance the friction of the claws on smooth substrates, whereas decreasing the friction on rough ones [68]. For the underwater adhesion of the teleost (Garra gotyla), tubercles with hooks on the jaw sheathes may function through an interlocking mechanism [68]. In addition, Johal and Rawal suggested that long hooks on the adhesive apparatus of the hillstream fish (Glyptothorax garhwali Tilak) may also interact with the irregular substrates by the same mechanism.

Figure 2.6 Fly adhering on the smooth glass surface. © Mani Mohan Tiwari, 2023.

In addition to that numerous insects, such as common houseflies, as well as certain amphibians and reptiles are able to walk on and cling to seemingly smooth surfaces--including glass doors and windows, as shown in Fig. 2.6. A study by Fell *et al.* added some other detail that the segments, or tarsi, at the end of insect legs possess claw like structures that help the insect hold on to different types of surfaces [69]. These tarsal claws are used to grip the tiny irregularities on rough surfaces. But in some cases, insects do make use of a kind of adhesion. If the surface is smooth, the insect can hold on using the adhesive action of hairs located on sticky pads on the tarsi.

2.5.2 Artificial surfaces for adhesive bonding

Due to the tremendous importance of adhesive bonding in today's emerging technologies, many efforts have been made to replicate nature. The term "bio-mimicking" is commonly used to denote the typical artificial methods for fabricating wet surfaces with different

surface micro/nanostructures as the technology to make them involves copying nature's solutions. The applications of adhesive bonding are diverse due to their unique bonding abilities. The most common areas where adhesive bonding attract attention include manufacturing anti-rust joints in boats [70], bio-chips [71], biomedical applications [72], microfluidics [73], interior joints for automobiles [74], textiles and many others.

A literature survey on the various attempts to prepare a surface for adhesive bonding has shown that the methods can be basically divided into chemical, mechanical and physical process. Extensive literature exists concerning the treatment of various surfaces for their suitability in adhesive bonding. A selection of these treatments is outlined below.

(i) Surface treatment using electrochemical anodization

Electrochemical anodization is a widely used surface treatment method for enhancing the properties of various materials, particularly metals like aluminum and its alloys. The process involves controlled oxidation of the material's surface in an electrolyte solution, forming a protective oxide layer. Research by Smith *et al.* highlighted the role of applied voltage, electrolyte composition, and anodization time in determining the oxide layer's thickness and characteristics [75]. A fundamental understanding of adhesively bonded joints requires an examination on both macroscopic and microscopic levels. On a microscopic level, adhesion is only achieved if the adhesive comes in molecular contact with the substrate. Numerous studies have been reported in literature, where electrochemical surface treatment was performed on metals to achieved a high SLS strength of adhesively bonded joint. The kind of bond that is formed and its strength depend on the chemical nature of the substrate, the type of adhesive and their compatibility with the properties of adherent's surface. In a classic

work done by Zhang *et al.* has reported the effect of various acid electrolytes to form a porous oxide that would lead to additional mechanical interlocking [76].

Table 2.1 The etching and anodizing processes prior to bonding. Adapted from [76] with authorization from Elsevier.

Process	**Composition**		**Conditions**
Dichromate/sulfuric acid etching	$Na_2Cr_2O_7 \cdot 12H_2O$	33 g/L	Etched: at about 68 °C for about 10 min
	H_2SO_4	330 g/L	
Sulfate/sulfuric acid etching	H_2SO_4	370 g/L	Etched: at about 65 °C, for about 10 min
	Fe_2SO_4	150 g/L	
Chromic acid anodizing	Cr_2O_3	50 g/L (Bengough–Stuart process)	Anodizing: at 40 ± 2 °C, increasing voltage from 0 V to 40 V in 10 min and lasting for 20 min, then increasing voltage up to 50 V in 5 min and lasting 5 min
Phosphoric acid anodizing	H_3PO_3	10 wt.%	Anodizing: at a constant voltage of 20 V (about 0.4 A/dm^2) for 20 min and about 20 °C
	H_2SO_4	5 wt.%	

Process	Composition		Conditions
Boric/sulfuric acid anodizing	H_3BO_3	0.8 wt.%	Anodizing: at a constant voltage of 15 ± 1 V (about 0.35 A/dm^2) at about 26 °C for 20 min
Phosphoric/boric/sulfuric acids anodizing	H_2SO_4	5 wt.%	Anodizing: at a constant voltage of 18 ± 1 V (about 0.45 A/dm^2) at about 22 °C for 20 min
	H_3BO_3	0.8 wt.%	
	H_3PO_4	50 g/L	

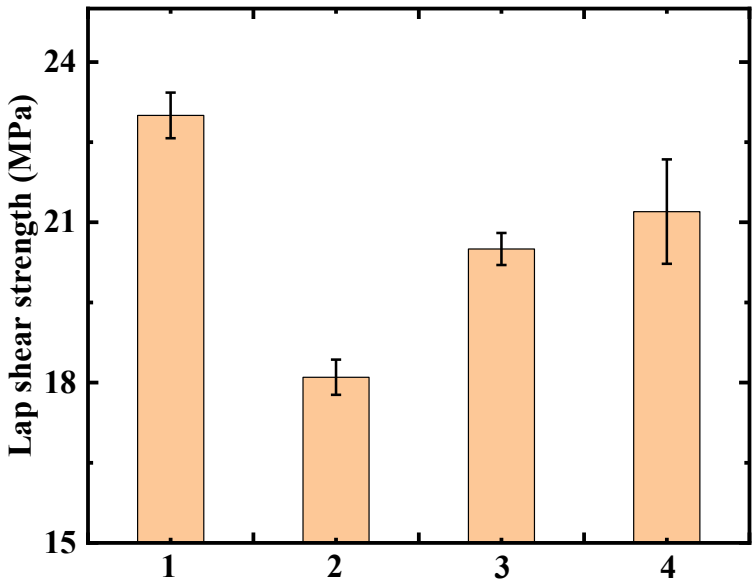

Figure 2.7 Effect of different anodizing process on the lap-shear strength of adhesion joints. The numbers on x-axis represents the types of process that described as-(1): Sulfate/sulfuric acid etching + phosphoric acid anodizing. (2): Sulfate /sulfuric acid etching + boric/sulfuric acids anodizing. (3): Sulfate/sulfuric acid etching + phosphoric/boric/sulfuric acids anodizing. (4): Dichromate/sulfuric acid etching + chromic acid anodizing. Adapted from [76] with authorization from Elsevier.

Fig. 2.7 has been replotted based on the data given in the Zhang *et al.* [76]. Zhang *et. al* reported that for the processes of phosphoric acid anodizing and chromic acid anodizing, which are most popular and accepted methods as pretreatment for structural bonding, the maximum lap-shear strengths of the bonding joints were close to 23 MPa, exhibiting excellent adhesive properties. For the boric/sulfuric acids anodizing process, the bonding strength was found to be much lower, implying that the process was unsuitable for structural bonding. For the process of phosphoric /boric/sulfuric acids anodizing, the maximum lap-shear strength of the bonding joints was found to be up to 20 MPa, close to the values of

phosphoric or chromic acids anodizing. The authors concluded that maximum SLS strength of the bonding joints by different processes decreased in order: phosphoric acid anodizing ≈ chromic acid anodizing > phosphoric /boric/sulfuric acids anodizing > boric/sulfuric acids anodizing.

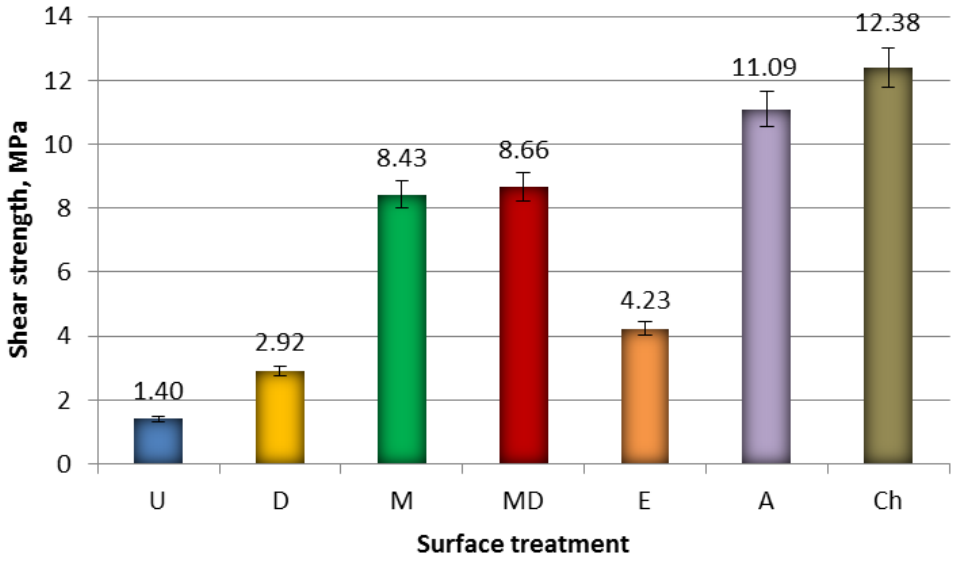

Figure 2.8 SLS tests of EN AW-2024PLT3 aluminium alloy sheet adhesive joints after different surface treatment methods: U - untreated, D - degreasing (chemical cleaning), M - mechanical treatment, MD - mechanical treatment and degreasing, E - etching A – anodizing, Ch - chromate treatment. Adapted from [77] with authorization from InTech.

In another study by Anna Rudawska, had reported a study addressing the effect of various surface treatments on the SLS strength of adhesively bonded EN AW-2024PLT3 Al alloy [77]. The results of SLS tests on EN AW-2024PLT3 aluminium alloy sheet adhesive joints are presented in Fig. 2.8. He specified that application of anodizing and chromate operations as an EN AW-2024 aluminium alloy sheet surface treatment method produced adhesive joints of maximum shear strength of 11.09 MPa and 12.39 MPa, respectively. Similarly, good results in promoting joint strength were also observed when the surface of EN AW-

2024PLT3 aluminium alloy sheets was subjected to exclusively mechanical treatment; the results in that case amounted to 8.43 MPa and 8.66 MPa; therefore, the joint strength was six times higher than in the case where no surface treatment was applied.

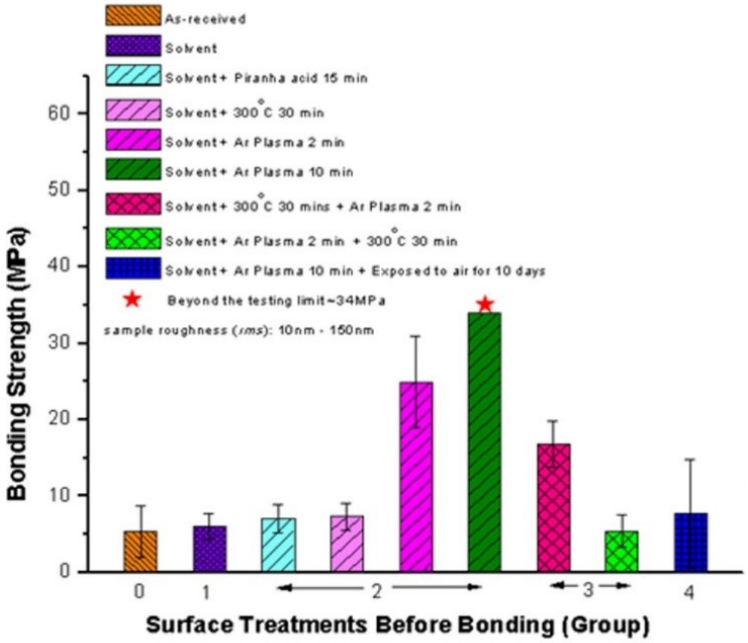

Figure 2.9 Effect of different types of surface treatment on SFE. Adapted from [78] with authorization from Elsevier.

Further, Lim *et al.* had also contributed by studying different surface cleaning techniques and treatment sequences were studied for their effect on Cu film adhesion with polycrystalline Al_2O_3 substrate [78]. It was found that organic solvent cleaning, heat-treatment, and piranha acid soaking have very limited impact in improving the adhesion strength, as shown in Fig. 2.9. Argon plasma cleaning is the most effective pre-treatment, and it can increase the bond strength by more than six times with the SLS strength of 33 MPa. The authors reported that reason for such a drastic increase is the effective removal of the surface contaminants as well as the creation of surface dangling bonds.

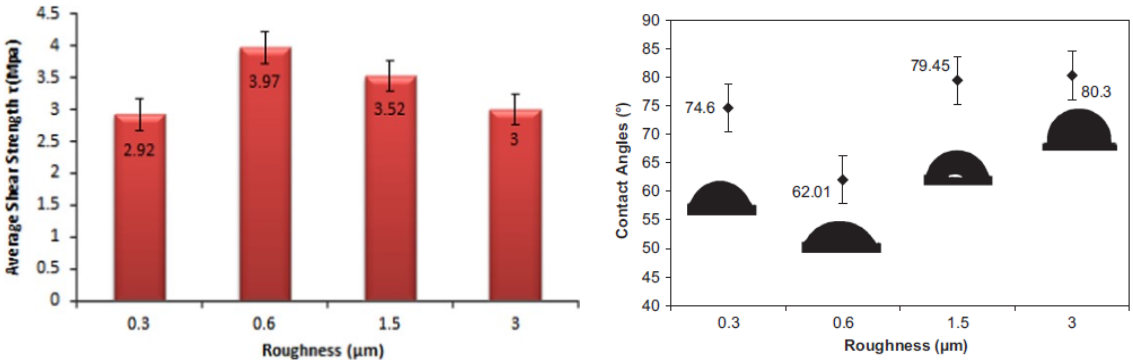

Figure 2.10 Variation of the shear strength as a function of roughness and Contact angles as function of surfaces roughness. Adapted from [79] with authorization from Elsevier.

Furthermore, the relationship between roughness and adhesion is not very simple. Optimum surface profile varies from one adhesive to another and depends upon the type of stress applied [79]. As well the roughness of adherend surfaces has frequently been used as a design parameter for adhesive joints. Therefore, in the same regards, a study conducted by Boutar *et al.* had comprehended the effect of roughness on the durability of single-lap joint, as shown in Fig. 2.10. The results indicate that the changes in joint properties associated with roughened surfaces can not be explained simply by the increased roughness characteristics, such as mechanical keying and increased effective bond area. It is evident that changes in physical and chemical properties of the surface, arising from the polishing process contributed significantly to the joint behaviour. Therefore, the characterisation of the interphase and its formation mechanisms are important in order to get a better understanding of the fundamental mechanisms of adhesion and to explain the joint durability [79].

Hu *et al.* have practiced the adhesive bonding between carbon fibre reinforced plastics and Al alloys, which is extensively advantageous to achieve optimum lightweight and reliable structures for multiple applications ranging from aerospace, automotive and agricultural machine industries [80]. An ultrasonic etching process was carried out in alkaline solutions

to investigate the influence of NaOH concentration on adhesive bonding characteristics, as shown in Fig. 2.11. An ultra-thin layer of acetone-diluted resin pre-coating (RPC) without hardener was then applied to the etched substrates to seal micro-cavities before adhesive bonding. The SLS test was used to evaluate the adhesive bond strength under different surface conditions [80].

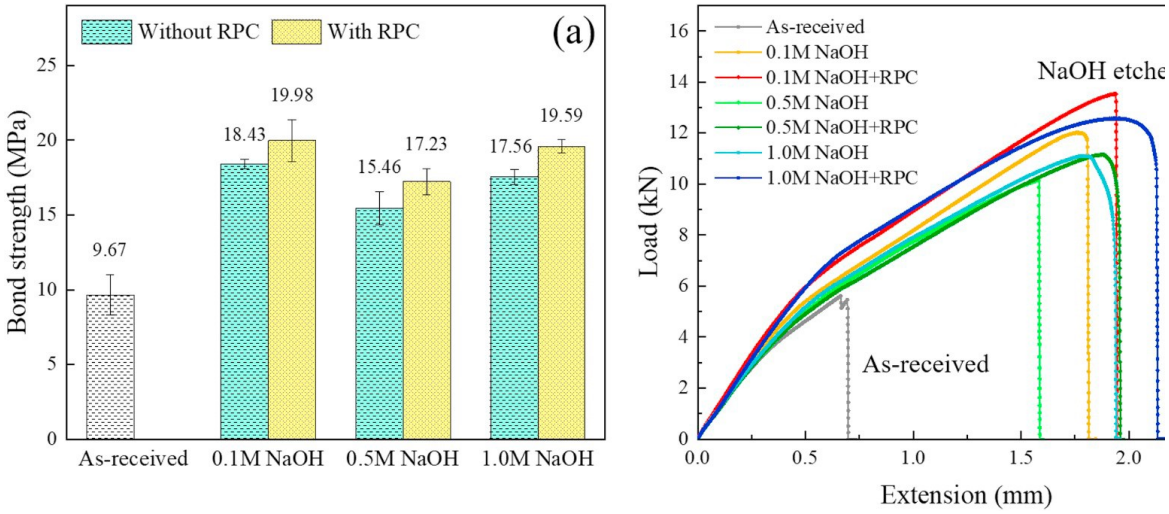

Figure 2.11 SLS test results: (a) average bond strength and (b) representative load-extension curves. Adapted from [80] with authorization from Elsevier.

2.3.2 Effect of self assembled monolayer silanes

Silane coupling agents are adhesion promoters to chemically unify dissimilar materials. The impacts of silane chemical insertion on the SLS strength and interfacial properties were thoroughly investigated. In a work by Underhill *et al.* explored the relationship between silane cured Al and relative humidity, as shown in Fig. 2.12. They reported that the sensitivity to the ambient humidity increased with increasing temperature and enhances the SLS strength. Furthermore, Abel *et al.* reported about the effects of silane application conditions on the bond durability [81]. In another systematic study performed by Qiu *et al.*, phenolic

adhesive was directly joined to Al using three different silane coupling agents, AEAPS (N-(β-aminoethyl)-γ-aminopropyl trimethoxy silane), McPS (γ-mercaptopropyl trimethoxy silane), and GPS (γ-glycidoxypropyl trimethoxy silane) [82]. The authors reported that joint strength was raised about 1.6–2.6 times that of the untreated Al when joined to phenolic adhesive.

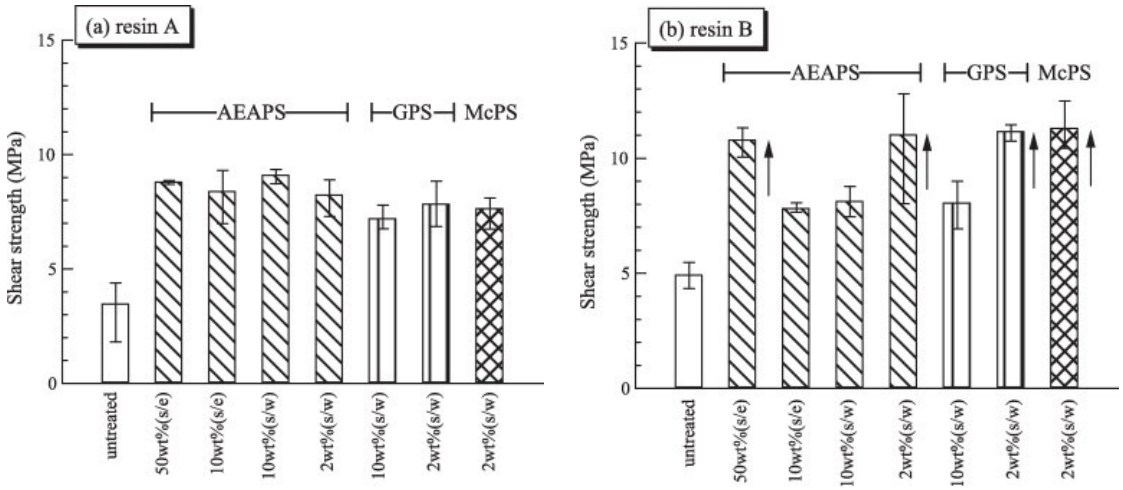

Figure 2.12 Changes of SLS strength by different silane solutions: (a) adhesive A and (b) adhesive B. Adapted from [82] with authorization from Elsevier.

Jianhui Qiu *et al.* reported that the SLS strength between Al and phenolic adhesive (after just the pre-treatment) was seen to be about 3.5-5.0 MPa whereas it was increased after the surface treatment [82]. They reported that the SLS strength of adhesive B after joining was found to be ~ 11 MPa, when Al was surface-treated with four of the silane coupling agent solutions 2 wt% AEAPS, 2 wt% GPS, 2 wt% McPS and 50 wt% AEAPS.

Zain *et al.* had demonstrated the effect of a SAM promotor on the shear strength of adhesive joint of metal substrate. Al alloy 2024-T3 was treated by two different methods of surface treatments i.e., by alkaline etching and warm water treatment followed by silanization method in order to enhance the adhesive bonding, as shown in Fig 2.13. The effects of both

the substrate surface condition and the adhesive properties on single–lap shear resistance was analysed. Three different formulation of polyurethane adhesive by varying the NCO:OH ratio which were prepared from polyol based on polycaprolactone (PCL)/palm kernel oil (PKO) with an aromatic and cycloaliphatic diisocyanate. The highest SLS strength of 16 MPa has been found for the NCO:OH ratio of 1.7, which was 15 times higher then the as-received counterpart [83].

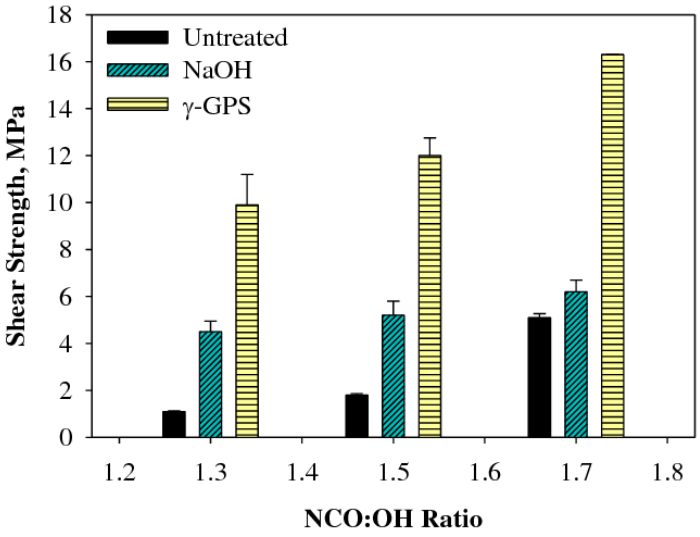

Figure 2.13 The effect of surface treatment on shear strength of adhesive bonding. Adapted from [83] with authorization from Trans Tech.

2.3.3 Effect of mechanical abrasion on surface roughness and SLS strength

Surface roughness is one of the important factors which influence the bonding strength of the joints. The literature indicates that sufficient surface roughness plays a critical role in obtaining a reliable bond by enlarging the contact area and inducing strong mechanical interlocking between the adhesive and the substrate [84]. A few mechanical treatments to alter the roughness are grit blasting [85], grinding [86] and sand blasting [87]. An investigation on effect of adherend surface roughness on adhesive bond strength was

performed by A. Ghumatkar and *et al.* The authors reported that optimum surface roughness exists for a maximum bonding strength and the roughness range depends on the adherend material, as shown in Fig. 2.14 [88]. A. Ghumatkar and *et al.* reported that a maximum of 40% increment in SLS strength was observed when the adherent surface roughness was in the range of 2.05±0.19 µm as compared to the non-abraded adherend surface (1.55± 0.15µm).

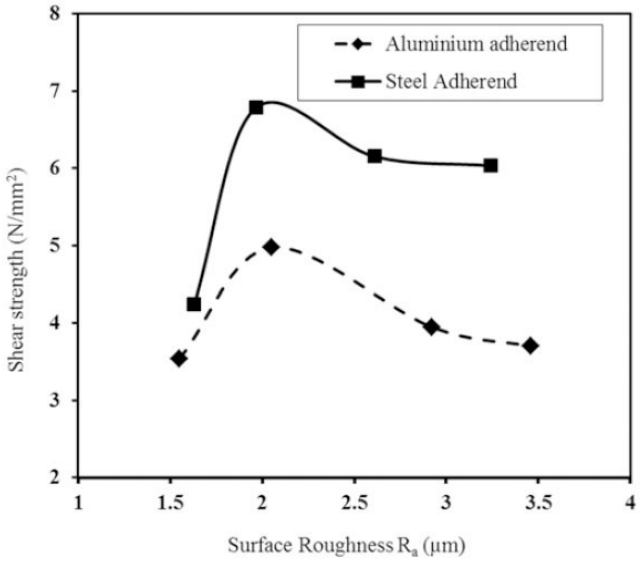

Figure 2.14 SLS strength with respect to the adherend surface roughness of Al and mild steel adherend joints. Adapted from [88] with authorization from SciELO - Scientific Electronic Library Online.

Besides the previously mentioned work, Farhad shafiei *et al.* had reported the effect of sand blast technique to improve the shear stress of adhesive joints. In Fig. 2.15, the results exhibited that the mean bond strengths in sandblasted groups were higher than non-sandblasted one. These differences were significantly higher in the sandblasted groups of Panavia F 2.0 and RU cement ($P < 0.05$). The mean bond strength values between GC and Panavia F 2.0 were not statistically significant ($P > 0.05$). The highest bond strength was

recorded for Panavia F 2.0 with the surface treatment of both sandblasting and Metal Primer II [89].

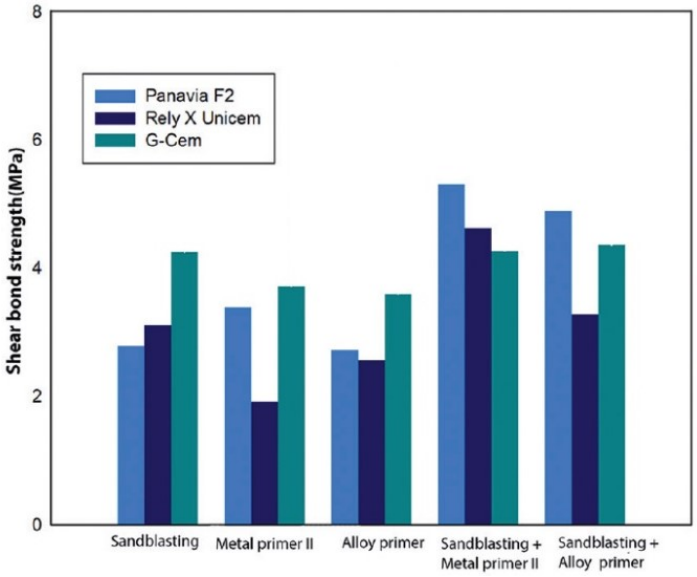

Figure 2.15 Bar chart of the effect of adhesive type and surface treatment on the shear bond strength of resin adhesive to base metal alloy. Adapted from [89] with authorization from Wolters Kluwer Medknow Publications.

Furthermore, Dawei Zhang and Ying Huang presented a systematic study over various grit blasting surface conditions of the steel adherend, including ground (G0.25, G0.5, and G1), fine- (F0.25, F0.5, and F1), medium- (M0.25, M0.5, and M1), and coarse-blasted (C0.25, C0.5, and C1) surface conditions for 0.25 mm, 0.5 mm, and 1 mm bondline thicknesses, respectively, as shown in Fig. 2.16 [90]. The authors reported that increases of SLS strength become relatively limited on high-roughened surfaces, the increments of toughness were still as high as 303 % and 302 % from the bondline thickness of 1 mm to 0.5 mm and from 0.5 mm to 0.25 mm respectively, with the highest SLS strength of ~24 MPa.

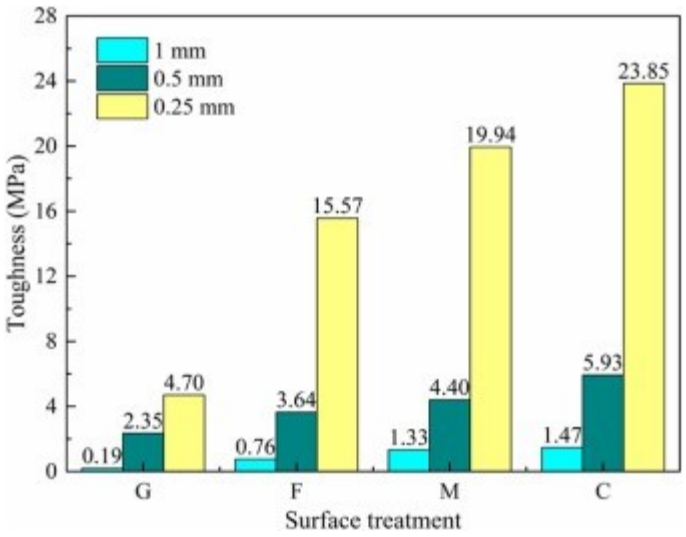

Figure 2.16 Comparisons of the toughness with different bondline thicknesses. Adapted from [90] with authorization from Elsevier.

Binhua Wang *et al.* also presented detailed study on the metal substrate surface treated by grit blasting, and then proposes a simple resin pre-coating method aiming at full wetting of the substrate surface for stronger adhesive bonding, as shown in as shown in Fig. 2.17 [91]. They examined four different surface conditions in this study: (i) Grit-Blasted (GB) steel surface, (ii) GB-surface with ultrasonic cleaning, (ii) GB-surface with our proposed resin Pre-Coating (PC), but without ultrasonic cleaning, and (iv) GB-surface with both ultrasonic cleaning and PC. They concluded that the SLS strength from GB/PC was 50% higher than that of base grit-blasted specimens and the highest SLS strength were obtained as 27 MPa for the GB/cleaning/PC specimen.

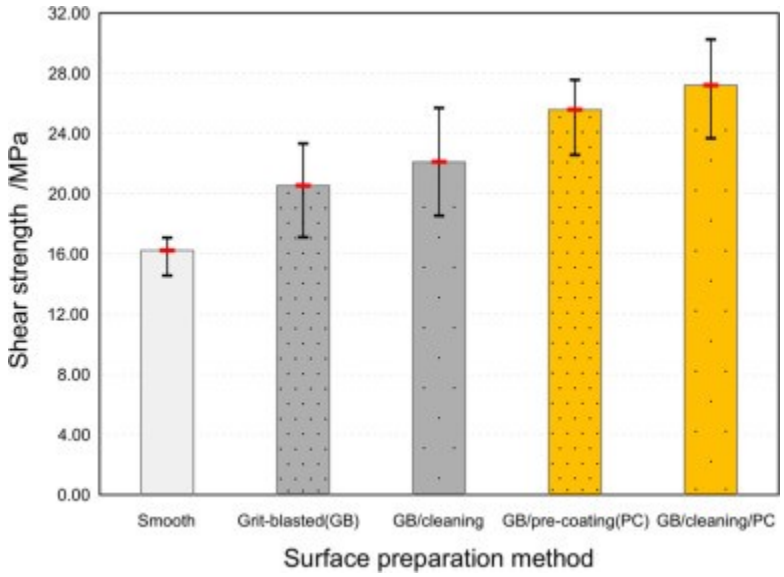

Figure 2.17 SLS strength of the grit-blasted steel samples with four different surface conditions. Adapted from [91] with authorization from Elsevier.

2.3.4 Surface treatment by physical process

Frequently, especially when dealing with plastic materials, chemical treatment and mechanical abrasion often fall short in terms of effectiveness. In such cases, alternate methods known as 'physical approaches' come into play to alter the surface reactivity of plastics and modify surface chemistry for improved adhesion. Among the commonly employed physical techniques are flame treatment, corona discharge, and plasma treatment [92]. Flame treatment entails briefly exposing the intended bonding surface to a gas flame. This exposure oxidizes the surface, creating higher-energy functional groups and increases surface energy. Meanwhile, corona discharge generated by ionizing the air between two closely spaced electrodes, reacts with the surface of the substrate to form free radicals. These free radicals quickly react with oxygen in the atmosphere and increase the surface energy of the substrate to be bonded. This treated substrate with higher surface energy allows the surface to be easily wet by the adhesive. Plasma treatment stands apart from corona discharge

and flame treatments due to its distinctive approach. It is usually conducted within a partial vacuum environment. Within plasma treatment, gas plasma is energized using suitable techniques, resulting in a greatly excited, ionized gas that interacts with the plastic substrate. Kruse *et al.* reported that the SLS strength of polybutyleneterephthalate after gas phase fluorination (for 10 s with 0.5 vol % F) treatment reached up to 6.1 MPa. Whereas, upon treating the polyetheretherketon with corona treatment, the maximum achieved SLS strength were found to be 7 MPa [93]. In an exemplary work, Gang Han *et al.* presented a technique for strengthening the adhesive-bond strength between Al and CFRP using physical surface treatment with carbon nanotubes (CNTs), as shown in as shown in Fig. 2.18. CNTs bridging across the interface between the adhesive joint and Al substrate enhanced the interfacial SLS bond strength between the Al substrate and CFRP by ~ 134 % [94].

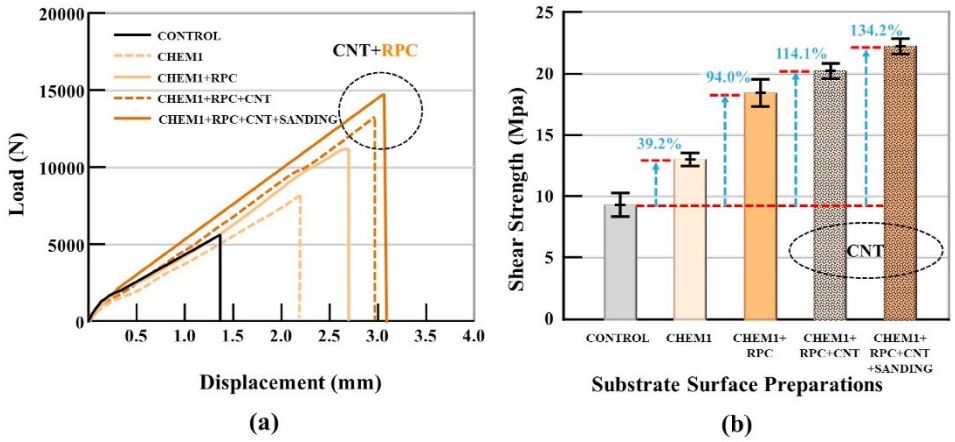

Figure 2.18 (a) The load and displacement curves (b) The average SLS strength with the techniques applied as surface treatment. Adapted from [94] with authorization from Elsevier.

A classic exemplary work on the effectiveness of CO_2 laser treatment of metals for adhesive bonding was document by G.W. Critchlow and *et al.* The authors reported the effect of CO_2 laser treatment on the wettability of mild steel and presented SLS strengths of joints formed

between a single-part epoxide and both mild steel and Al [95]. They found that the CO_2 laser treatment provided the SLS strength of ~16MPa which was ~45% higher compared to degrease only and concluded that the laser treatment gives comparable initial results to the commercially used grit blast plus silane treatment.

Table 2.2 Initial joint strengths data from treated CRI mild steel joints bonded with a single-part epoxide. Adapted from [95] with authorization from Elsevier.

Treatment	Initial joint strength (N)
Degrease only	3550
CO_2-laser treatment, SET 30s	5200
CO_2-laser treatment, SET 2760s	4940
Grit-blast	5240
Grit-blast+silane	5160

Frank L. *et. al* reported the surface treatment of Ti-6Al-4V alloy faying surfaces using a laser ablation technique [96]. They reported the use of neodymium doped yttrium Al garnet (Nd:YAG) laser to clean and create topographical patterns, and modify adherend surface chemistry prior to bonding with PETI-5 adhesive. The authors reported that that the highest SLS strength of the bonded joints had been reported as ~35 MPa, with the improvement of 250% compared to the non-ablated samples.

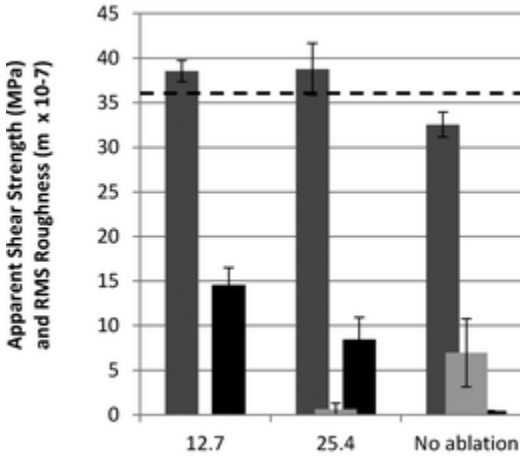

Figure 2.19 Results for SLS specimens with and without Laser ablation. Dashed lines indicate the highest apparent shear strength values measured for SLS specimens. Adapted from [96] with authorization from NTRS - NASA Technical Reports Server.

On the other hand, an investigation of surface treatment of titanium by plasma ion implantation under atmospheric pressure plasma had been carried out by Akram, *et al.* [97]. The authors reported that the SLS strength of as-received titanium/titanium with polyimide adhesive were found to be 3.65 MPa, as shown in Fig. 2.20. Whereas, the grit blasting for 120 s provided an increase in SLS strength up to 7.75 MPa. Further, modified by atmospheric pressure plasma, the SLS strength reached up to 10.10 MPa with the increase of 176% as compared to as-received counterparts.

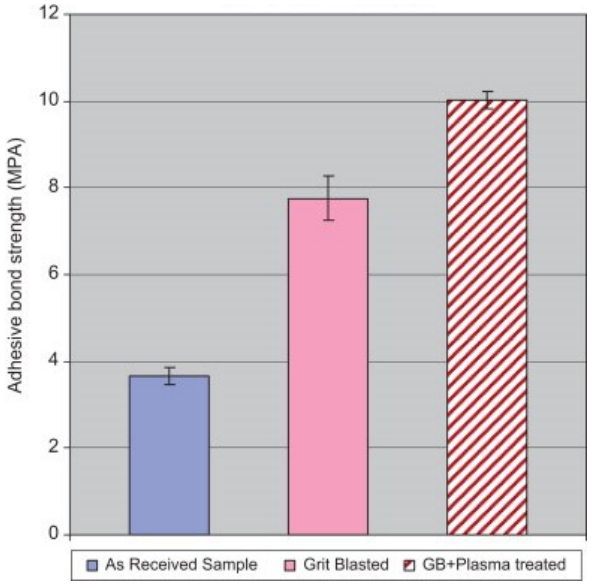

Figure 2.20 Adhesive joint strength of as received titanium and surface modified titanium. Adapted from [97] with authorization from Elsevier.

Chapter 3: Experiment

In this chapter, the techniques used for synthesizing and characterizing the materials will be discussed along with the experimental procedures used. This chapter will be divided into two sections - Materials synthesis and Materials analysis.

3.1 Preparation of adhesive joints

Adhesive joints were produced using three successive steps - (i) substrate cleaning; (ii) creation of surface microroughness on the substrates; (iii) preparation of adhesive joints. The substrate materials used were mainly AA 3031-T4, AA 6061-T6 (1.5 mm thick), AA 6061-T6 (3 mm thick) Al and PVC.

3.1.1 Substrate cleaning

Prior to any treatment, the Al substrates were always ultrasonically cleaned for 15 minutes with acetone (Sigma Aldrich) followed by ultrasonication in deionized water for 15 minutes and dried on hotplate at 70 °C for several hours to remove excess water. Whereas, the PVC substrates were ultrasonicated in 2-Propanol and dries on open environment at room temperature.

3.1.2 Creation of surface microroughness on the substrates

The major procedures of this research work consist of the following steps:

The erection of microrough structures are accomplished by mechanical abrasion surface treatments , where, SiC abrasive pads are used to alter the surface features of Al. The ultrasonically cleaned substrates of Al are mechanically abraded using grit (G)-80, G-120,

G-240, G-320, G-400 and G-600 SiC abrasive paper. Furthermore, the growth of microrough porous structures are achieved through the electrochemical anodization of Al into an aqueous salt solution of Na_2HPO_4. In addition to that the organosilane are incorporated using in-situ silanization during anodization technique, where the anodization is conducted in aqueous electrolytes of the organic GPS and an inorganic salt of zinc nitrate ($Zn(NO_3)_2$. On the other hand, the PVC surface are treated using corona discharge in order to introduce polar functional groups to enhance their hydrophilicity.

The detailed description of the experimental procedures is provided in the respective chapters. The bonding process of all the prepared surfaces are described in the following section.

3.1.3 Preparation of adhesive joints

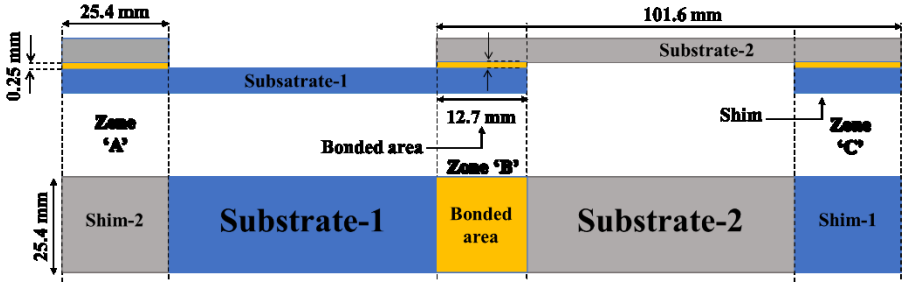

Figure 3.1 Schematic representation of bonded Al with PVC utilizing structural adhesive for SLS test according to ASTM-D1002. © Mani Mohan Tiwari, 2023.

Fig. 3.1 shows the schematic of a general SLS specimens of two substrates according to the ASTM-D1002 standard [98]. The blue part depicts substrate-1 and gray portion represents substarte-2 bonded with adhesive (shown as yellow portion) with defined bondline thickness of 0.25 mm. In order to understand well, the schematic can be divided into three different

zones, where zone 'A' represents the first end of SLS specimen prepared by mounting a square shaped shim-2 (made of substrate-2) over substrate-1 with the bondline thickness of 0.25mm. Zone 'B' depicts the adhesively bonded are of two substrates of area of 25.4 mm × 12.7 mm, with the maintained bondline thickness of 0.25mm. Zone 'C' represents the last end of SLS specimen prepared by mounting a square shaped shim-1 (made of substrate-1) over substrate-2 with same daimonion. The adhesively joined substrates have been allowed to cure according to the manufacturer's recommendation prior to mechanical testing. The SLS strength were determined using an INSTRON 8801 at a recommended traction speed according to the used adhesive. Rupture modes of the failed specimen have been visually analyzed.

3.2 Materials analysis

3.2.1 Optical profilometry

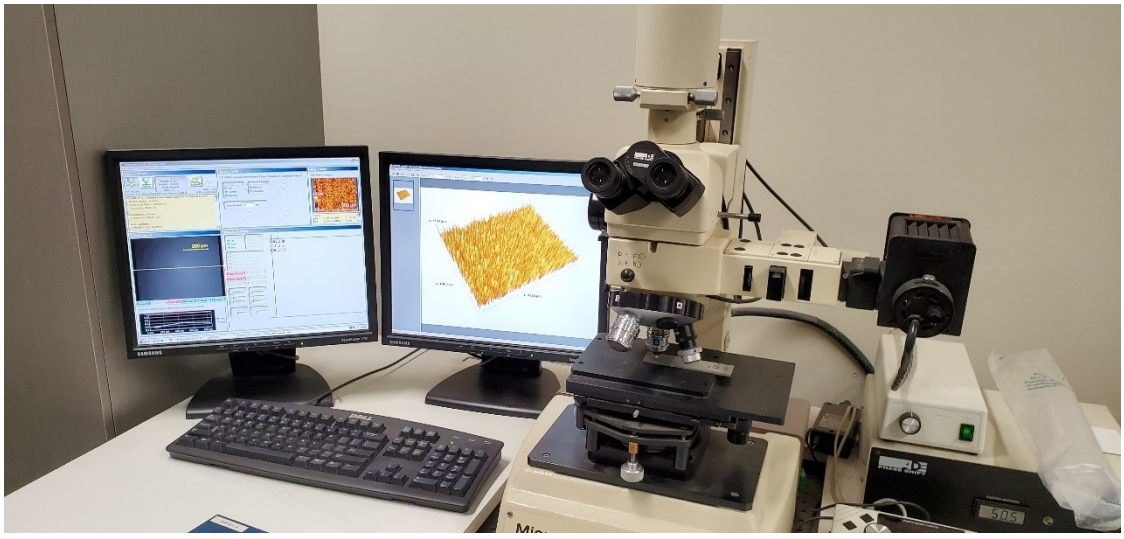

Figure 3.2 Instrument of Optical profilometry (at the laboratory of CURAL, UQAC).

The MicroXAM surface profiling microscope is used to measure the roughness of a surface in this work. A MapVue software is used to record the data received from the microscope and the SPIP software allows the analysis of the resulting image by modeling the surface in 3D. This device works as an optical microscope, as shown in Fig. 3.2. It is necessary to focus on the surface of the specimen to be analyzed and then start the acquisition. The microscope scans the surface of the specimen with great accuracy in order to give a detailed image of the surface of the sample. From the image obtained, MicroXAM determines the root mean square (*rms*) surface roughness of a surface.

3.2.2 Infrared absorption analysis

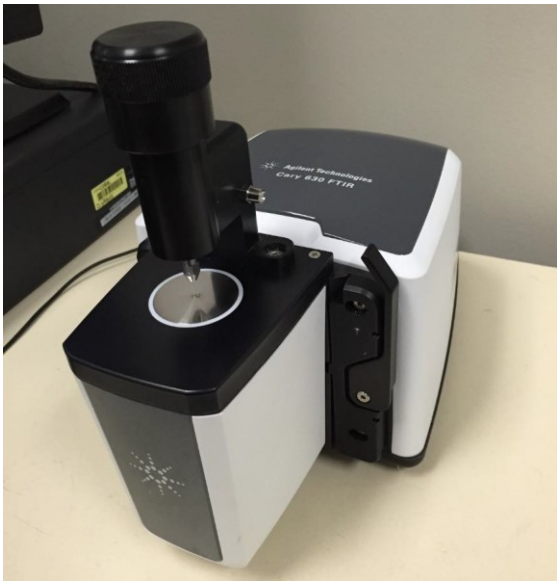

Figure 3.3 Attenuated Total Reflectance-Fourier Transform Infrared Spectroscopy (ATR-FTIR) Cary 630 Agilent Technologies instrument (at the laboratory of CURAL, UQAC).

The chemical composition of the samples was analyzed by Attenuated Total Reflectance-Fourier Transform Infrared spectroscopy (ATR-FTIR Agilent Technologies Cary 630) in the wavenumber range of 4000-450 cm^{-1}, as shown in Fig. 3.3. Generally, the infrared radiation

is passed through the sample, some of this radiation is absorbed by the sample, and some of it is transmitted. The resulting ATR-FTIR spectra represents the specific molecular absorption and transmission, creating a molecular fingerprint of the sample. This reason makes ATR-FTIR a useful tool for the chemical analysis of the samples.

3.2.3 Microstructural characterization by scanning electron microscopy

Figure 3.4 Scanning Electron Microscope SEM Jeol (model JSM 6480LV) instrument (at the laboratory of CURAL, UQAC).

The surface morphology and its evolution of the samples was carried out using a Scanning Electron Microscope (SEM, JEOL JSM 6480LV), equipped with energy dispersive X-ray spectroscopy (EDS), as shown in Fig. 3.4. To analyze the surface morphology of the surfaces, the samples were first placed in a vacuum environment. Furthermore, the samples prepared are mounted on the supporting stage using a conductive adhesive. All these manipulations help to obtain a better resolution of the images and avoids charging effects. This device is also coupled to an Energy Dispersive X-ray Spectroscopy (EDS) allowing the identification

and quantification of the elements present on samples surfaces for the chemical compositional analysis.

3.2.4 Determination of tensile SLS strength

Figure 3.5 INSTRON universal testing machine (at the laboratory of CURAL, UQAC).

The adhesively bonded joints were tested using an INSTRON 8801 universal testing machine, as shown in Fig. 3.5. Under the pulling type of loading something, it can be very quickly determined how the material will react to these types of forces being applied in tension. As the materials are being pulled from one end, its strength and elongation can be finding out. A lot of about a substance can be learned from tensile testing. This system continues to pull on the material until it breaks, a good, with a complete tensile profile displays on the associated computer. The curve shows how it reacted to the forces being applied. In the tension test a specimen is subjected to a continually increasing one directional

tensile force while simultaneous observations are made of the elongation of the ductile specimen.

Chapter 4: Parametric influence of roughness due to mechanical abrasion on the structural adhesive bonding of Al/Al.

4.1 Introduction

The ongoing climate change and future sustainable green environment necessitate the reduction in the emission levels of greenhouse gases (GHGs). The automotive industry requires manufacturers to reduce the fuel consumption of their vehicles not only to suppress GHG emissions but also to satisfy consumer expectations [99-100]. To increase the fuel efficiency, significant research effort has been spent to decrease the vehicular weight by replacing steel with lighter materials, such as aluminum, magnesium, and fiber-reinforced composites. However, joining materials in the vehicle design plays a significant role in reducing the overall body weight. Structural adhesive bonding has emerged as a technique used in modern lightweight designs. Although it represents a suitable alternative to conventional joining techniques by increasing the overall bonding efficiency, bonding two similar or dissimilar materials remains a challenging task in the development of next-generation vehicle structures for marine technology and the medical and aerospace fields [101-107].

Despite the extensive research studies on adhesive bonding reported in the literature, the commercialization of their findings is limited by various factors such as high fabrication costs, significant time consumption, material toxicity, limited material availability, poor stability, and the complexity of preparation methods [105, 106]. The strength and stability of the bond between the adhesive and substrate strongly depends on the preparation method

[105-107]. The key aspects of structural adhesive bonding process include the (1) substrate surface treatment and (2) selection of a suitable adhesive with specific curing conditions.

The structural adhesive bonding of aluminum has a wide range of practical applications in the aircraft, automotive, and marine industries owing to its various advantages such as light weight, low density, ductility, and high strength [104, 107-115]. However, the presence of a weakly bound surface oxide layer on the aluminum surface weakens the bonding of adhesive molecules to this surface. For this reason, the surfaces of aluminum alloys are frequently subjected to mechanical, chemical, and electrochemical pretreatments before adhesive bonding [106, 116-118]. Other conditions that influence the bond strength include temperature, humidity, and chemical compatibility between the substrate and adhesive. Surface roughness is an important factor which affects the bonding strength of joints. Mechanical treatments performed to change surface roughness include grit blasting, grinding, and sandblasting [119-131]. According to the literature, a sufficiently high surface roughness plays a critical role in forming a reliable bond by increasing the contact area and inducing strong mechanical interlocking between the adhesive and substrate [112, 119, 122, 129, 131-137]. Abid *et. al.* has used mechanical abrasion as a surface treatment to study the effect of surface roughness on the adhesive bonding of aluminum–aluminum substrates [132]. Da Silva *et al.* examined the compositions of different aluminum alloys, their geometries, and various surface treatments for adhesive bonding applications [134]. They found that the SLS strength of adhesive joints was directly proportional to the (i) bonding area, (ii) yield strength of the aluminum alloy, and (iii) toughness of the used adhesive. Similarly, the effect of surface roughness on the SLS strength of steel–steel bonded joints was investigated via profilometry by Ghumatkar *et al.* [133]. In their study, different

roughness values were achieved using mechanical abrasion, and an optimal average roughness of 1.97 μm was established. The observed improvement in the SLS strength was attributed to possible mechanical interlocking. Zielecki *et al*. also studied the effects of surface roughness and topography on the mechanical strength of steel–steel adhesive joints [135]. They concluded that the SLS joint strength was proportional to the effective interfacial surface area. Similarly, an earlier work conducted by Watts and Castle demonstrated that the surface roughness effect could be attributed to the increased interfacial surface area and associated with an increase in the number of interactions across the interface [136]. Rudawska also investigated the effect of mechanical treatment on surface roughness; however, the geometrical structure of the surface, which determined the penetration capability of the adhesive, was found to be more important than the surface area [137]. The aforementioned studies indicate that most researchers have recognized the importance of surface roughness and its positive influence on the bond strength. However, the relationship between surface roughness and adhesion is complex and has not been thoroughly examined in the literature.

To the best of our knowledge, no detailed work has been systematically conducted to investigate the effects of the surface roughness of aluminum materials on adhesive bonding and environmental aging on its durability. Hence, the main objective of this study was to gain a comprehensive understanding of the effect of surface roughness on the SLS strength of aluminum joints and elucidate the mechanisms of SLS strength variations in joints aged in various environments. For this purpose, the AA 6061-T6 aluminum alloy was mechanically abraded using silicon carbide (SiC) grid papers to achieve different roughness values for its substrates. A strong correlation was observed between the SLS strength of the

adhesive joints and SiC grit size. Furthermore, the effect of the SLS strength on environmental aging was discussed, and a suitable model was proposed.

4.2 Materials and methods

In this study, a 3-mm-thick flat sheet of AA 6061-T6 aluminum alloy (Russel Metals Inc., Ontario, Canada) was used. A set of AA 6061-T6 substrates with dimensions of 101.6 mm × 25.4 mm were mechanically abraded via two different methods using 80, 120, 240, 320, 400, and 600 grit SiC abrasive papers before preparing the adhesive joints.

Mechanical abrasion with SiC abrasive papers was performed using an automated grinding and polishing machine (Struers Laboforce-100 polishing system). Fig. 4.1, shows a schematic illustration of steps involved in this method. The machine was operated in a continuous rotation mode at a rotation speed of 50 rpm and pressure of 0.003 MPa for 1 min. In addition to the machine mode, the AA 6061-T6 substrate was also manually abraded with SiC abrasive materials of various grit sizes for one minute. Water was used as the lubricant throughout the entire mechanical abrasion process.

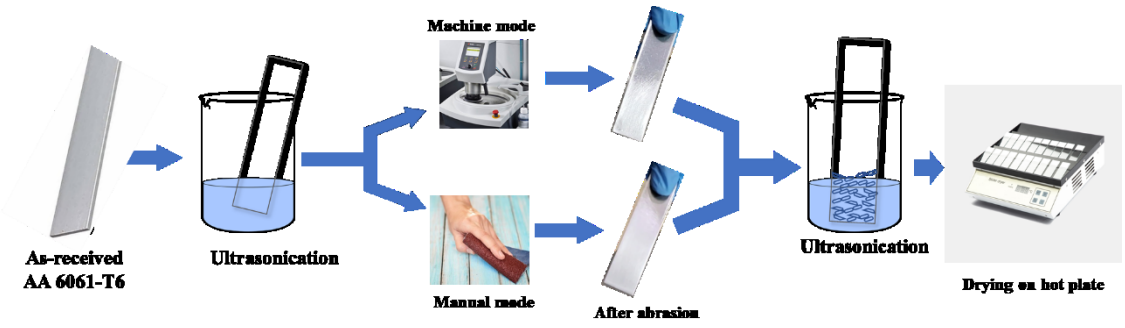

Figure 4.1 Schematic illustration of mechanical abrasion of AA6061-T6. © Mani Mohan Tiwari, 2021.

After abrasion, three ultrasonic cleaning steps were performed to remove loosely bound particles from the aluminum alloy substrates. The first stage of the ultrasonication cleaning of the mechanically abraded AA 6061-T6 substrates involved 15 min of degreasing in acetone followed by 15 min of ultrasonication in propanol and 15 min of ultrasonic cleaning in deionized (DI) water. Each ultrasonicated AA 6061-T6 substrate was air-dried under ambient conditions. The morphologies and chemical compositions of the prepared surfaces were characterized via scanning electron microscopy (SEM, JEOL JSM-6480) and energy-dispersive X-ray spectroscopy (EDS, JEOL). Furthermore, the root-mean-square (*rms*) surface roughness was measured with a MicroXAM-100 HR 3D optical surface profilometer. The ultrasonically cleaned and dried mechanically abraded AA 6061-T6 substrates were bonded using Adhesive #1 and Adhesive #2 with a bonding area of 12.7 mm × 25.4 mm and nominal bond-line thickness of 0.254 mm under the recommended curing conditions. All bonded specimens were tested using an INSTRON mechanical testing system (MTS). Depending on the adhesive type, the crosshead speed of the MTS utilized in lap shear tests was 1.0 mm/min for the Adhesive #1 and 0.5 mm/min for the Adhesive #2. Following Table 4.1 elucidates the properties of adhesives used in the preparation of SLS specimens:

Table 4.1 Properties and recommended curing conditions of adhesive

S. No.	Entity	Adhesive #1	Adhesive #2
1.	Name	2C-epoxy (LOCTITE EA L9460)	2C-methyl methacrylate (LOCTITE AA H8003)
2.	Curing conditions	Room temperature cure (72 hours)	Room temperature cure (1 hour)

3.	Crosshead speed	1.0 mm/min	0.5 mm/min
4.	characteristics and properties of adhesives	Specific Gravity at 25 °C= 1.33 Viscosity at 25°C, mPa·s (cP)= 150,000 to 250,000 Peak Exotherm Temperature (°C)= 93	Specific Gravity at 25 °C= 0.97 Viscosity, Cone & Plate, 25 °C, mPa·s (cP): Cone CP25-2 at shear rate 20 s^{-1}= 40,000 to 50,000
5.	chemical base of adhesive ingredients	Chemical Type: Epoxide	Chemical Type: Methacrylate
6.	stoichiometric ratio of adhesives components	Components Two part= Resin and Hardener Mix Ratio, by weight - Resin : Hardener =1 : 1 Appearance (Mixture)= gray	Components Two part= Resin and Hardener Mix Ratio, by weight - Resin : Hardener =10 : 1 Appearance (Mixture)= Light green
7.	method of their preparation	Mix using hands in a weighing boat.	Mix using hands in a weighing boat.
8.	amount of prepared mass	~ 5 g	~ 5 g
9.	methods of applying adhesives	Pasted over the Al specimens using a Bamboo Kabob Skewers.	Pasted over the Al specimens using a Bamboo Kabob Skewers.

4.3 Surface characterization

4.3.1 Roughness and topography

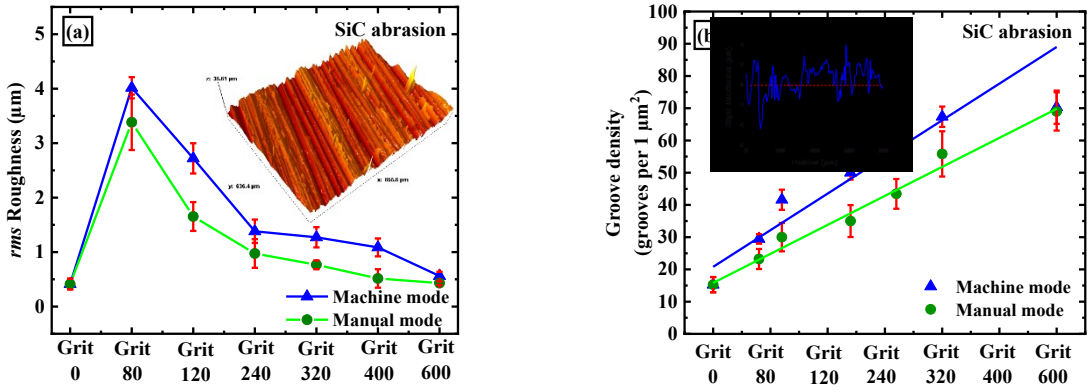

Figure 4.2 (a) Surface roughness values and (b) calculated grooves densities of the SiC-abraded surfaces. The insets show the (a) 3D surface and (b) cross-sectional profiles, respectively.

Table 4.2 Rms roughness of AA 6061-T6 as a function of the SiC grit size.

Sample	***Rms* roughness (µm)**	
Grit-0 (As-received)	0.41±0.09	
	SiC abrasion (machine mode)	**Sic abrasion (manual mode)**
Grit-80	4.01±0.64	3.38±1.05
Grit-120	2.72±0.27	1.65±0.21
Grit-240	1.38±0.21	0.97±0.26
Grit-320	1.27±0.18	0.76±0.08
Grit-400	1.08±0.16	0.51±0.16
Grit-600	0.56±0.07	0.42±0.03

Fig. 4.2 (a) and Table 4.2 present the obtained *rms* surface roughness values of various AA6061-T6 surfaces abraded with SiC abrasive papers of different grit sizes in the machine and manual modes. The *rms* surface roughness of the as-received (grit-0) AA6061-T6 surface is equal to 0.41±0.09 µm. In the machine mode of operation, the *rms* surface

roughness obtained for the grit-80 SiC paper is 4.01±0.64 μm. After increasing the grit size to 120, 240, 320, 400, and 600, the *rms* surface roughness monotonically decreases to 2.72±0.27, 1.38±0.21, 1.27±0.18, 1.08±0.16, and 0.56±0.07 μm, respectively. A slightly lower set of *rms* surface roughness values was obtained for the manual mode of operation using the SiC abrasive paper of the same grit size. For example, the *rms* surface roughness values obtained in the machine and manual modes of abrasion using the grit-80 SiC paper is equal to 4.01±0.64 and 3.38±1.05 μm, respectively. The *rms* surface roughness of the mechanically abraded AA6061-T6 surfaces monotonically decreased with increasing SiC abrasive paper grit size because the higher grit size makes the surface smoother owing to the larger number of finer SiC particles in the grid [138, 139]. The formation of localized microrough structures occurred during the rolling and sliding motions between SiC particles and the AA6061-T6 substrates. This process primarily removed the oxide layers from the surfaces of the as-received AA6061-T6 samples and created localized grooves and scratches for better mechanical interlocking between the adhesive molecules and treated surfaces as compared with the as-received surface of AA 6061-T6. The cross-sectional surfaces of the abraded samples were also analyzed to characterize the properties of the textured grooves. Fig. 4.2 (b) shows the groove densities calculated for the AA6061-T6 samples abraded with the SiC abrasive papers of different grit sizes. The emergence of localized grooves in the machine and manual modes of operation resulted in the formation of microrough structures on the AA6061-T6 surfaces, and a linear relationship was established between the number of grooves and abrasive material properties. The groove densities determined in the machine and manual abrasion modes were similar. The slope values obtained after the linear fitting of the generated counts exhibited similar trends but were systematically higher in the

machine mode than in the manual mode of operation. The corresponding insets of Fig. 4.1 (a) and (b) depict the three-dimensional (3D) topographic profile and cross-section of the mechanically abraded AA6061-T6 surface, respectively. Furthermore, a mathematical relationship between the SLS strengths and calculated groove densities of the SiC abrasive materials of various grit sizes is presented in Fig. 4.3, where the SLS strengths of the Al/Al bonded joints are normalized with respect to the groove area (true area).

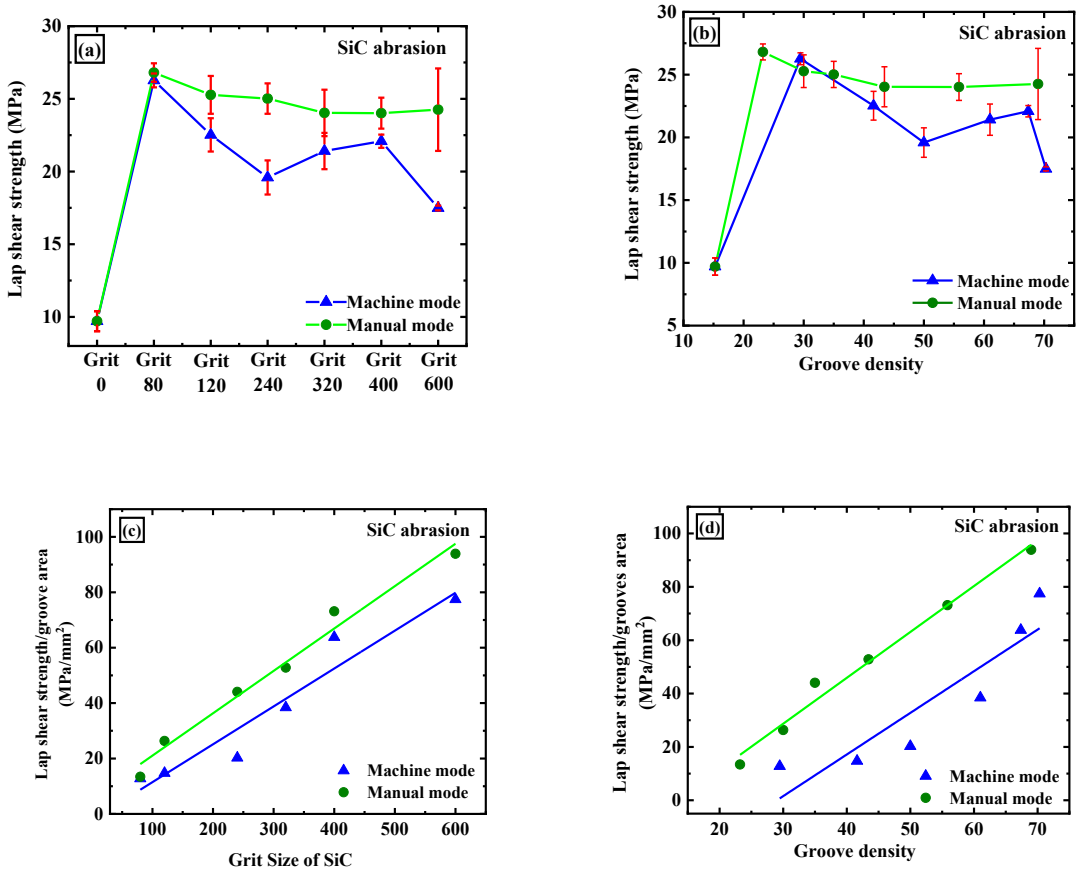

Figure 4.3 SLS strength of the Al/Al joints plotted as a function of the (a) SiC grit size and (b) calculated groove density. Normalized SLS strength with respect to the true bonding area plotted as a function of the (c) SiC grit size and (d) calculated groove density.

Fig. 4.3 displays the mechanical properties (SLS strengths) of the bonded joints measured at different SiC grit sizes and calculated groove densities. Fig. 4.3 (a) shows the SLS strengths of the adhesively bonded AA6061-T6 substrates. The highest lap shear strengths of 27.15±1.84 and 26.38±1.12 MPa are obtained for the surfaces abraded at a SiC grit size of 80 in the machine and manual modes, respectively. Fig. 4.3 (b) depicts the variations in the SLS strength with the calculated groove density (see Fig. 4.1 (b)), which exhibits a trend similar to that presented in Fig. 4.3 (a) because the calculated groove density varies linearly with the SiC grit size (Fig. 4.1 (b)). This confirms the correlation between the alloy mechanical properties and surface roughness (Fig. 4.1 (a)) and suggests that an optimal SiC grit size of 80 results in the highest SLS strength regardless of the operation mode. The obtained SLS strengths were normalized with respect to the true bonding area and plotted against the SiC grit size in Fig. 4.3 (c). The plot of the normalized SLS strength versus the groove density is shown in Fig. 4.3 (d). In both cases, linear relationships are observed.

4.3.2 Morphological analysis

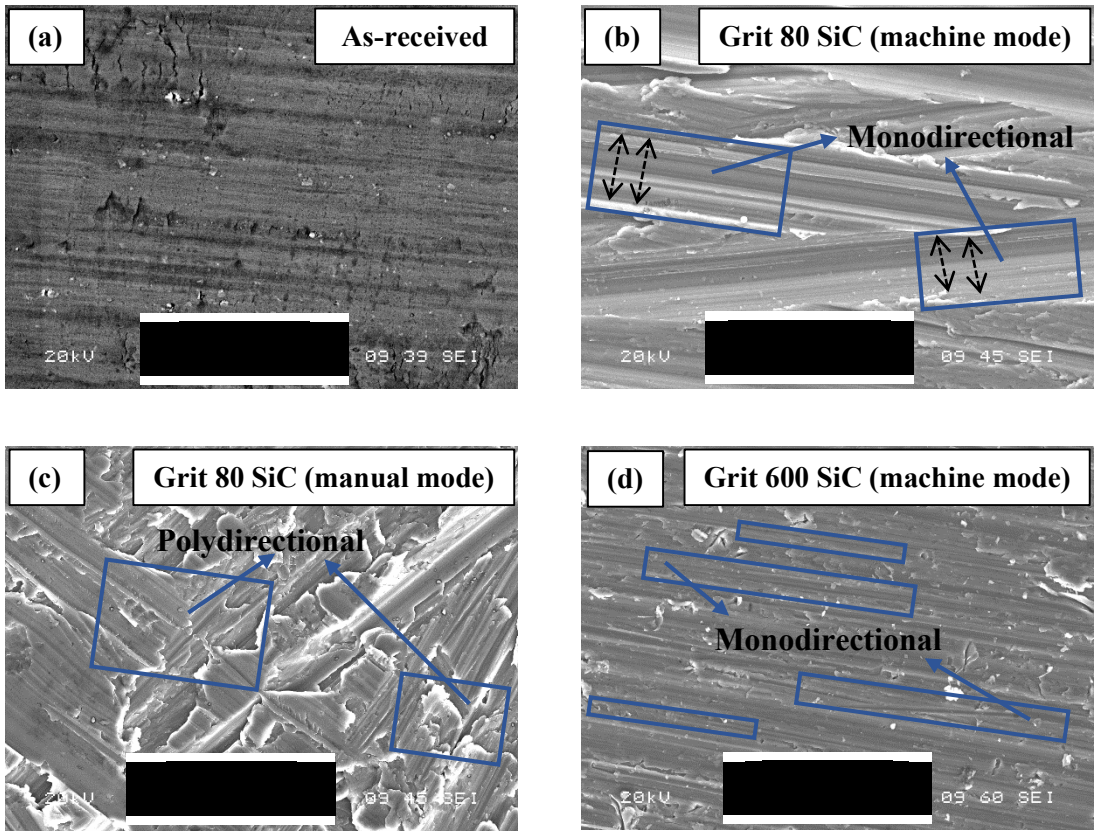

Figure 4.4 SEM images of the (a) as-received AA6061-T6 sample and AA6061-T6 surfaces abraded with the grit-80 SiC abrasive paper in the (b) machine and (c) manual modes and (d) grit-600 SiC paper in the machine mode.

Fig. 4.4 shows the morphologies of the AA6061-T6 specimen observed before and after mechanical abrasion. Fig. 4.4 (a) depicts the SEM image of the as-received AA6061-T6 surface, while Fig. 4.4 (b) illustrates the microstructural evolution that occurs during mechanical abrasion at a SiC grit size of 80 in the machine mode. Similarly, Fig. 4.4 (c) shows the microstructural evolution observed during abrasion in the manual mode at a SiC grit size of 80. It is noteworthy that after mechanical abrasion, the surface appears much rougher than that of the as-received surface. Furthermore, the difference between the terraced

microstructures during manual abrasion is clearly visible in Fig. 4.4 (b) and (c). The microfeatures created by the paper with the SiC grit size of 80 contain polydirectional interaction sites (which differ from monodirectional ones) when abrasion is performed in the manual mode instead of the machine mode. Moreover, the general morphological characteristics of the AA6061-T6 surfaces abraded by the grit-80, grit-120, grit-240, grit-320, grit-400, and grit-600 SiC abrasive papers have been studied but are not presented here. Fig. 4.4 (d) depicts the mechanically abraded surface at a SiC grit size of 600 in the machine mode. Its morphology appears to be similar to the morphology of the as-received sample surface. However, the morphological features of the mechanically abraded surfaces at a SiC grit size of 600 SiC in the machine and manual modes are also similar; therefore, the SEM image of the surface abraded in the machine mode is presented to avoid redundancy. The SEM images discussed above are consistent with the roughness data listed in Table 4.2. In addition to the morphological analysis, EDS was performed to examine the chemical compositions of the as-received and mechanically abraded AA6061-T6 substrates.

4.3.3 Chemical compositional analysis

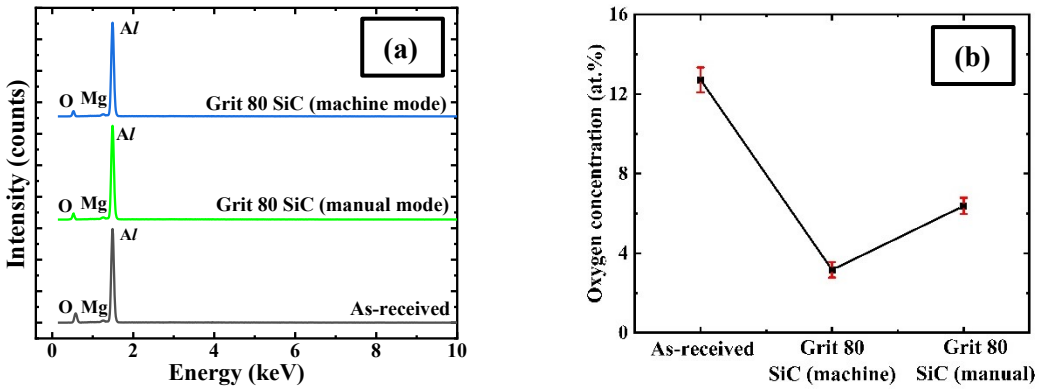

Figure 4.5 (a) EDS spectra of various AA6061-T6 samples and (b) the corresponding oxygen concentrations measured before and after mechanical abrasion.

Fig. 4.5 (a) shows the EDS spectra of the as-received Al substrate and mechanically abraded aluminum surfaces using the SiC paper with a grit size of 80 in the machine and manual modes. They confirm the presence of O, Mg, and Al elements with their Kα peaks at 0.53, 1.25 and 1.49 keV, respectively. Fig. 4.5 (b) shows the oxygen concentrations of these samples. The oxygen concentration on the as-received sample is 6.56±1.22 at.%. After the abrasion with the grit-80 SiC paper in the machine and manual modes, its magnitude decreases to 1.09±0.10 at.% and increases to 1.34±0.39 at.%, respectively. This indicates that abrasion favours the depletion of the naturally formed oxide layer on the surface of the as-received AA 6061-T6 substrate, which in turn promotes the interactions between adhesive molecules and the metal surface of the AA6061-T6 substrate.

4.4 SLS strengths of the adhesive joints

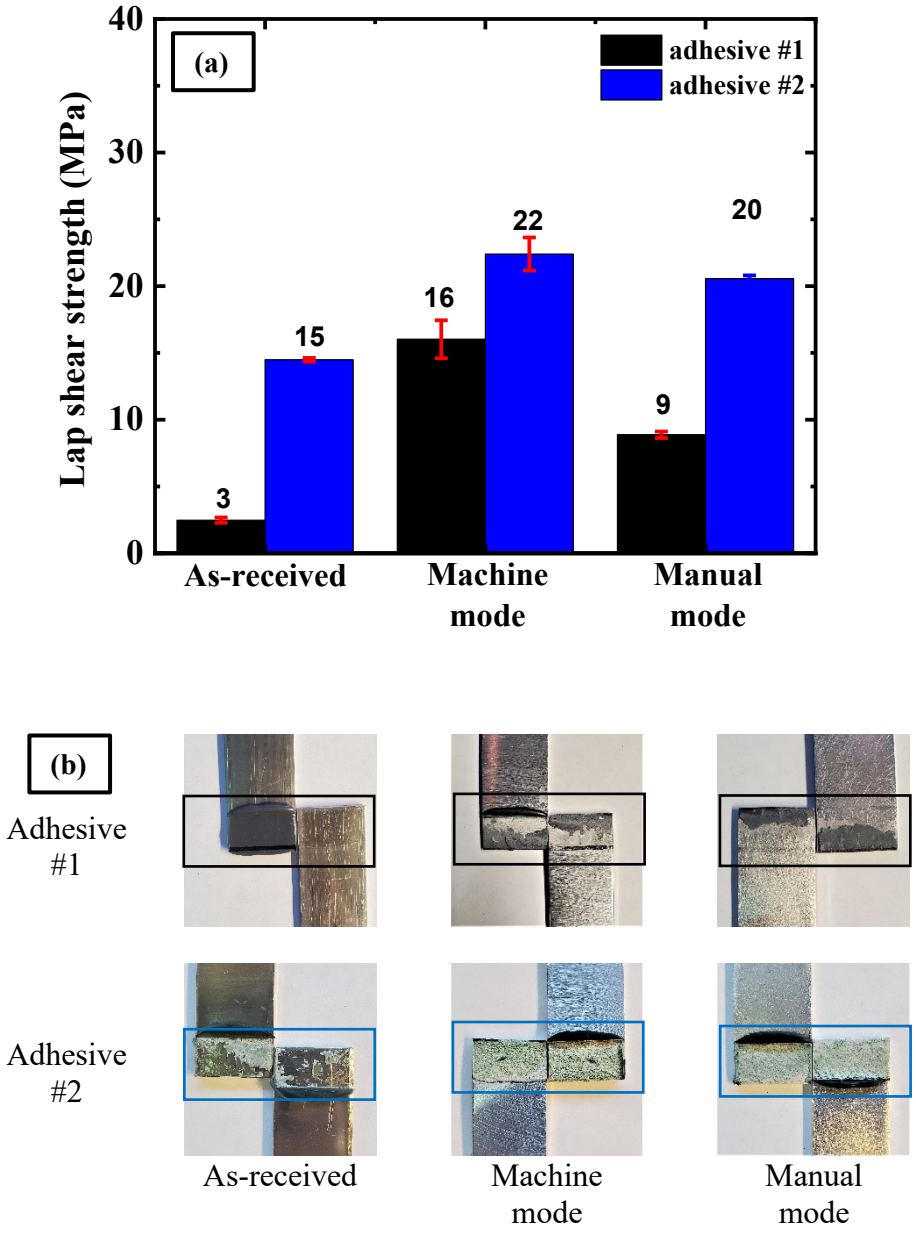

Figure 4.6 (a) SLS strengths of the as-received Al specimens and Al specimens abraded with the grit-80 SiC paper in the machine and manual modes and bonded using the Adhesive #1 and Adhesive #2. (b) Images of the ruptured SLS specimens.

Fig. 4.6 (a) shows the SLS test results obtained for the as-received and mechanically abraded specimens. Adhesion strength was measured for the adhesive joints prepared using the Adhesive #1 and Adhesive #2. Mechanical characterization of the bonded surfaces revealed that the surfaces abraded with grit-80 SiC in the machine mode could potentially exhibit high adhesive bond strengths using both adhesives. The as-received specimen demonstrates a cohesive rupture with shear strengths of 3.58±0.73 and 15.36±0.21 MPa obtained for the Adhesive #1 and Adhesive #2, respectively. The SLS strengths of the specimens treated with grit-80 SiC in the machine and manual modes and bonded with Adhesive #1 are equal to 16.79±3.42 and 9.44±1.12 MPa, respectively. Meanwhile, the SLS strength of the specimens prepared using the Adhesive #2 adhesive and treated with grit-80 SiC in the machine and manual modes are 22.40±1.23 and 20.56±0.24 MPa, respectively. Interestingly, the structural adhesive joints fabricated using the Adhesive #1 adhesive exhibited not only lower SLS strengths as compared with those bonded with the Adhesive #2, but also their rupture modes were complete adhesive failures even after the corresponding substrate surfaces were abraded with the grit-80 SiC paper. The results of cross-sectional roughness studies supported this observation, as the deepest rough microscale surface texture was obtained only for the surface treated with SiC (grit-80) in the machine mode with the highest *rms* roughness of 4.01±0.64 μm. Therefore, the optimum surface roughness value of 4.01±0.64 μm obtained for the surfaces treated with SiC (grit-80) in the machine mode was required to achieve the highest joint bond strength. The lap shear strengths values obtained for the specimens treated with SiC (grit-80) in the machine mode are comparable with those obtained by various anodization processes, which are generally considered benchmark surface treatment methods in adhesive bonding [140]. Li et al. reported the highest adhesion

strength of 18.9 MPa for the unsealed samples anodized in sulfuric acid and 16.3 and 18.8 MPa for the anodized surfaces of hot water-sealed and agent-sealed samples, respectively [141]. However, the anodization process consists of multiple steps and requires the use of toxic inorganic acids. In the present study, the application of the SiC abrasive paper in a single step was sufficient to obtain adhesion strengths comparable to those reported for the anodized surfaces. Furthermore, the adhesively bonded specimens with the highest SLS strengths, i.e. the specimens prepared with Adhesive #2, were exposed to air, DI water, and aqueous salt solutions to observe the effect of the environment on the SLS strength. Based on the SLS results, a suitable model was proposed to explain the effects of these environmental factors on the SLS strength.

4.5 Environmental aging

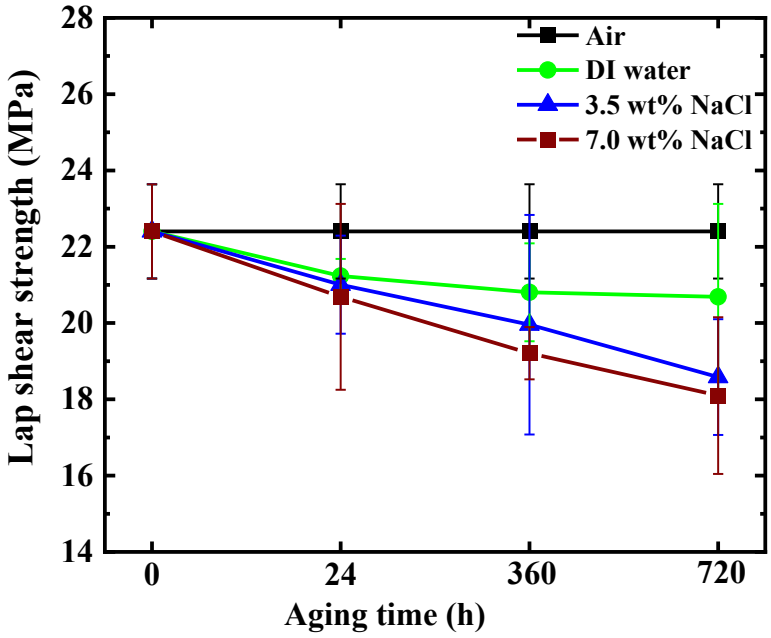

Figure 4.7 SLS strengths of the adhesive joints measured at air (0 h) and after treatments with DI water and the 3.5 and 7 wt.% NaCl solutions for 24, 360, and 720 h.

Table 4.3 Residual SLS strengths of the Al specimens measured in different environments at various aging times.

Aging time (h)	Residual SLS strength (MPa)		
	DI water	3.5 wt.% NaCl	7 wt.% NaCl
0	22±1.2	22±1.2	22±1.2
24	21±0.4	21±1.2	20±2.4
360	20±1.2	19±2.8	19±0.6
720	20±2.4	18±1.5	18±2.0

The first point in Fig. 4.7 shows the SLS strength of the Adhesive #2 based aluminum SLS joints in air. These joints were also tested after degradation by immersing into (i) DI water, (ii) the 3.5 wt.% NaCl solution, and (iii) the 7 wt.% NaCl solution at 25 °C for different times varying from 0 to 720 h. The obtained residual SLS strengths are presented in Figure 6 and listed in Table 4.3. The SLS strength of the reference specimen, i.e. the adhesive joint exposed only to air, is 22±1.2 MPa. After immersing in DI water for 24 h, the residual SLS strength is equal to 21±0.4 MPa, which corresponds to a reduction of only 3%. However, upon increasing the immersion time to 360 and 720 h, the bond strength decreased to 20.8±1.2 and 20.6±2.4 MPa with reductions of 7.3% and 8%, respectively. The residual SLS strengths of the bonded joints exposed to the 3.5 wt.% NaCl aqueous salt solution for 24, 360, and 720 h are equal to 21±1.2, 19±2.8, and 18±1.5 MPa with relative strength losses of 7%, 13%, and 17%, respectively. Furthermore, these adhesive joints were immersed in the 7 wt.% salt solution to investigate the effect of accelerated aging. The resulting residual SLS strengths amount to 20±2.4, 19±0.6, and 18±2.0 MPa with relative losses of 10.7%, 14.2%, and 19.6%, respectively. The observed decreases in the residual SLS strength can be explained using the model presented in Fig. 4.9. It is noteworthy that the relative strength

losses after 720 h of immersion in DI water and the 3.5 and 7.0 wt.% NaCl aqueous salt solutions amount to 8%, 17%, and 19%, respectively.

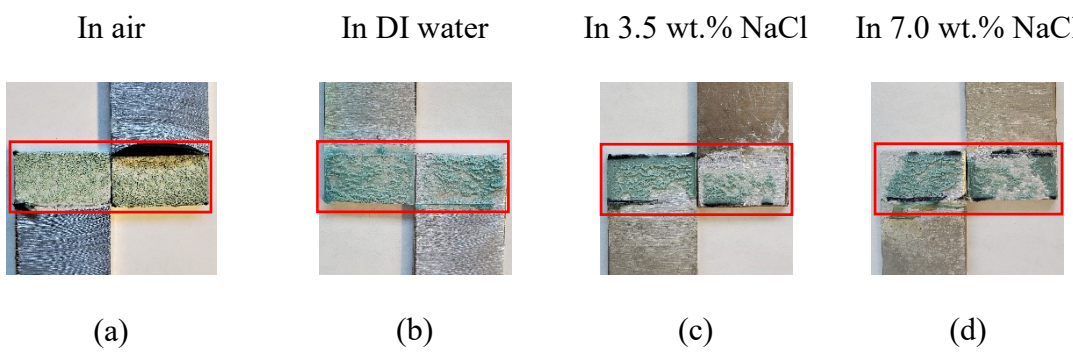

Figure 4.8 Fracture surfaces of the bonded joints after failure, which were aged for 720 h in air, DI water, and the 3.5 and 7.0 wt.% NaCl aqueous solutions.

Fig. 4.8 shows the fractured surfaces of the Adhesive #2 bonded Al substrates after the mechanical tests. The specimens were exposed to air, DI water, and the 3.5 and 7.0 wt.% NaCl aqueous salt solutions for 720 h before mechanical testing. Note that the failure mode of the reference specimen (exposed to air) was cohesive in nature, whereas it was partially cohesive and partially adhesive in DI water. The fracture surfaces of the specimens immersed into the 3.5 and 7.0 wt.% NaCl aqueous salt solutions exhibited completely adhesive failures owing to the formation of white patches. The following schematics describe the deboning mechanisms of the studied specimens and their corresponding failure modes upon exposure to air, DI water, and the aqueous salt solutions.

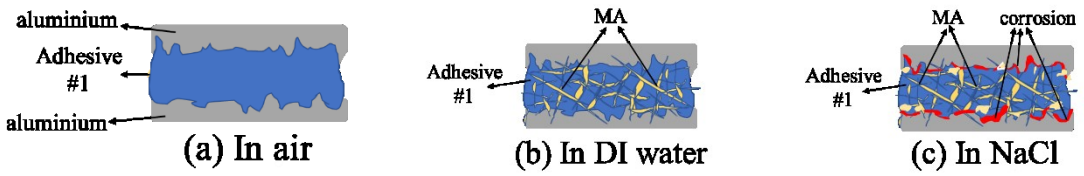

Figure 4.9 Schematic illustrations of the debonding mechanisms of the Adhesive #2-based aluminum adhesive joints in air, DI water, and the NaCl aqueous salt solution. © Mani Mohan Tiwari, 2023.

Fig. 4.9 shows a schematic model of the Adhesive #2 and two interfaces between the MMA adhesive and aluminum exposed to (a) air, (b) DI water, and the (c) NaCl aqueous solution. This model was established to explain the SLS strengths presented in Fig. 4.9, which were obtained after exposing the prepared samples to different environments for various aging times. Fig. 4.9 (a) illustrates the Adhesive #2 based SLS joints, where the adhesive layer is sandwiched between two the aluminum substrates exposed to an air environment. These joints are aged for a maximum period of 720 h. The bond strength and ruptured specimen remains intact, as shown in Fig. 4.9 and 4.8 (a), because no perturbation was observed for the sandwiched adhesive layer owing to the air exposure. In contrast, in the case of DI water, the sandwiched adhesive joints were exposed to H_2O molecules. The immersion of Adhesive #2 based SLS joints in DI water enables water intake into the adhesive layer, which degrades both its chemical and mechanical properties [142]. According to the literature, Adhesive #2 (CH_2=C(CH_3)─$COOCH_3$) reacts with H_2O molecules to produce metacrylic acid (MA: CH_2=C(CH_3)─COOH), which reduces the hardness of the Adhesive #2 adhesive [143-145]. Therefore, the immersion of the Adhesive #2 adhesive-based joint into DI water, where H_2O molecules react with Adhesive #2 and form MA as a by-product in the sandwiched adhesive

layer, is schematically illustrated in Fig. 4.9 (b). The presence of MA in the Adhesive #2 adhesive weakens the intramolecular adhesive bonds formed by Adhesive #2 and significantly reduces its mechanical strength, which considerably decreases the SLS strength of the adhesive joints. Therefore, the global SLS strength was reduced by 7.3% and 8% after immersion in DI water for of 360 and 720 h, respectively.

Furthermore, the Adhesive #2 based SLS joints were also immersed into the NaCl environments (3.5 and 7.0 wt.% aqueous solutions), where the sandwiched adhesive layer was exposed to H_2O molecules and Na^+ and Cl^- ions. This produced a similar effect by weakening the Adhesive #2, and corrosion occurred on the aluminum surface, as illustrated in Supporting Fig. I.1 of appendix I. The corrosion process minimized the contact area between the adhesive and aluminum substrate, which reduced the mechanical strength of their interface (Fig. 4.9 (c)). Hence, the global SLS strengths of the Adhesive #2 based SLS joints in the NaCl aqueous salt solution decreased because of the reductions in the (i) hardness of the Adhesive #2 due to the water exposure and (ii) contact area between the Adhesive #2 and aluminum surface due to the corrosion by Cl^- ions. Therefore, the global SLS strengths were reduced by 17% and 19.6% after immersing into the 3.5 and 7.0 wt.% NaCl aqueous salt solutions for 720 h, respectively. In a previous study, Mu *et. al.* explored the influence of humidity on the adhesively bonded carbon fiber-reinforced polymer/aluminum alloy joints and demonstrated that the bond strength decreased from 19 to 15 MPa in a humid environment [147]. In their study, the mechanical strength was reduced by 21% after exposing the specimens to humidity for 720 h. In another study conducted by Hua *et. al.*, the effect of a 3.5 wt.% salt spray on Al/Al joints fabricated using an epoxy adhesive was explored [148]. The authors found that the initial SLS strength of 8 MPa was

reduced to 7.6 MPa after 720 h of aging in the salt spray. The observed differences in the adhesive strength could be due to the used adhesive type and salt spray instead of the immersion in the aqueous salt solution performed in this work.

4.6 Summary and Conclusions

A simple and effective one-step process for removing a weak native oxide layer from the AA6061-T6 alloy surface was demonstrated by the surface treatment with SiC abrasives in two different modes. The results of SEM morphological analyses and profilometry studies revealed that an optimum roughness of ~ 4 μm could be achieved through abrasion with the grit-80 SiC paper in the machine operation mode. The EDS chemical analyses of the studied surfaces confirmed the formation of alumina species. The maximum SLS strength of the specimens treated with grit-80 SiC in the machine mode was 22.40 MPa. These surfaces were further examined to elucidate the debonding mechanisms of the Adhesive #2 and aluminum interfaces exposed to DI water and the 3.5 and 7.0 wt.% aqueous sodium chloride solutions. A substantial decrease in the measured SLS strength (17%) was observed when the Adhesive #2 based aluminum joints were exposed to the 3.5 wt.% NaCl aqueous salt solution for 720 h. The formation of MA from Adhesive #2 in the presence of DI water and inclusion of Cl^- ions from the aqueous NaCl salt solution due to the initiation of corrosion at the interfaces between the aluminum surface and adhesive were the contributing factors to the decrease in the contact area that effectively minimized the global SLS strength.

Chapter 5: Synthesis of porous oxide layer on Al substrates by anodization in a salt electrolyte of sodium phosphate (Na_2HPO_4) for the application of structural adhesive bonding of Al/Al

5.1 Introduction

Climate change policies focus more on energy efficiency as a central strategy for greenhouse-gas emissions reduction [1, 2]. To mitigate the impact of the materials on greenhouse gases emissions is to improve material efficiency (light-weighting); reducing yield losses in the manufacturing processes; minimizing the byproducts; and using products more intensely or at a higher capacity. Structural adhesive joining of lightweight materials, namely aluminum (Al), has a considerable role in industrial applications, particularly in transportation industries, on CO_2 emission reduction due to reduced fuel consumption associated with light weighting [3]. Structural adhesive bonding is well known in aircraft industry, since they provide greater structural efficiency and performance due to low structural weight, large area bonding with uniform stress distribution (compared to localized stresses in rivets), excellent bondability of similar and dissimilar materials of different shapes and dimensions [4, 5]. Though a huge research, dedicated to the advancement in the structural adhesive bonding, has been conducted and documented in the literature [6, 7], limitations such as high cost, long cure times, fatigue and durability, health and safety issues, availability and so on still poses challenges in their wide usage in many application areas [8-10]. The strength and stability of the bond between adhesive and the adherent surface are generally controlled by surface preparation, which governs the chemical and geometrical features of the surface favorable to adhesion of adhesives [11, 12]. Controlling the surface features of Al, therefore, becomes primordial in obtaining robust adhesive joints with high

mechanical strengths. Several methods have been used to modify the surface properties in terms of morphology and chemistry [13, 14]. Acid anodizing, among many, is an electrochemical process that promotes the formation of a strong porous oxide layer (anodic layer) on the surface of the metal, which helps protect the material from atmospheric agents or their environment in general [15], but also add various factors in regards of degradation of electrolyte. Although, acid anodization is a benchmark treatment for Al in adhesive bonding, use of acids as anodizing electrolyte poses health and environmental risks due to release of hazardous gases in addition to requiring more prudence in manipulating acids [6, 16, 17].

Considering the ecological and safety challenges, we have, in this study, used an environmentally friendly salt solution as anodizing electrolyte instead of standard acids to anodize the Al surfaces prior to bonding with Adhesive #3. The effect of the pore diameters of the anodized porous oxide layer on the adhesion strength of SLS specimens were investigated. The anodization induced surface roughness and the pore size on the resulting surfaces, characterized by SEM/EDS and roughness measurements, presented a strong correlation with the mechanical strength of the bonded joints.

5.2 Methods

The AA6061-T6 Al sheets of 4″ × 1″ × 0.12″ were cleaned ultrasonically in a dilute soap solution and dried at ambient condition. The anodization process was carried out using a voltage-controlled DC power supply at a constant current mode, by utilizing an optimized current density (j) of 30 $mA \cdot cm^{-2}$. Clean and dry AA6061-T6 substrates connected to the positive output of the power supply served as anodes, as shown in Fig. 5.1. The process was

carried out in a 60 ml electrolyte prepared by mixing ~14 g of solid Na_2HPO_4 salt diluted into 1 L of deionized water, at a controlled electrolytic bath temperature of 5±1 ^oC for a duration of 15, 30, 45, and 60 minutes. The anodized samples were further washed with deionized water and dried on hot plate at 150 ^oC for 2 hours prior to bonding with a two-component (2-C) epoxy adhesive. The prepared surfaces were characterized for surface morphology and chemistry using scanning electron microscopy (SEM, JEOL JSM-6480), equipped with energy-dispersive X-ray spectroscopy (EDS). Chemical analysis was also performed using attenuated total reflection-Fourier transform infrared (ATR, Agilent Technologies, Cary 630 FTIR). The root mean square (*rms*) surface roughness was measured and analyzed using a MicroXAM-100 HR 3D optical surface profilometer.

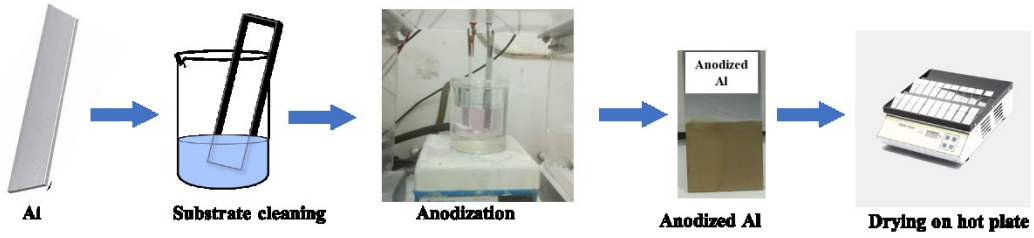

Figure 5.1 Schematic illustration of electrochemical anodization of AA6061-T6. © Mani Mohan Tiwari, 2021.

SLS specimens were prepared with the Adhesive #3 according to the ASTM-D1002 standard and allowed to cure according to the manufacturer's recommendation prior to mechanical testing. The joint strengths of the SLS were determined using an INSTRON 8801. Rupture modes of the failed specimen were visually analyzed. Following Table 5.1 elucidates the properties of adhesives used in the preparation of SLS specimens:

Table 5.1 Properties and recommended curing conditions of adhesive

S. No.	Entity	Adhesive #3

1.	Name	2C-epoxy (LOCTITE EA E-20HP)
2.	Curing condition	Room temperature cure (40 minutes)
3.	Crosshead speed	1.0 mm/min
4.	characteristics and properties of adhesives	Specific Gravity at 25 °C = 1.03 Tensile Elongation ASTM D-638 = 8% Hardness ASTM D-1706, Shore D= 80 Glass Transition Temperature (Tg)= 60 ºC
5.	chemical base of adhesive ingredients	Chemical Type: Epoxy
6.	stoichiometric ratio of adhesives components	Components Two part= Resin and Hardener Mix Ratio, by weight - Resin : Hardener =100 to 55 Appearance (Mixture)= Off-white
7.	method of their preparation	Mix using hands in a weighing boat.
8.	amount of prepared mass	~ 5 g

9.	methods of applying adhesives	Pasted over the Al specimens using a Bamboo Kabob Skewers.

5.3 Surface characterization

5.3.1 Effect of electrochemical anodization time on roughness

The salt anodization process results in the formation of a porous oxide layer on the aluminum surface, leading to a rough microstructure. Fig. 5.2 shows the *rms* roughness obtained on the salt anodized Al surfaces at an optimized current density (j) of 30 $mA \cdot cm^{-2}$ as a function of anodization time. The untreated Al surface presented a rms value of as low as 0.33 μm. However, it is observed that the surface, once anodized, presented an increase in their *rms* values. It is clear from Fig. 5.1 that the roughness increased with the increase in anodization times and reached the maximum value of 1.04 μm after 60 minutes anodization. This increase in roughness may be attributed to the increasing growth of porous oxide layer with the pores of varied dimensions contributing to the micro rough structure. The surface with anodized pores having such high roughness value can be expected to promote the mechanical anchoring of the adhesive into the rough pores, thereby enhancing the interfacial bonds between the adhesive and the surface.

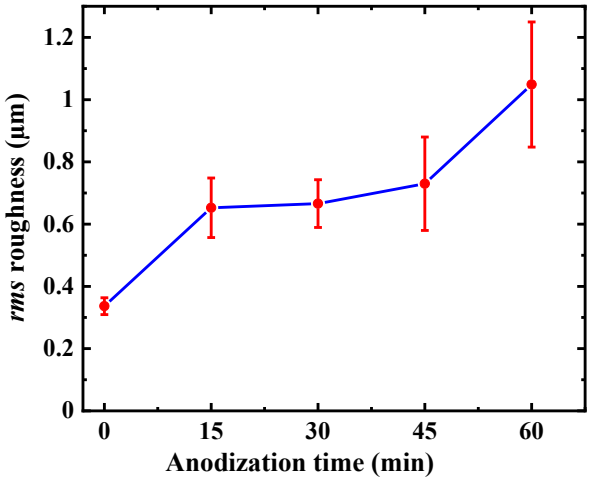

Figure 5.2 Variation in rms roughness of anodized AA6061-T6 Al surfaces as a function of anodization time.

5.3.2 Morphology and chemical composition

The morphological and chemical analysis by SEM/EDS (Fig. 5.2 (a-c) corroborates with the surface roughness measurements. Fig. 5.3 (a) and (b) show the SEM images of the surfaces of as-received clean Al and the 60 minutes anodized counterpart, respectively. The anodized surface revealed the emergence of porous microstructures with wide pores of diameter ~0.60 µm as confirmed by Fig. 5.3 (b). A comparison of the SEM images of all the surfaces studied (*Figures not shown*) showed the evolution and emergence of microporous structures contributing to the enhancement of *rms* surface roughness with increasing anodization time. The morphology of the surfaces, however, presented porous texture in all cases.

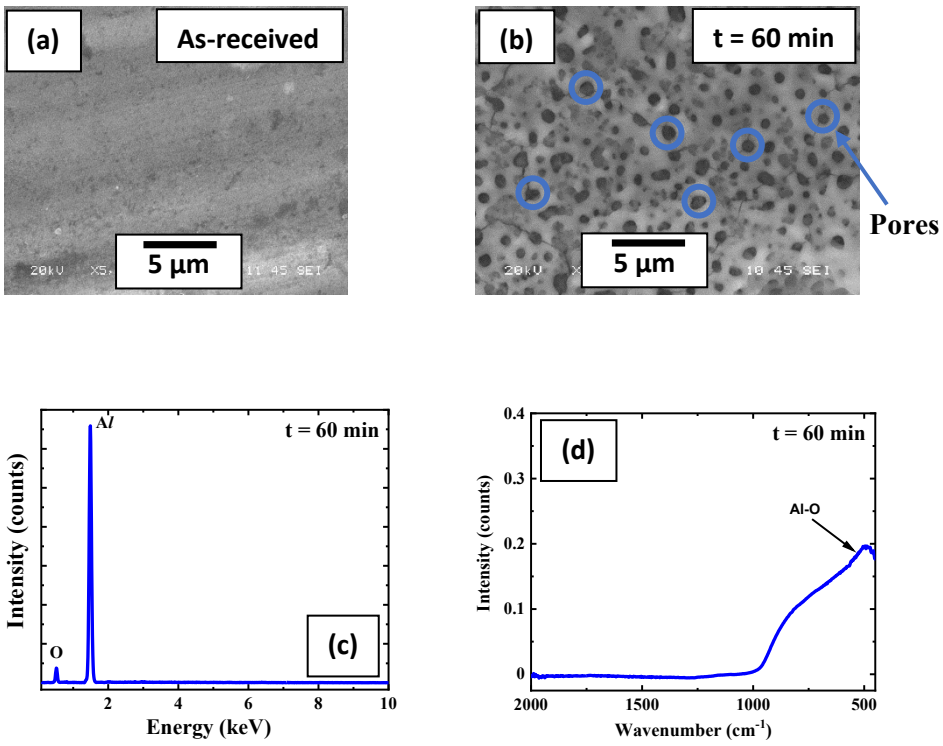

Figure 5.3 SEM images of (a) as-received Al; (b) 60 minutes salt anodized Al (some pores are highlighted by blue circles), (c) EDS spectrum of (b) and (d) ATR-FTIR spectra of (b)

The chemical nature of the treated surfaces was analyzed by both EDS and ATR-IR spectral analyses. The EDS spectrum (Fig. 5.3 (c)) confirmed the presence of O, which can be associated with the formation of the anodic aluminum oxide layer. The ratio of atomic percentage of O and Al on the anodized surface was found to be 1.37±0.20, close to the theoretical value of 1.5. Fig. 5.3 (d) depicts the corresponding ATR-FTIR spectrum of the surface shown in Fig. 5.3 (b). A broad band at 490–1000 cm^{-1}, is attributable to the Al-O vibrations confirming the presence of an oxide of aluminum on the surface, as well corroborating with the EDS results shown in Fig. 5.3 (c) [149]. These observations indicate that the 60 minutes salt anodized aluminum surfaces have potential of providing high joint strength between these surfaces and the adhesive, when bonded together.

5.4 SLS strengths of the adhesive joints

Mechanical testing was carried out on the SLS specimens prepared by bonding the 60 minutes salt anodized aluminum coupons with a 2-C epoxy adhesive and their failure modes were further examined. Fig. 5.4 (a) shows the SLS test results obtained on the as-received and treated specimens. It is evident that the lap shear strengths of the treated specimens were higher than that of the as-received Al (10±1 MPa). A maximum lap shear strength of 21±1 MPa was obtained with specimens prepared with surfaces anodized for 60 minutes. The increase trend in the lap shear strengths was similar to the values of *rms* surface roughness. Therefore, a linear fit of the SLS values with the *rms* roughness was established, shown in the Fig. 5.4 (b). This behavior can be attributable to the microstructural evolution and the chemical changes occurring on the treated Al surfaces with varied anodization times. Furthermore, the rupture modes of the failed specimens, shown in Fig. 5.4 (c), presented 100 % cohesive failure on specimens prepared with surfaces treated for 60 minutes, indicating that the adhesion at the adhesive/surface interface was strong enough to make the failure within the adhesive. All other specimens showed 100% adhesive failure at the interface between the adhesive and the surface, indicating that the porous texture and dimensions with lower surface roughness values on these surfaces anodized for less than 60 minutes were not sufficient to obtain a strong interfacial bond between the adhesive and the surface and thereby failing at the interface.

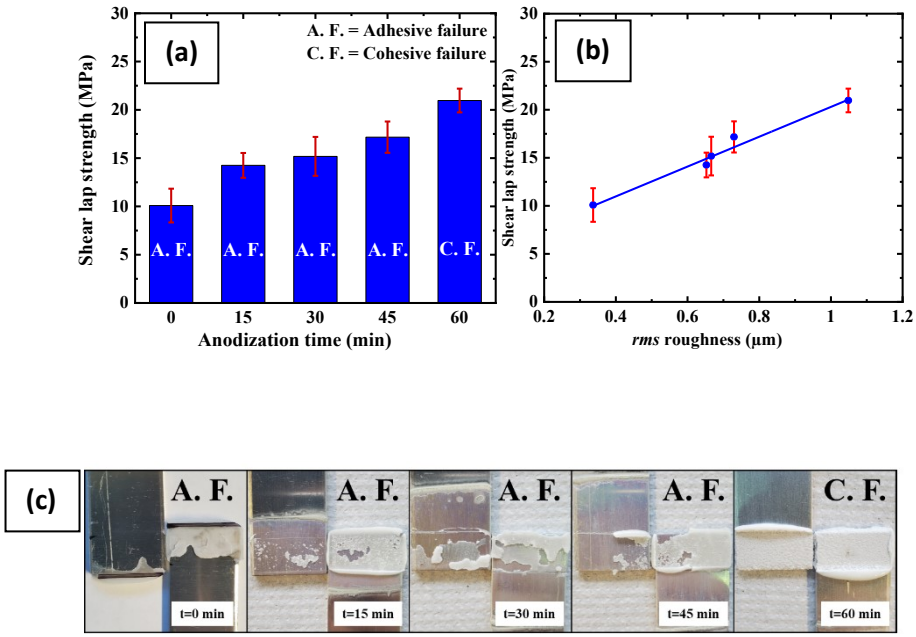

Figure 5.4 (a) SLS strengths vs anodization time of adhesively bonded SLS specimens and (b) SLS strengths as a function of rms roughness (c) images of ruptured specimens (A.F. – Adhesive Failure, C. F. – Cohesive Failure).

Therefore, 60 minutes of anodization time was required to achieve strong mechanical interlocking of the adhesive within the anodized pores. The strong oxide as evidenced by EDS measurements and IR spectral analyses may be expected to play an additional role of chemical enrichment of the surface with high surface energy, allowing the adhesive thoroughly wet the surface.

5.5 Summary and Conclusions

An environmentally friendly salt anodization technique using a Na_2HPO_4 salt electrolyte has revealed the formation of porous anodic oxide layers on the aluminum surfaces with varied surface features. Morphological analysis presented porous structure on the treated surfaces, while the EDS and the FTIR analyses confirmed the growth of strong oxides upon

salt anodization. A correlation between the anodization time and the surface roughness was established indicating increase in rms roughness values as a function of anodization time (0.33 μm on as-received to 1.4 μm on 60 minutes anodized surface). The same trend has further been evidenced with the mechanical strengths of the adhesively bonded joints showing systematic increase in the shear lap strengths with anodization time. Maximum shear strength of ~21 MPa was obtained at 60 minutes of anodization, while the as-received SLS specimens reached only ~10 MPa, proving the effectiveness of the salt anodization. The Al surfaces anodized for 60 minutes presented 107% enhancement in adhesion strengths compared to the as-received counterpart.

Chapter 6: Incorporation of the organosilane of GPS by in-situ silanization and anodization using inorganic salt electrolyte of zinc nitrate ($Zn(NO_3)_2$) for the application of structural adhesive bonding of Al/Al

6.1 Introduction

Climate change policies focus more on energy efficiency as a central strategy for greenhouse-gas emissions reduction [1-3]. Structural adhesive joining of lightweight materials, namely aluminum, is of great importance in industrial applications, particularly in transportation on carbon dioxide emission reduction due to lightweight and reduced fuel consumption [4]. Structural adhesive bonding is well known in aircraft industry, since they provide greater structural efficiency and performance due to low structural weight, large area bonding with uniform stress distribution (compared to localized stresses in rivets), excellent bond ability of dissimilar materials of different shapes and dimensions, and other advantages [5, 6]. Adhesion mechanism involves the interface between the substrate (aluminum) and the adhesive controlled by interfacial bonds, which can be chemical, mechanical or a combination of both [7]. Controlling the surface of aluminum, therefore, becomes primordial in obtaining robust mechanical strengths of the joints. Several methods have been used to modify the surface properties in terms of morphology (mechanical) and chemistry [8, 9]. Anodizing, among many, is an electrochemical process that promotes the formation of a thin layer of oxide (anodic layer) on the surface of the metal, which helps protect the material from atmospheric agents or their environment in general [10, 11]. Due to the rich oxide layer, aluminum anodization has been found to enhance the durability of bonds formed when treated with a silane compound and bonded with an epoxy adhesive [12, 13]. In this study,

the effect of the morphological and chemical evolution, produced in a one-step simultaneous anodization and silanization process, on the formation of an anodic film on the aluminum alloy and their bonding properties have been investigated. An attempt has been made to correlate the anodization induced surface roughness and the silane modification generated during the one-step process with the mechanical properties of the bonded joints.

6.2 Methods

AA 3031-T4 alloy substrates of 4"×1"×0.05" were cleaned ultrasonically in a dilute soap solution and dried at ambient conditions. The anodization process was carried out using a voltage-controlled direct current power supply at a constant current mode, using four different current density (j) of 10, 60, 120 and 150 m A cm^{-2}. Clean and dry aluminum substrates connected to the positive output of the power supply served as anodes. The electrolyte was prepared by using 30 ml of 0.1 M zinc nitrate and 30 ml of 1% glycidoxy propyl-trimethoxy silane. The 1% glycidoxy propyl-trimethoxy silane solution had been prepared by adding 4 ml glycidoxy propyl-trimethoxy silane into 400 ml acetic acid diluted in distilled water to pH = 5 in a 2 L container. The anodization process was carried out in the prepared electrolyte, at the controlled electrolytic bath temperature of 5±1 ºC for 5 minutes. The anodized samples were further washed with deionized water and dried on hot plates at 150 ºC for 2 hours prior to bonding with Adhesive #4. The prepared surfaces were characterized for surface morphology and chemistry using scanning electron microscopy (JEOL JSM-6480), equipped with energy-dispersive X-ray spectroscopy (JEOL), on the individual sample. The chemical compositions have been analyzed by attenuated total

reflection-Fourier transform infrared (Agilent Technologies, Cary 630). The surface roughness (root-mean-square) was measured using a MicroXAM-100 HR 3D surface profilometer.

SLS specimens were prepared according to the ASTM-D1002 standard and cured according to the manufacturer's recommendation prior mechanical testing [98]. The bond strengths of the SLS were tested using an INSTRON 8801 at a traction speed of 1.3 mm minute^{-1}. Rupture modes of the failed specimen were visually analyzed.

6.3 Surface characterization

6.3.1 Effect of electrochemical anodization time on roughness

Anodization process results in the formation of a porous oxide layer while silanization is expected to impregnate silane molecules in the anodized pores of the aluminum surface. This mechanism which results in such morphological changes may contribute to a rough microstructure. The root-mean-square roughness values has been obtained on the surfaces anodized at varying j, Fig. 6.1. The untreated clean aluminum surface presented a root-mean-square roughness value of as low as 0.24 µm. However, it is clear that the surface once treated presents an increase in root-mean-square value. It is clear that the roughness increases with increasing j values up to 120 m A cm^{-2}, where the roughness was a maximum of 6.95 µm. This increase in roughness may be attributed to the increasing growth of porous oxide layer while simultaneously silane molecules deposit into and near the pores adding a second degree of roughness to the porous structure. However, with further increase in *j*, there is a decline in the roughness value. This declining nature in root-mean-square roughness can be attributed to the falling of porous material as well as the increased deposition of silane

molecules filling the constantly evolving pores minimizing the surface's roughness to a smoother surface. These results indicate that the critical roughness required to help enhance the mechanical interlocking corresponds to the surface anodized at j = 120 m A cm^{-2}. Presence of silane molecules is expected to add covalent interfacial bonds between the adhesive and the surface in addition to the mechanical interlocking favored by the roughness.

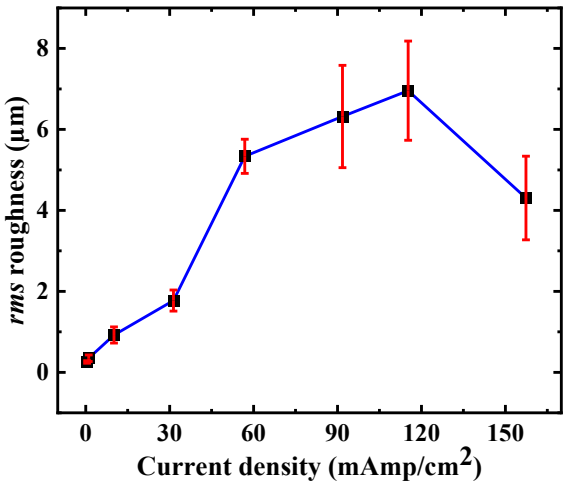

Figure 6.1 rms roughness of anodized AA3031 Al substrates at varying current density.

6.3.2 Morphology and chemical composition

The morphological and chemical analysis by scanning electron microscopy/energy-dispersive X-ray spectroscopy corroborates with the surface roughness measurements. The treated surfaces reveal the emergence of clustered microstructures with different sizes and shapes. The scanning electron microscopy images of the surfaces of as-received clean aluminum and the anodized aluminum at j = 120 m A cm^{-2} have been analyzed, Fig. 6.2 (a) and (b), respectively. The presence of a porous sponge-like structure arising from the anodization and silanization processes can be clearly seen, Fig. 6.2 (b). A comparison of the

scanning electron microscopy images of the various samples studied showed the evolution of enhancing rough structures with increasing current density (figures not shown to avoid repetitive images). The morphology, however, changed to a smoother texture with increase in j to 150 m A cm^{-2} (figure not shown). As explained above, this may be attributable to a denser silane deposition on the larger pores reducing the texture to a less rough one.

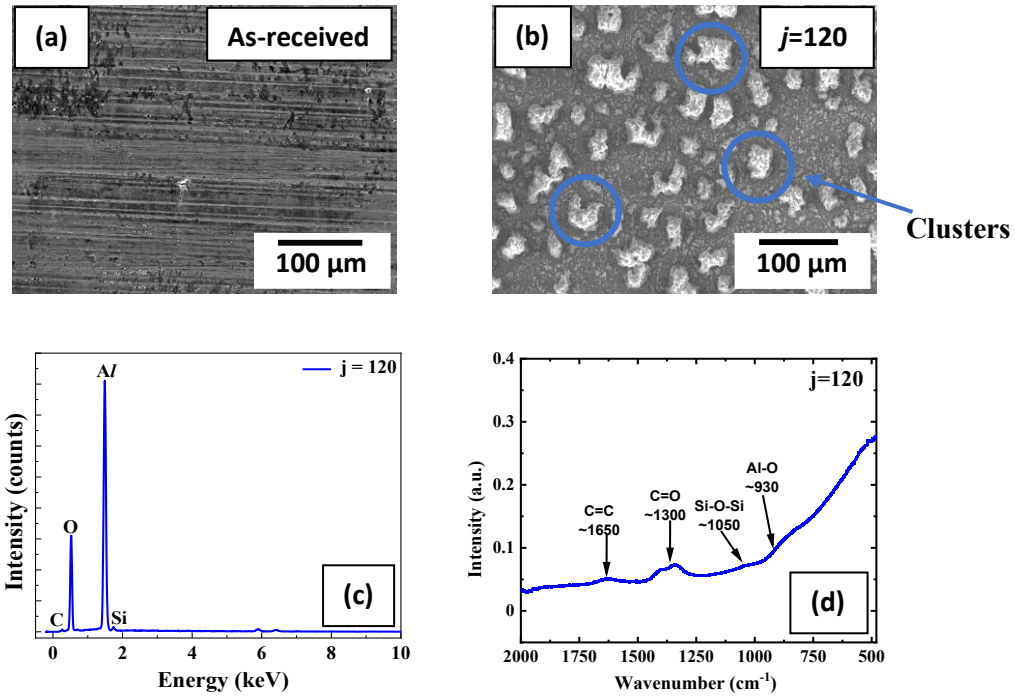

Figure 6.2 Scanning electron micrographs of (a) as-received; (b) anodized at j=120, AA3031 Al sheets (some clusters are highlighted by blue circles) with their corresponding; (c) EDS measurement and (d) ATR-FTIR spectra

The chemical nature of the treated surfaces was analyzed by both energy-dispersive X-ray spectroscopy and attenuated total reflection-Fourier transform infrared spectral analyses. The energy-dispersive X-ray spectroscopy spectra (Fig. 6.2 (c)), confirmed the presence of oxygen (O), aluminum (Al), and silicon (Si) with their corresponding K_α peaks at 0.53 keV,

1.15 keV and 1.74 keV. The energy-dispersive X-ray spectroscopy result clearly shows a strong peak of oxygen, which can be associated with the formation of the anodic oxide (Al─O) layer as well as from the silane molecules deposited in the pores as silanol (Si─O─H). In addition, the presence of silicon confirms the silane impregnation in the porous anodic layer. Corresponding to the scanning electron microscopy surface (Fig. 6.2 (b)), the characteristic peak of attenuated total reflection-Fourier transform infrared spectrum obtained, Fig. 6.2 (d). The attenuated total reflection-Fourier transform infrared spectrum presents a broad peak at around 930 cm^{-1} attributable to the formation of anodic aluminum oxide upon anodization [150]. The Si─O─Si bonds at around 1050 cm^{-1} confirms the silane impregnation during the anodization process [151]. Additionally, 1650 cm^{-1} and 1300 cm^{-1} can be assigned to the ─C=C and ─C=O stretching modes of glycidoxy propyl-trimethoxy silane.

6.4 SLS strengths of the adhesive joints

The characterization of the surfaces studied indicates that the surfaces anodized and silanized at j = 120 m A cm^{-2} has potential of providing high adhesive bond strength when bonded with an Adhesive #4. Mechanical testing was further carried out on these surfaces to investigate the lap shear strengths and their modes of rupture after failure. The SLS test results obtained on the as-received and treated specimens, Fig. 6.3 (a). It is clear from this graph that the lap shear strengths of the treated specimens were higher than that of the as-received aluminum (12±1 MPa). A maximum lap shear strength of 18±1 MPa was obtained with specimens treated at the anodization current density of 120 m A cm^{-2}. The trend in the

increase and decrease observed on the lap shear strengths were in agreement with that of the root-mean-square surface roughness values as well as the morphological evolution. The increase in SLS strengths were observed up to j = 120 m A cm^{-2} and then the strength declines at j = 150 m A cm^{-2}. This behavior can be attributable to the microstructural evolution and the chemical changes occurring on the treated surfaces with varied current density. A critical j value of 120 m A cm^{-2} has been found beneficial to achieve the highest SLS strengths. Further, the rupture modes of the failed specimens (Fig. 6.3 (b)) elucidates a substrate failure at 120 m A cm^{-2} indicating the adhesion at the adhesive/surface interface is very strong while all other specimens showed 100 % adhesive failure at the interface between the adhesive and the surface. Therefore, a current density of 120 m A cm^{-2} was required to obtain a uniform distribution of the adhesive attributable to the right surface conditions obtained at this value.

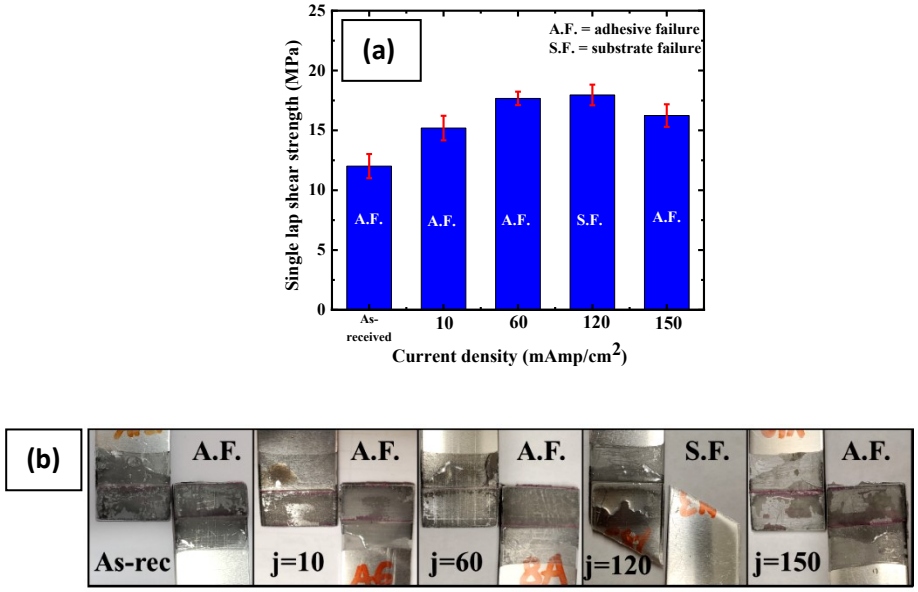

Figure 6.3 (a) SLS strengths of adhesively bonded SLS specimens and (b) images of ruptured specimens (A.F. – Adhesive Failure, S. F. – Substrate Failure).

6.5 Summary and Conclusions

A one-step approach of simultaneous anodization and silanization has been used to prepare adhesively bonded SLS specimens and the effects of the various surface conditions on the adhesion strengths between the adhesive and the treated surfaces have been investigated. Although an increase in the SLS strengths has been observed with treated surfaces as a function of increasing current density, a decile in SLS strength has also been observed at very high current density of 150 m A cm^{-2}. Therefore, a critical j value of 120 m A cm^{-2} has been found essential to obtain the highest SLS strength of ~18 MPa with a failure mode where the substrate failed first. This indicates that the surface has presented the benefits of mechanical interlocking by providing highly textured surface as confirmed by the roughness measurements and scanning electron microscopy analyses, as well as chemically rich surface as confirmed by energy-dispersive X-ray spectroscopy and infrared spectra. All other specimens failed 100 % adhesively indicating weak surface natures. The aluminum surfaces anodized at 120 m A cm^{-2} presented 50 % enhancements in adhesion strengths as compared to the as-received counterpart. The results show potential for this easy one-step process as a green method for use in industrial components and large-scale productions.

Chapter 7: Effect of corona discharge on PVC for structural adhesive bonding applications at Al/PVC interface.

7.1 Introduction

Climate change and environmental legislation for greenhouse gas emissions have become primary concern in our society [152-156]. For the sectors, such as, the automotive industries, aviation and aerospace technology, the development of variety of highly engineered and high-performance materials is crucial for successful reduction of global greenhouse gas (GHG) emission [157-159]. A potential solution to a significant reduction in the overall body weight may be attained by using lightweight multi-material components, such as polymers and light weight metals, with high strength-to-weight ratio in the vehicle bodies. Assembling metals and polymers can be a challenging task as polymers can't be welded [160]. Traditional arc welding and friction stir welding, for instance, is not a viable option, as, polymers and metals have different melting temperatures [161, 162]. Among the various joining techniques, the most feasible technique to join metals and polymers together is by using structural adhesives [163-167]. Due to wide range of applications of metal-polymer hybrid systems in aerospace, automotive, robotics, electronic, packaging, defense, nuclear, medical, etc., these systems become of high importance [164, 168-172]. As compared to similar materials, namely, metal-metal or polymer-polymer adhesive joints, the metal-polymer hybrid adhesive joints hold many unique properties in terms of low density and light weight, high bending strength as well as good sound, vibration and damping characteristics [173-175]. Owing to the low weight and mechanical properties of aluminum, adhesive bonding of polymers with Al can contribute to light weighting of overall body structure [176]. Polyvinyl

chlorides (PVC) are the largest class of synthetic thermoplastic polymers that are employed in a wide variety of applications, particularly in food packaging, consumable products, structural plastics, and medical applications [177-179]. This is because these polymers are distinguished by light weight, excellent chemical and physical properties, cost-effectiveness, as well as ease of processing [180, 181]. PVC materials have low surface reactivity and hydrophobic nature due to the lack of hydrophilic functional groups on their surfaces, and hence demonstrate low adhesion with adhesives [182. 183].

In recent decades, several surface modification methods have been developed in order to facilitate the adhesive joining of polymer-metal hybrid system. All these methods assist in increasing the surface energy of the polymer material, resulting in better wettability depicted by the decrease in water contact angle and thus higher bond strength. These surface modification methods are basically classified into three categories: physical methods based on plasma technologies and flame treatment, chemical methods via surface functionalization, and mechanical methods by abrasion [184-186]. Generally, abrasion/solvent cleaning, grit blasting, peel-ply, tear-ply, acid etching, corona discharge treatment, plasma treatment, flame treatment and laser treatments are the common techniques employed to activate the polymer surface to favor adhesive joining of multi-material system [187]. Kruse *et al.* performed a detailed investigation on the effect of corona treatment, the low-pressure plasma process, and the fluorination on polypropylene, polybutyleneterephthalate and polyetheretherketon substrates [188]. They reported that the highest SLS strength of polybutyleneterephthalate after gas phase fluorination (for 10 s with 0.5 vol % F) treatment reached up to 6.1 MPa. Whereas, upon treating the polyetheretherketon with corona treatment, the maximum achieved SLS strength were found to be 7 MPa. Chin *et al.*

considered the effect of several surface engineering processes, including grit-blasting, on the composition, surface energy, and surface topography of composites. They found that after grit-blasting the total surface energy was increased from 31.3 mJ/m^2 to 39.1 mJ/m^2 [189]. Many works highlight the effects of chemical treatments on the strength and durability of adhesive joints using chemical etching [190]. One of the main issues in chemical etching of the surfaces is the environmental hazards produced by the chemical reagents [191]. The best performing chemical treatments are often the most aggressive ones, complex during the bonding operations, and hazardous for the environment [192]. The wetting properties of polypropylene have been studied by Williams *et al.* using flame treatment and they have shown that the water contact angle reduces from 98±1.1 to 62±3.2 [193]. Among these processes, the laser or plasma treatment are claimed to increase the surface energy, a key parameter to provide good bonding [194, 195]. However, previous studies found that, these methods are not always easy to implement and are not cost effective when applied in an industrial context [196-198]. The flame treatment is also challenging to control, and bonding must be carried out shortly after exposure to flame [199]. Corona discharge techniques and selected chemical methods are, therefore, found to be preferable in the surface treatment of PVC. On the industrial scale, corona treatment is a preferred surface treatment for the surface modification of PVC substrates. It promotes surface activation, which leads to enhanced wetting and adhesion characteristics for applications related to adhesive bonding and printing [200-203]. Corona treatment is characterized by fast operation, cost-effectiveness, adaptability to in-line operations, and being environmentally friendly without the need to use aggressive chemicals in the process [203, 204].

In the present study, we have used corona discharge surface treatment method to activate PVC surfaces to favor adhesive bonding with AA 6061 aluminum alloy as second substrate. The effect of time of exposure of corona discharge on the PVC surfaces on the adhesive joint strengths when bonded with aluminum (Al/PVC, PVC/etched Al and PVC/anodized Al), using Adhesive #3. The corona treatment on PVC surfaces is found to enhance the PVC surface wettability. The chemical changes were monitored using attenuate total reflection–Fourier transform infrared spectroscopy (ATR–FTIR). The surface morphological features have been found unaltered as the optical profilometry measurements show no change in their surface roughness values following treatment. Mechanical tests performed on the SLS specimens of PVC bonded aluminum multimaterial systems shows improvement in the shear strengths of the joints presenting a cohesive mode of failure of the adhesive.

7.2 Materials and Methods

In this study, 1.5 mm-thick flat sheet of AA6061 aluminum alloy from Russel Metals Inc. (Ontario, Canada) and the 6.35 mm-thick PVC Type 1 Plastic from McMaster-Carr (USA) of dimension 101.6 mm × 25.4 mm have been utilized. All substrates of Al alloy and PVC have been ultrasonically degreased in propanol solution at room temperature for 15 min, then dried in open air at ambient conditions. Prior to bonding with adhesive, the clean and dry substrate surfaces were pretreated individually: corona treatment on PVC surfaces and etching, anodization on the surfaces of Al. These methods have been described below in sections 7.2.1, 7.2.2 and 7.2.3, respectively. The prepared surfaces have been characterized for surface morphology with optical microscope. Chemical analysis was performed using attenuated total reflection-Fourier transform infrared (ATR, Agilent Technologies, Cary 630

FTIR) system. Further, the *rms* surface roughness was measured and analyzed using a MicroXAM-100 HR 3D optical surface profilometer. Wettability of the PVC surfaces have been investigated by using digital images of the water drops (~ 5 μL) and measuring the contact angle of the drops using ImageJ software. The clean and dry substrates have been bonded with a two-component room temperature cure epoxy adhesive from Henkel corporation. SLS specimens were prepared using an Adhesive #3 according to the ASTM-D1002 standard and allowed to cure according to the manufacturer's recommendation prior to mechanical testing [98]. The joint strengths of the SLS specimens were determined using an INSTRON 8801 at a traction speed of 1.0 mm/min. The rupture modes of all tested SLS specimen have been analysed visually as well as using the contrast-colour change mode in imageJ software to determine the percentage of cohesivity. Following Table 7.1 elucidates the properties of adhesives used in the preparation of SLS specimens:

Table 7.1 Properties and recommended curing conditions of adhesive

S. No.	Entity	Adhesive #3
1.	Name	2C-epoxy (LOCTITE EA E-20HP)
2.	Curing condition	Room temperature cure (40 minutes)
3.	Crosshead speed	1.0 mm/min

4.	characteristics and properties of adhesives	Specific Gravity at 25 °C = 1.03 Tensile Elongation ASTM D-638 = 8% Hardness ASTM D-1706, Shore D= 80 Glass Transition Temperature (Tg)= 60 ºC
5.	chemical base of adhesive ingredients	Chemical Type: Epoxy
6.	stoichiometric ratio of adhesives components	Components Two part= Resin and Hardener Mix Ratio, by weight - Resin : Hardener =100 to 55 Appearance (Mixture)= Off-white
7.	method of their preparation	Mix using hands in a weighing boat.
8.	amount of prepared mass	~ 5 g
9.	methods of applying adhesives	Pasted over the Al specimens using a Bamboo Kabob Skewers.

7.2.1 Surface modification of PVC substrates using corona surface treatment

The PVC surface have been treated using corona discharge in order to introduce of polar functional groups, as illustrated in Fig. 7.1. A laboratory scale corona discharge system (BD-20AC, 115 V, USA) has been employed for surface treatment of PVC under atmospheric

pressure using 300 W of nominal power and frequency of 17.20 kHz. The effect of corona treatment process on PVC has been studied by varying treatment time from 0 to 30 s, where the treatment time of 0 s represents as-received PVC. By maintaining a gap of ~1.5 mm between the corona head and the substrate surface, a high voltage potential was applied between the tip of the electrode and the PVC substrate to ionize the air molecules in the open atmosphere, that effectively modify the PVC substrate chemically.

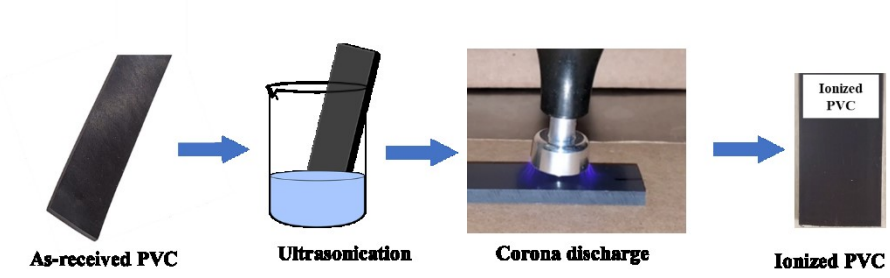

Figure 7.1 Schematic illustration of corona discharge treatment on the surface of PVC. © Mani Mohan Tiwari, 2022.

7.2.2 Preparation of AA 6061 substrates by chemical etching

Clean AA 6061 substrates have been immersed in 1M sodium hydroxide solution maintained at 55°C for a period of 3 minutes, followed by rinsing in distilled water. These surfaces were further desmutted in 10 % (w/v) solution of HNO_3 at room temperature for 1.5 minutes, inside a fume hood chamber. The etched AA 6061 substrates have been ultrasonicated in distilled water for 15 minutes and then dried at 150° C for 1 hour to remove any excess water on the surface.

7.2.3 Anodization of AA 6061 substrates

Clean and dry AA6061-T6 substrates have been used as both cathode and anode separated by a distance of 1.5 cm during the anodization process. In this study, the anodization process

has been carried out using a voltage-controlled DC power supply at a constant current mode, by utilizing an optimized current density of 30 $mA \cdot cm^{-2}$. The process was carried out in 60 ml of 0.1M Na_2HPO_4 salt electrolyte, at a bath temperature of 5 ^oC for 1 hour. The anodized samples were further washed with deionized water and dried on hot plate at 150 ^oC for 2 hours. These surfaces were used for bonding with PVC using the Adhesive #3.

7.3 Surface characterization

7.3.1 Surface roughness and topography of corona treated PVC

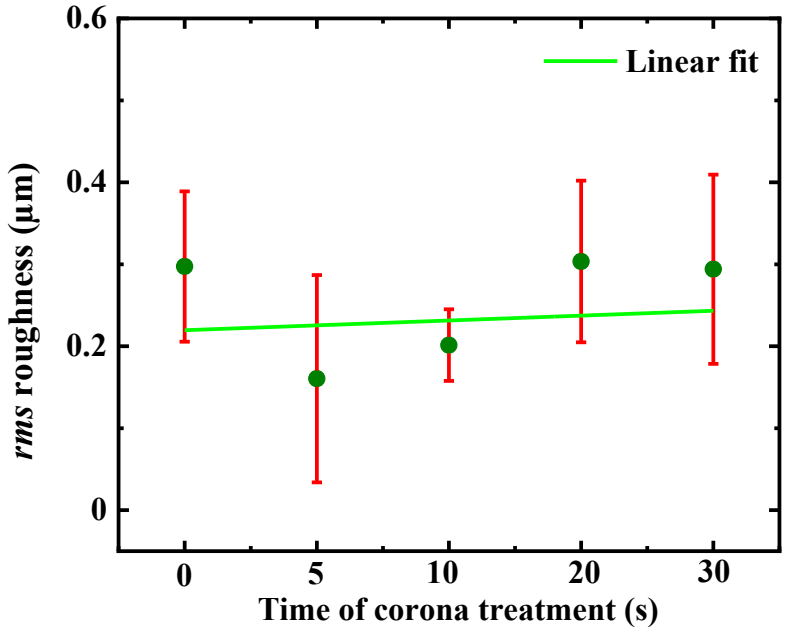

Figure 7.2 (a) Variation in rms roughness of PVC surfaces treated by corona discharge as a function of treatment time.

Fig. 7.2 shows that the *rms* roughness of the corona treated PVC surfaces with the varied times treatment. The *rms* roughness of the as-received PVC surfaces has been measured to be ~ 0.3 µm. Following varied times of corona treatment of 5 s, 10 s, 20 s and 30 s, the *rms* roughness values were found to remain similar and measured to be ~ 0.2 µm for 5 s and 10 s and ~ 0.3 µm for 20 s and 30 s. These results show that the corona discharge employed on the PVC surfaces does not alter the surface roughness indicating that the topography of the surface remain unchanged. This observation is corroborated with the optical microscopy images as shown in Fig. 7.3 (a-e) and the 3-D profiles obtained from the optical profilometry

during the roughness measurements as shown in Fig. 7.3 (f-j). The optical micrographs and the 3-D images obtained on the treated surfaces shows similar surface topography as obtained on the as-received PVC surfaces. The optical study is also in agreement with a previous study on polypropylene surface where the authors demonstrate no change on the surface topography following corona discharge treatment of these surfaces [205].

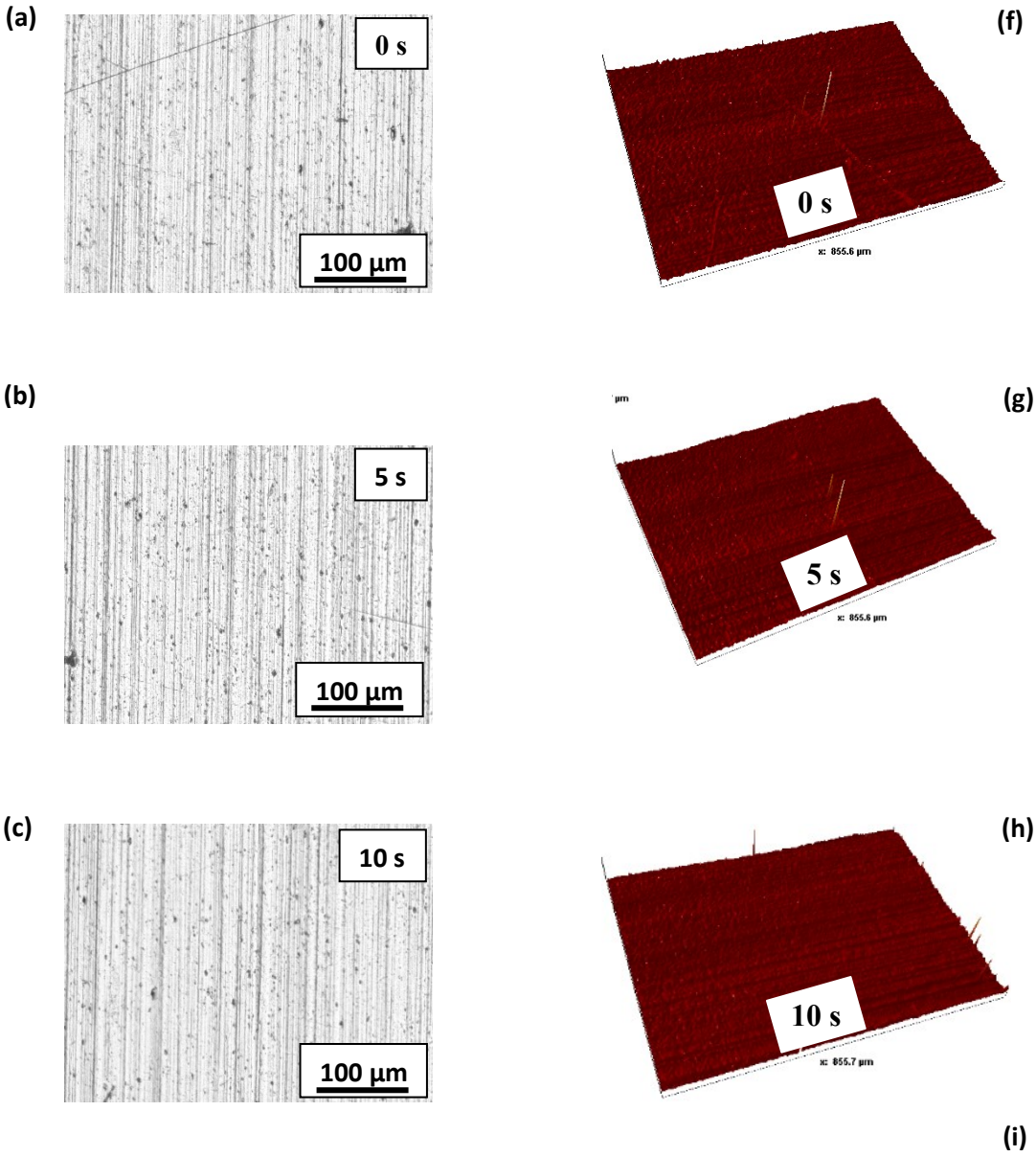

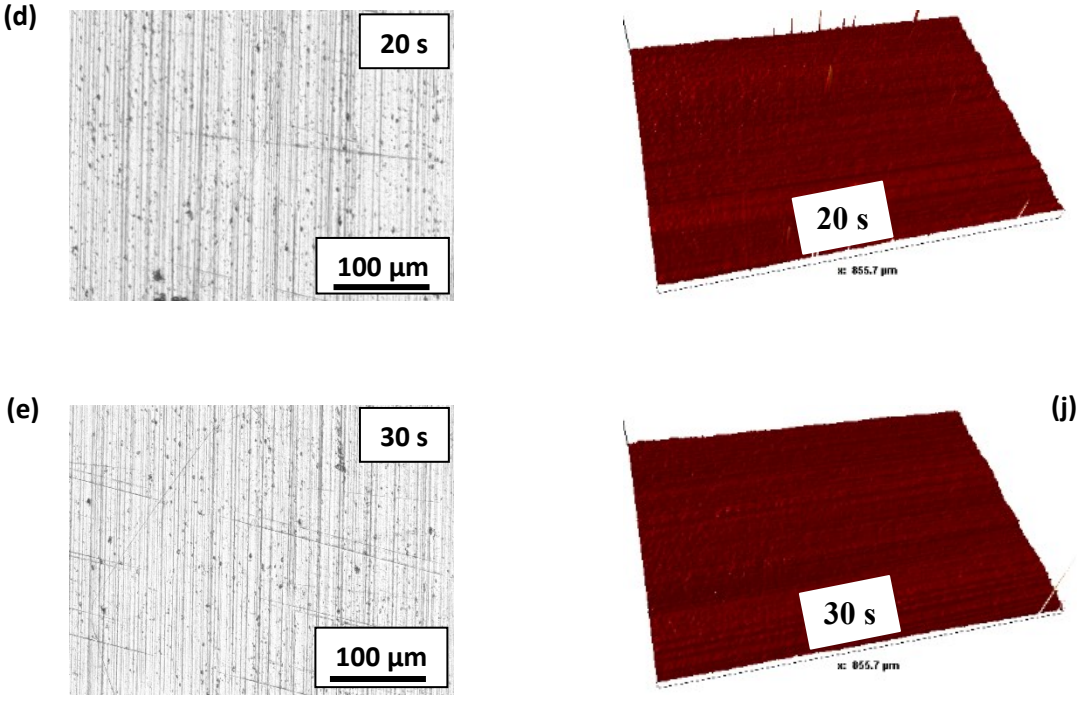

Figure 7.3 Optical micrographs and 3-D profiles from optical profilemtry of PVC surfaces (a, f) as-received; after corona discharge surface treatment for (b, g) 5 s, (c, h) 10 s, (d, i) 20 s and (e, j) 30 s.

7.3.2 Chemistry and wettability of surface

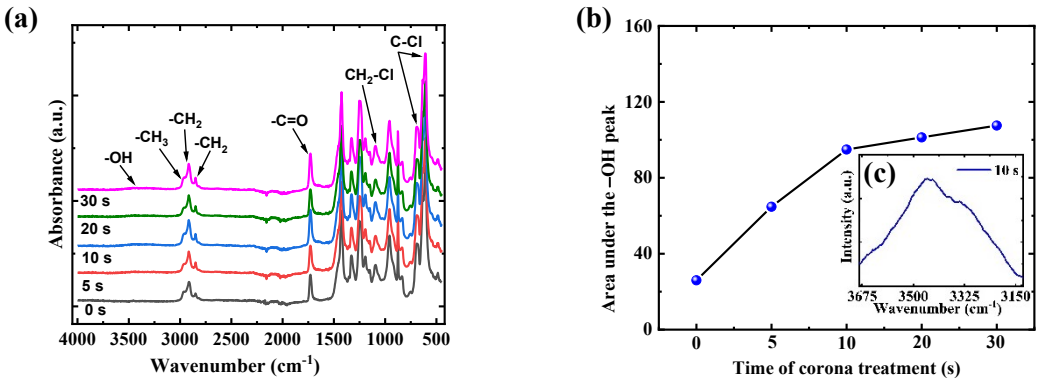

Figure 7.4 (a) ATR-FTIR spectra of corona discharge treated PVC surfaces, (b) area under the –OH peak as a function of time of time of treatment, and (c) inset showing the IR peak of –OH after 10 s of treatment time.

Fig. 7.4. (a) shows the ATR-FTIR spectra of corona treated PVC surfaces for 0 s, 5 s, 10 s, 20 s and 30 s. The principal characteristics peaks of PVC appear in the spectral ranges of 500–1750 cm^{-1} and 2750–3000 cm^{-1}. At the low-wavenumber region, the peaks at 611 cm^{-1} and 689 cm^{-1} represents C–Cl bonds. The peak at 1095 cm^{-1} may be attributed to CH_2–Cl stretching mode [206] while the peak at wavelength of 1727 cm^{-1} may be assigned to carbon C=O bond. Further, the two intense peaks in the high wavenumber region at 2852 cm^{-1} and 2921 cm^{-1} are ascribed to the asymmetric and symmetric C-H stretching modes of $–CH_2$ groups, respectively, and a very small peak at 2961 cm^{-1} arises from the asymmetric in-plane C-H stretching mode of the $–CH_3$ group [206, 207]. As the time of corona treatment increases, the formation of the polar functional group, –OH, at 3390 cm^{-1} becomes significantly noticeable unlike on the as-received PVC surfaces where the hydroxyl groups are apparently absent or negligible owing to the PVC surface chemical composition. Fig. 7.4 (b) depicts the variation in area under the –OH peak with the variation in time of corona treatment and the inset shows the presence of –OH peak formed following 10 s of corona discharge treatment on PVC surfaces. It is clear from this investigation that the area under the –OH peak increases with the treatment time directly indicating that the corona treatment incorporates these polar functional groups in greater quantity as the time of treatment increases. The incorporation of these polar functionalities is an important criterion in adhesive bonding as they are responsible for the hydrogen bonding with the adhesive components during the curing reaction. These functional groups also render the PVC surface hydrophilic by enhancing its water wettability properties, which is also an important criterion in adhesive bonding to enhance the wettability of the adhesive over the –OH rich surface [208, 209]. The formation of these –OH groups on the PVC surface arises from interaction

of the surface with the ionized air (O_2 and H_2O) molecules, ionized as a result of its exposure to corona discharge in the vicinity of the surface [167, 205].

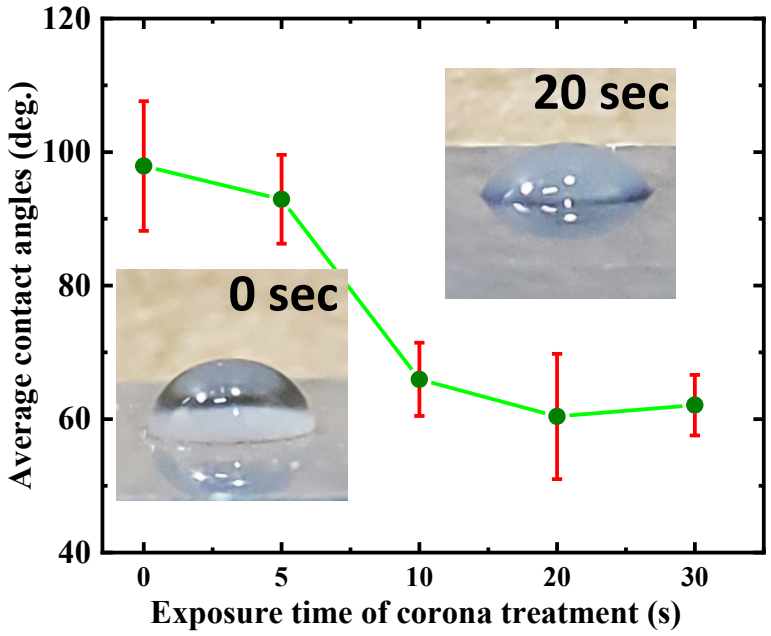

Figure 7.5 Contact angles of a water droplet on corona discharge treated PVC surfaces as a function of treatment time; insets show images of water droplet on the PVC surfaces treated at 0 and 20 s. . © Mani Mohan Tiwari, 2022.

As the FTIR spectra clearly showed the evidence of the formation and increase in intensity of –OH peaks upon increased time of corona treatment responsible for better wettability, water contact angle measurements were further carried out on these surfaces. High wettability, *i.e.*, lower water contact angle, of a surface is considered as indicative of better adhesive bonding [210-213]. A water break test was carried out on the corona treated PVC surfaces [214]. Figure 8.4 shows the variation in the water contact angle of PVC surfaces treated with corona discharge for 0 s, 5 s, 10 s, 20 s and 30 s. The water contact angle of the

as-received PVC surface is found to be 98 ± 19°. Upon treatment for a period of only 5 s, the contact angle reduced to 92±6°, which further reduces to a further lower value of 62 ± 8° when treated at an increased period of 20 s. A slight increase of water contact angle to 66 ± 4° was observed upon further increasing the treatment time to 30 s. This increase may lie within the standard deviation and therefore may be considered similar to that obtained on the surface treated for 20 s. This also corroborates with the area under the –OH peak where the area of –OH peak was similar on the surfaces treated for 20 s and 30 s (Fig. 7.4(b)). These observations indicate that 20 s of treatment time is critical to obtain the lowest water contact values on the PVC surface which is, by nature, a hydrophobic material [205, 215, 216]. This wettability behavior is in close agreement with previous studies by plasma methods and corona treatments. For example, Kusano *et al.* indicated that polar functional groups could be introduced on the surfaces in a short time of treatment [217]. Similarly, Bormashenko *et al.* showed that the wettability of PVC reaches to saturation in short time of plasma treatment [218]. The results obtained in the current study shows that the corona treatment is effective in incorporating –OH functional groups and thereby enhancing the hydrophilic nature of the PVC surface by exposing these surfaces to corona discharge for a period of a critical treatment time of 20 s.

7.4 SLS strengths of the adhesive joints

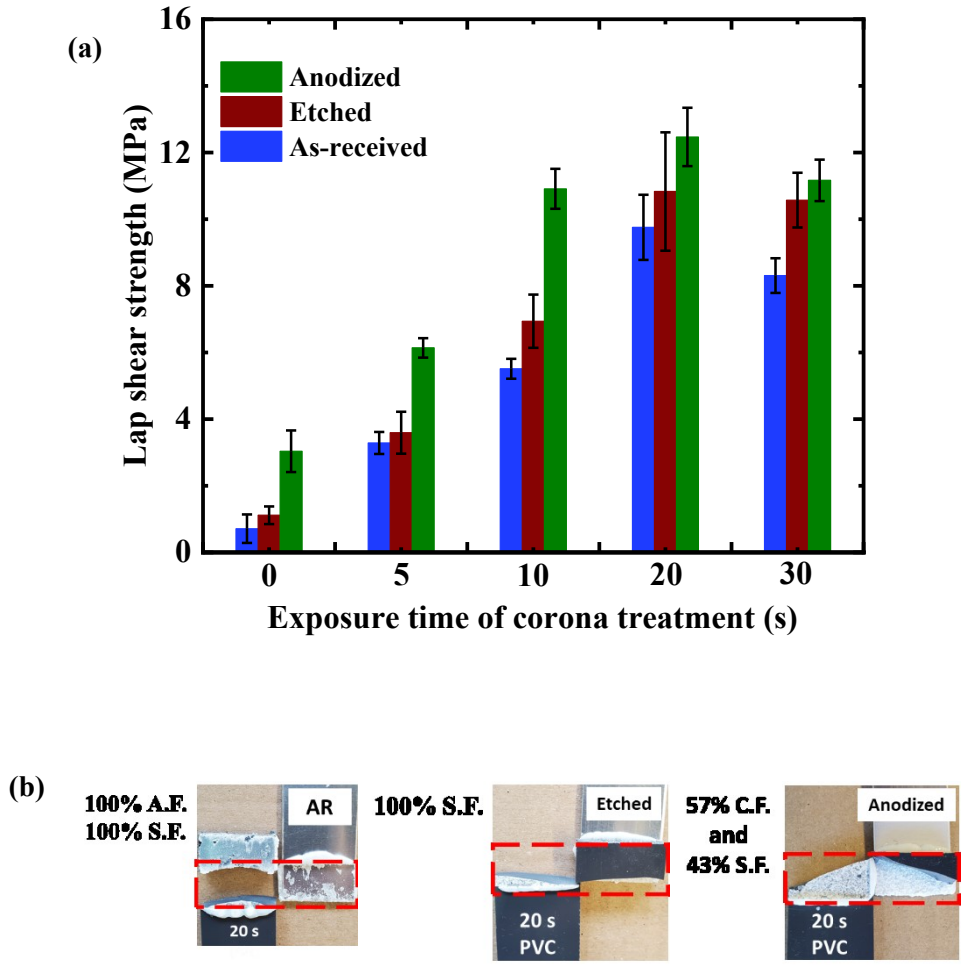

Figure 7.6 (a) SLS strengths as a function of corona treatment time of PVC/AR, PVC/Etched Al, PVC/Anodized Al SLS specimens and(b) images of ruptured SLS specimens (A.F. – Adhesive Failure, C. F. – Cohesive Failure, S.F. – Substrate Failure).

Fig. 7.6. (a) shows the SLS strengths of the adhesive joints of as-received and corona treated PVC bonded with the as-received, etched and anodized Al substrates. The SLS strength of as-received PVC/as-received Al, as-received PVC/etched Al and as-received PVC/anodized Al have been found to be 0.7±0.4 MPa, 1.1±0.2 MPa and 3.0±0.6 MPa, respectively,

indicating that a maximum comparative shear strength is obtained when bonded with anodized aluminum. With PVC corona treated for 5 s, the joint strengths of the bonded joints have been found to have increased to 3.3±0.3 MPa, 3.6±0.6 MPa and 6.1±0.3 MPa, respectively, with as-received, etched and anodized Al. Furthermore, upon increasing the time of corona treatment on PVC substrates to 10 s, the strengths of the PVC/as-received Al, PVC/etched Al and PVC/anodized Al have been further increased to 5.5±0.2, 6.9±0.8 and 10.9±0.8 MPa, respectively. It is observed that the shear strengths are increased with the increase of the time of corona treatment and maximum shear strength is obtained when 20 s of corona treatment time was used. When treated for 20 s, the obtained SLS strengths are 9.8±1.0 MPa, 10.8±1.8 MPa and 12.46±0.8 MPa, for the PVC/as-received Al, PVC/etched Al and PVC/anodized Al joints, respectively. However, upon increasing the time of treatment to 30 s, a slight change in the SLS strengths of the Al/PVC adhesive joints has been observed compared to 20 s treated PVC surfaces, still, higher than 10 s treated PVCs. When treated for 30 s, the SLS strength of PVC/as-received Al, PVC/etched and PVC/anodized Al have been found to be 8.3±0.5, 10.6±0.8 and 11.2±0.6 MPa, respectively. This slight change may be attributable to the similar wetting properties on the PVC surfaces treated for 20 s and 30 s with similar water contact angle values on both surfaces as shown in Fig. 7.2. The improved shear strengths obtained on surfaces treated for longer time may be attributable to the sufficient time allowing the corona discharge to breakdown the hydrocarbon (C-H) bonds on the PVC structure and incorporate oxygenated species from the atmosphere (air) present in the vicinity of the surface resulting in a surface enriched with –OH groups. These –OH groups play a vital role in enhancing the adhesive strengths at the PVC-adhesive interface due to improved wettability of the surface to the adhesive. The effect of mechanical

interlocking on improved joint strengths can be eliminated as the corona treatment does not affect the topology of the surface as demonstrated by the profilometry measurements and optical micrographs (Fig. 7.1 and 7.2). Therefore, the improved joint strengths are principally attributable to the changes in the surface chemistry of the PVC surfaces upon corona treatment, which shows an increase in the hydrophilic nature of the surface by increasing the corona treatment time. This is evidenced by the observation that the lap shear strengths of the Al/PVC specimens, when PVC surfaces are treated for varied time periods, are always higher than that of the as-received PVC counterparts with as-received, etched and anodized Al. The 20 s treated PVC/as-received Al joints provided 14 times higher SLS strength than the as-received PVC/as-received Al joints with an enhanced adhesive strength of 1314% (from 0.7 MPa to 9.8 MPa). The SLS strength of 20 s treated PVC/etched Al joints has found to be 9 times higher than that of as-receivedPVC/etched Al joints with an enhancement of 881% (from 1.1 MPa to 10.8 MPa). Similarly, 20 s treated PVC/anodized Al joints show 4 times higher strengths than that of as-received PVC/anodized Al joints with a gain in the SLS strength of 313% (from 3.0 MPa to 12.4 MPa). A global percentage gain in the SLS strength of 1.6×10^3 % (from 0.7 MPa to 12.5 MPa) have been also recorded in SLS strength of 20 s treated PVC/Anodized Al joints compared to that of as-received Al/PVC counterparts. These results indicate that a treatment time of at least of 20 s on PVC surface has been found to be critical to achieve the highest SLS strengths when bonded adhesively with anodized Al. Fig. 7.6 (b) shows the specimens of ruptured images of 20 s corona treated PVC surfaces with Al. The Al/PVC joints not only failed with 100% S.F at PVC end but also presented 100% A.F. at the interface between adhesive and as-received Al. Subsequently, in the case of PVC/etched Al, 100% S.F. have been observed in all specimens. The emergence of 57% C.F.

together with 43% S.F. in 20 s treated PVC/anodized Al specimen, indicates that the adhesion at the adhesive/surface interface was strong enough to make the partial failure within the Adhesive #3 itself.

Table 7.2. SLS strength of adhesively bonded Al/PVC treated by corona discharge for various times.

Treatment time (s)	SLS strength (MPa)		
	PVC bonded with as-received Al	PVC bonded with etched Al	PVC bonded with anodized Al
0	0.7±0.4	1.1±0.3	3.0±0.6
5	3.3±0.3	3.6±0.6	6.1±0.3
10	5.5±0.2	6.9±0.8	10.9±0.8
20	9.8±1.0	10.8±1.8	12.4±0.9
30	8.3±0.5	10.6±0.8	11.2±0.6

The obtained SLS strength values of PVC and Al adhesive joints on the corona treated PVC surfaces are comparable with those obtained by activating the substrate surfaces using various other physical treatment processes such as laser and gas plasma, which are generally considered as common physical surface treatment methods in the adhesive bonding of multi-material system. For example, in the work of Bagiatis *et al.* studied the effect of plasma treatment with different gas compositions using combinations of helium, argon and oxygen on polymethyl methacrylate substrate [219]. They showed that argon/0.5 vol % oxygen plasma treatment presented approximately a 190 % improvement in bonding strength with the obtained value of 1.6 MPa on the polymethyl methacrylate with glass substrates with silicone adhesive [219]. Similarly, Carrado *et al.* studied the effect of corona treatment on the adhesion at the metal–polymer interface using an epoxy adhesive and reported that the SLS adhesion reached to 8.4 MPa with the enhancement of 22% [220]. In another work, Palkowski and Carradò had demonstrated that adhesion strength with corona treatment and

bonded by using epoxy adhesive (Köratec FL201) for the Zn-coated steel with polymer had been reached to 11 MPa, with the ~ 22 % increment compared to SLS joints prepared by acetone wiped substrates only [221]. Furthermore, an investigation lead by Rheea and Yang showed the acetylene and nitrogen plasma-treated aluminum and Ar^+ ion irradiated CFRP specimen exhibited SLS strength of 0.75 MPa with the gain of 108 %, when joined with epoxy adhesive [222]. These studies show the influence of plasma treatments on polymeric surfaces to improve the strength of adhesive joints when bonded with metallic surfaces. The current study has demonstrated the same with a simple technique of corona discharge, showing higher percentage of gain in the joint strengths when compared with the existing literatures.

7.5 Summary and Conclusions

The effect of time of corona treatment on the SLS strengths of the adhesive joints of bonded with the as-received, etched and anodized Al have been studied. The analysed surface chemistry revealed the linear increase in –OH polar functional groups on the of PVC substrate surface after an increased treatment time of corona discharge. However, the *rms* micro-roughness of PVC substrate surface remained unchanged as the corona treatment does not alter the topographic features of the PVC surfaces. The wetting properties of the PVC surface has been analyzed by water contact angle measurements and are found to increase after increased time of corona treatment as compared to as-received PVC surface. Investigations into the wetting properties of these surfaces demonstrated decrease in water contact angles by ~ 36° from 98°. The maximum SLS strength were found to be 12.4 MPa, with the gain of 313% for corona treated PVC with anodized Al joints.

Chapter 8: Chemical affinity of mixed adhesive for structural adhesive bonding applications at Al/PVC interface

8.1 Introduction

The development of the aerospace and automobile industries requires lightweight materials with high reliability and good dimensional stability, and thus promotes the application of polymers such as polyvinyl chloride (PVC) and light metal materials, such as aluminum (Al) alloys [152-154]. Compared with conventional mechanical joining approaches, such as welding, bolting and riveting, adhesive bonding stands out for several reasons, including its uniform stress distribution, low weight and good bondability of multi-material systems [5–8]. Bonding multi-material systems such as polymers to lightweight metals increases the efficiency in weight reduction in automotive and transportation structures, and hence improves overall fuel efficiency. For example, Pantelakis and Tserpes [223] discussed the development and challenges of adhesive bonding technology for composite materials in aircraft structures, proposing a numerical design method for bonding polymer materials to an Al alloy. Wang et al. [224] studied the influence of bonding parameters, namely adhesive types, surface treatment, substrate shape and bonding area on the improvement of the mechanical strengths. Pitta et al. [225] demonstrated a three-times-higher strength for metal–polymer systems when bonded adhesively compared to riveted counterparts. All these studies show that joint strengths and weight reduction can be improved using adhesives for assembling polymers to metals. However, the durability of the joint is determined by the strengths of the interfacial bonds between the polymer surface and the adhesive. Appropriate surface treatment is known to have a significant impact on improving the interfacial bonds

between the treated polymer surface, such as PVC, and the adhesives [226–228]. Joining PVC with a metal using an adhesive is challenging as polymers have inherently very low surface energies, unfavorable for adhesion with adhesives. In addition to surface treatment, the selection of the right adhesive chemistry also plays a significant role for its compatibility with the polymer surface chemistry.

In the present work, we investigate the adhesion properties of two dissimilar materials, PVC and Al, adhesively bonded with a mixed adhesive chemistry by combining two different adhesive types, namely epoxy and silicone. The chemical compatibility of the mixed adhesive with the PVC substrate as well as Al and the improvements in the mechanical strengths of the bonded joints are presented.

8.2 Materials and methods

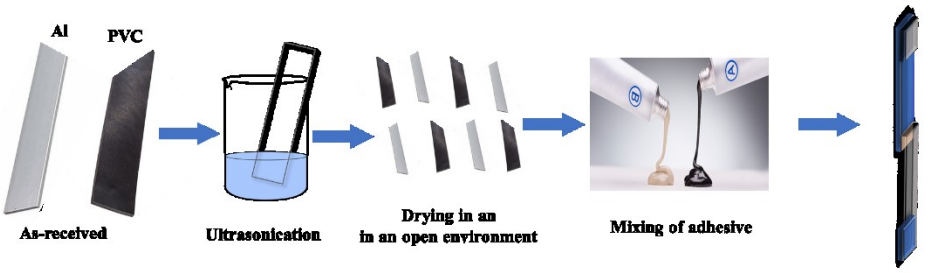

Figure 8.1 Schematic illustration of preparation of mixed adhesive based Al/PVC joints. © Mani Mohan Tiwari, 2023.

Fig. 8.1 shows the schematic illustration of the prepareation of SLS specimen of two different materails, namelt, Al and PVC. The commercially available 1.5-mm-thick AA 6061-T6 Al flat sheet from Russel Metals Inc. (Mississauga, ON, Canada) and the 6.35-mm-thick PVC Type 1 plastic from McMaster-Carr (USA) were utilized as substrates. Commercially

available silicone adhesive (SI 595) and epoxy adhesive (loctite EA E-20HP), provided by Henkel Inc., were used to bond the substrates. These two adhesives were mixed in equal volume proportions at an ambient temperature and pressure, as shown in Fig. 8.1. SLS specimens of PVC bonded to Al were prepared according to the ASTM-D1002 standard [98]. The geometrical and topographic characteristics of surfaces of PVC and Al were analyzed using an optical microscopy (Nikon Eclipse) and MicroX-AM-100 HR 3D surface profilometer, respectively. The chemical composition of mixed adhesive was studied using attenuated total reflectance Fourier-transform infrared (ATR-FTIR) spectroscopy. The SLS strength of the Al/PVC bonded joints were determined using an INSTRON 8801 mechanical testing unit. Following Table 8.1 elucidates the properties of adhesives used in the preparation of SLS specimens:

Table 8.1 Properties and recommended curing conditions of adhesive

S. No.	Entity	2C-epoxy	Silicone
1.	Name	LOCTITE EA E-20HP	LOCTITE SI 595
2.	Curing condition	Room temperature cure (40 minutes)	Room temperature cure (24 hour)
3.	Crosshead speed	1.0 mm/min	0.3 mm/min
4.	characteristics and properties of adhesives	Specific Gravity at 25 °C = 1.03 Tensile Elongation ASTM D-638 = 8% Hardness ASTM D-1706, Shore D= 80	Specific Gravity at 25 °C= 1.01 Odor = Acetic Acid

		Glass Transition Temperature (Tg)= 60 ºC	
5.	chemical base of adhesive ingredients	Chemical Type: Epoxy	Chemical Type: Acetoxy silicone
6.	stoichiometric ratio of adhesives components	Components Two part= Resin and Hardener Mix Ratio, by weight - Resin : Hardener =100 to 55 Appearance (Mixture)= Off-white	Appearance clear
7.	method of their preparation	Mix using hands in a weighing boat.	One component - requires no mixing
8.	amount of prepared mass	~ 5 g	~ 5 g
9.	methods of mixing of these two adhesives	Mixed in open enviromnet using a Bamboo Kabob Skewers.	

8.3 Surface characterization

8.3.1 Optical and 3D profile images

Fig. 8.2 presents the optical images and corresponding 3D profile images of the roughness for the as-received PVC and Al substrates, in which Fig. 8.2 (a, c) are for the PVC surface and Fig. 8.2 (b, d) for the Al surface, respectively. These topographic images show that both substrate surfaces presented naturally rough surface profiles in their as-received state. The

presence of crests (peaks) and troughs (valleys) in the surfaces provided certain microroughness: 0.34 ± 0.13 μm for the PVC and 0.61 ± 0.21 μm for the Al.

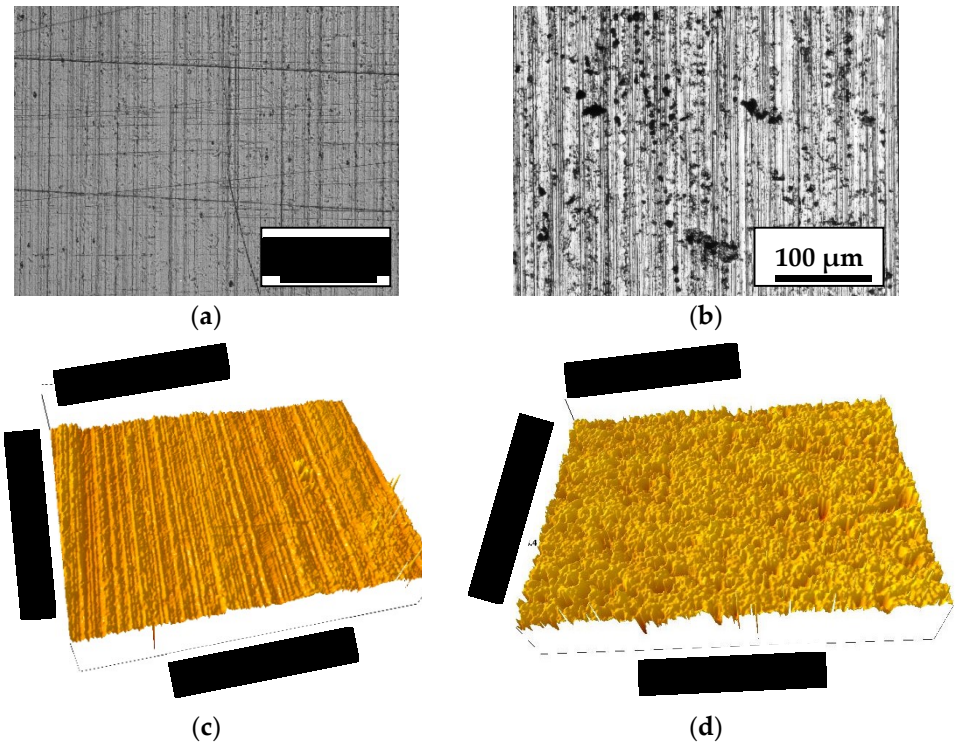

Figure 8.2 Optical images of as-received (a) PVC and (b) Al and their corresponding 3D pro-file images of the roughness in (c) and (d).

8.3.2 Water break test

Fig. 8.3 shows the digital images of droplets of water on the surfaces of the as-received PVC and Al substrates. The water drop placed on the surface of the PVC substrate provides a water contact angle of ~96°. On the other hand, the water contact angle on the surface of the Al substrate was found to be ~68°. The higher water contact angle on the PVC substrate is attributed to the lower surface energies of the PVC as compared with that of the Al.

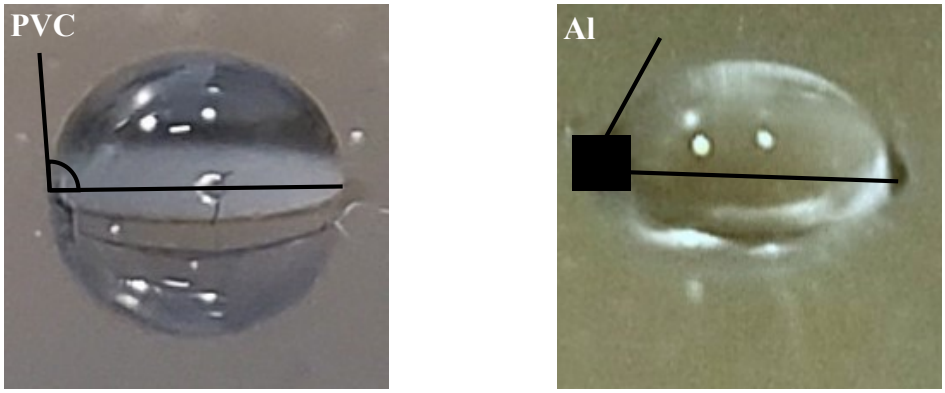

Water on PVC **Water on Al**

Figure 8.3 Digital image of a water droplet on the PVC and Al substrate surfaces showing the water contact angles. . © Mani Mohan Tiwari, 2023.

8.4 Chemical compositional analysis and SLS strengths

Fig. 8.4 shows the ATR-FTIR spectra of the mixed adhesives of the epoxy and silicone as well as of the PVC and Al substrate surfaces. The Al surface showed no IR absorptions, except for a small band at around ~950 cm^{-1} due to the possibility of the presence of an ultrathin oxide layer. However, the PVC substrate displayed multiple strong characteristic IR bands, such as 600 cm^{-1} (C–Cl stretching) and a broad absorption peak at 1425 cm^{-1} corresponding to $–CH_2$ bending, typical of PVC surfaces [229]. Small bands of $–CH_2$ and $–CH_3$ between 2800–3000 cm^{-1} were also observed [229]. Upon analyzing the epoxy-silicone adhesive mixture, overlapping peaks with PVC, namely (i) $–CH_2$, $–CH_3$ around 2800–3000 cm^{-1}, (ii) $Si–CH_3$ at 1260 cm^{-1} were observed. The presence of a characteristic Si–O–Si stretching mode at ∼1050 cm^{-1} and bending modes at 800 cm^{-1} were also observed, confirming the components from the silicone in the mixed adhesive. The presence of these

components effectively enhanced the bonding with the Al substrate due to their chemical affinity to PVC that has an inherently low-surface-energy chemical structure.

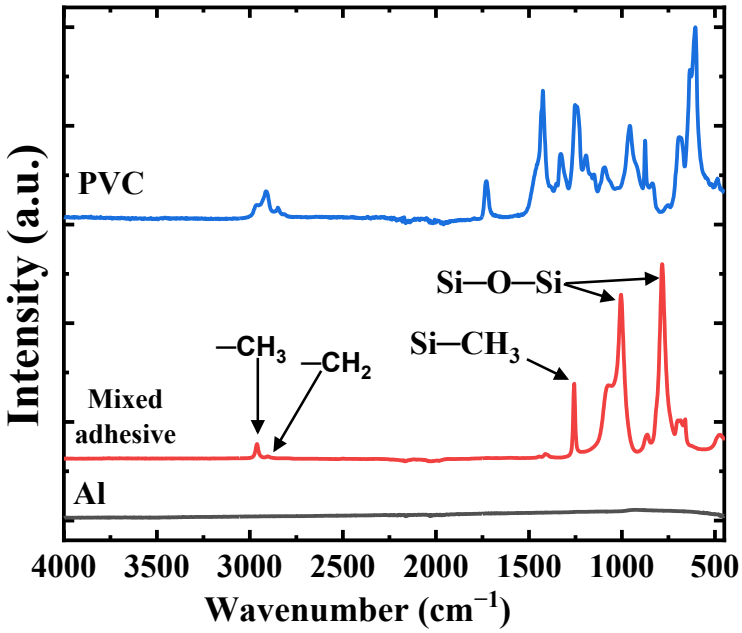

Figure 8.4 ATR-FTIR spectra of mixed adhesive of epoxy and silicone, PVC and Al surfaces.

The presence of Si components in the mixed adhesive shows promise for enhancing bonding with the mixed adhesive compared with those bonded with silicone individually. Further mechanical tests were carried out on the Al/PVC adhesive joints prepared using the pure silicone adhesive and mixed adhesive. The SLS strength of the Al/PVC bonded joints with pure silicone were found to be 0.43 MPa, while the joint strength using the mixed adhesive increased to 2.21 MPa, showing 413% enhancement. This behavior can be attributable to the affinity of low-surface-energy PVC to silicone. The results show that the mixing of epoxy with silicone at an equal proportion provides an increment in the joint strengths, with the mixed adhesive having excellent compatibility with Al/PVC.

8.5 Summary and Conclusions

A simple modification of the adhesive chemistry by combining epoxy and silicone resulted in a significant enhancement of the interfacial joint strength between the mixed adhesive and PVC when bonded with aluminum. The ATR-FTIR analysis presented the presence of overlapping $–CH_2$, $–CH_3$ and $Si–CH_3$ functional groups, which shows the chemical affinity of the mixed-adhesive molecules over the PVC surface. A maximum shear strength of ~2.2 MPa was obtained with 413% enhancement using the mixed adhesive compared to the joints prepared with the pure silicone adhesive. Further work is in progress to obtain an in-depth understanding of using and optimizing adhesive mixture proportions.

Chapter 9: Conclusions and future recommendations

9.1 Conclusions

Adhesive bonding between two surfaces is governed by two important properties: surface roughness and chemical affinity. Achieving surfaces with desirable properties involves precise engineering, accomplished through the careful optimization parameters of surface treatment. In the present work, a systematic study was carried out focusing on structural adhesive bonding between two similar (Al/Al) and two dissimilar (Al/PVC) materials. In this regard, the surfaces of Al and PVC were prepared employing a range of surface treatment techniques, including mechanical, electrochemical and physical. The subsequent changes in microrough structures of surfaces were methodically analyzed using scanning electron microscopy (SEM) and 3D-optical profilometry. The chemical compositions of these surfaces were analyzed using Attenuated Total Reflectance-Fourier Transform Infrared Spectroscopy (ATR-FTIR) and energy dispersive X-ray spectroscopy (EDS). The ASTM-D1002 standard was followed to bond these surfaces and their SLS strength was tested using a mechanical testing system (MTS).

Based on the results, the following conclusion can be drawn:

1. The mechanically abraded surfaces of Al, exhibited the emergence of micro-rough structures as a result of the removal of the ultrathin native oxide layer. This removal facilitated a more effective interaction between adhesive molecules and the aluminum metal, enhancing the adhesive bonding process. The adhesively bonded surface of Al/Al modified with 2C-methyl methacrylate (Adhesive #1), demonstrated a notable 46% increase in SLS

strength compared to the as-received Al/Al. Furthermore, the aging effect of SLS strength of adhesive joints in both DI water and aqueous NaCl salt solution showed higher degradation with increased concentration of salt.

2. The scanning electron microscopy analysis visibly confirmed the presence and growth of pores on the anodized aluminum surfaces. Additionally, the 3D-optical profilometer provided an optimum rms roughness of 1.4 μm. These porous microrough structures offered better mechanical anchoring to the adhesive as compared to as-received Al. As a result, the SLS strength of adhesively joined anodized Al surfaces increased significantly, reaching 21 MPa, i.e., 2.3 times higher than as-received Al surfaces.

3. A novel in-situ silanization during anodization of Al in the aqueous salt solution of $Zn(NO_3)_2$ were performed to incorporate silane (GPS) in the anodized pores for their chemical modification as well as obtaining two tire roughness. In situ silanization shows the microroughness of 7 μm, whereas, the microroughness is found to be 3.9 μm without silane. An enhancement in the microroughness was found to be 79% due to in-situ silanization. The ATR-FTIR spectra confirmed the impregnation of silane molecules with the presence of Si-O-Si peak around 1050 cm^{-1}. The SLS strength of adhesively bonded On bonding these surfaces adhesively, the SLS strength exhibited a relative gain of 160% as compared to the as-received Al.

4. Al and PVC were chosen to study the bond strength of two dissimilar materials. In this study three different types of Al surfaces were chosen, such as: (i) as-received (ii) chemically etched, and (iii) electrochemically anodized. In contrast, the corona discharge was performed

to modify the surfaces of PVC. With an increased time of exposure of corona discharge revealed, without altering the microroughness, a linear increase in –OH polar functional groups on the surfaces of PVC substrate. The observed water contact angle on the surface of PVC was analyzed to be decreased to 36° from 98° due to corona discharge. The highest SLS strength was found to be 12.4 MPa for the joint prepared with corona discharge PVC and anodized Al. The relative gain of bond strength was estimated to be 300%, as compared to as-received PVC and as-received Al.

5. Besides the surface treatments, an attempt has been made to understand the joining mechanism of multi-materials using mixed adhesives. In this study two chemically different adhesives, namely, epoxy and silicone were mixed to bond as-received Al and as-received PVC. The ATR-FTIR analysis confirmed the presence of overlapping $–CH_2$, $–CH_3$ and $Si–CH_3$ functional groups both in mixed adhesive and PVC surfaces. This overlapping provides the chemical affinity between the mixed-adhesive and PVC. Hence, the bonding strength is increased by 413%, as compared to the adhesive joints prepared with the only silicone.

6. In the case of Al/Al bonding, three surface treatments were utilized, e.g. (i) mechanical aberration, (ii) salt anodization and (iii) in-situ silanization during anodization. All the three cases the bond strength was found to higher as compared to the as-received Al surface. The highest relative gain in SLS strength was found in the Al samples prepared using in-situ silanization during anodization. Compared to conventional acidic electrolytes used during anodization, the SLS (strength of adhesively bonded surfaces) of aluminum subjected to aqueous salt electrolyte was remarkably similar. This provides a green process for surface preparation for large-scale industrial components.

9.2 Future recommendation

Based on the findings of this study, the following sections outlines potential research directions to extend our understanding of surface preparation fundamentals, which is crucial for the adhesive bonding mechanism.

1. In this research, it has been observed that electrochemical anodization of aluminum in an aqueous salt solution results in the growth of a thin porous oxide layer. This layer plays a crucial role in providing mechanical anchoring to the adhesive, particularly when its thickness is in the range of a few microns. Therefore, it becomes essential to explore ways of increasing the thickness of these porous layers. To achieve this, a careful selection of anodization parameters, such as voltage, temperature, and current density, is essential to promote the growth of a thick, porous oxide layer.

2. A novel method of in-situ silanization during electrochemical anodization uses an organosilane of GPS and an inorganic salt of zinc nitrate ($Zn(NO_3)_2$. A suitable combination of other organosilane with an inorganic salt may result in different surface morphology and change in chemical composition. Therefore, a potential chemically enriched surface can be produced, which can demonstrate a stronger chemical interaction to enhance the adhesive bonding at the interface of prepared surface and adhesive. An attempt should be made for in-situ silanization using inorganic acid as the porous structures are well controlled in the acidic electrolyte.

3 According to the finding of this thesis, incorporating polar functional groups onto the surface of PVC by corona discharge enhanced its hydrophilicity. This incorporation

increased the chemical affinity towards the adhesive material, promoting effective bonding with Al. However, the corona discharge treatment does not last longer, as PVC demonstrates an exponentially fast regaining capacity. In this regard, plasma etching could serve as a potential alternative to the corona discharge technique, as it might effectively modifies the surface topography and chemistry of PVC.

4 Although we have demonstrated that the surface treatments developed in this work are stable with respect to the protection of surfaces under laboratory conditions, further evaluation is necessary. Before proceeding to real-world applications, it is essential to assess the durability of the prepared surfaces. This evaluation should encompass factors such as resistance to rough handling, prolonged exposure to the environment, and the potential for corrosion and contamination of the surface.

5. Exploring fundamental aspects of surface preparation for adhesive bonding, as discussed in this dissertation, involves delving into various aspects like chemical bonding, van der Waals interactions, and mechanical anchoring. Further research in these areas, including theoretical work, would contribute to a deeper understanding.

References

1. Adams, R.D., Adams, R.D., Comyn, J., Wake, W.C. and Wake, W.C., *Structural adhesive joints in engineering*. Springer Science & Business Media, 1997.

2. Alexander, B.H., Checkoway, H. and Wechsler, L., Lung cancer in chromate-exposed aerospace workers. *Occupational Health and Industrial Medicine*, 1997. 3: p.119.

3. Lim, J.D., Lee, P.M., Rhee, D.M.W., Leong, K.C. and Chen, Z., *Effect of surface treatment on adhesion strength between magnetron sputtered copper thin films and alumina substrate.* Applied Surface Science, 2015. 355: p.509-515.

4. Hu, Y., Yuan, B., Cheng, F. and Hu, X., *NaOH etching and resin pre-coating treatments for stronger adhesive bonding between CFRP and aluminium alloy.* Composites Part B: Engineering, 2019. 178: p.107478.

5. Dahuri, S. M., Subri, N. H. A., & Noor, N. M., *Stress Analysis of Engine Camshaft from Light Metal.* 2018.

6. Eftekhari, A., & Corrochano, P., *Electrochemical energy storage by aluminum as a lightweight and cheap anode/charge carrier*. Sustainable Energy & Fuels, 2017. 1(6): p. 1246-1264.

7. Martin, J., & Plain, J., *Fabrication of aluminium nanostructures for plasmonics*. Journal of Physics D: Applied Physics, 2014. 48(18): p. 184002.

8. Zheng, S., Li, C., Fu, Q., Xiang, T., Hu, W., Wang, J., et al., *Fabrication of a micro-nanostructured superhydrophobic aluminium surface with excellent corrosion resistance and anti-icing performance.* RSC advances, 2016. 6(83): p. 79389-79400.

9. Ardelean, M., Lascău, S., Ardelean, E., & Josan, A., *Surface treatments for aluminium alloys*. In IOP Conference Series: Materials Science and Engineering, 2018. Vol. 294, No. 1, p. 012042.

10. Xiong, G., Kang, P., Zhang, J., Li, B., Yang, J., Chen, G., Zhou, Z. and Li, Q., *Improved adhesion, heat resistance, anticorrosion properties of epoxy resins/POSS/methyl phenyl silicone coatings,* Progress in Organic Coatings, 2019, 135: pp.454-464.

11. Sieber, M., Morgenstern, R., Kuhn, D., Hackert-Oschätzchen, M., Schubert, A., & Lampke, T., *Downscaled anodic oxidation process for aluminium in oxalic acid*. In IOP Conference Series: Materials Science and Engineering, 2007. Vol. 181, No. 1, p. 012044.

12. Wielage, B., Alisch, G., Lampke, T., & Nickel, D., *Anodizing–a key for surface treatment of aluminium.* In Key Engineering Materials, Trans Tech Publications Ltd., 2008. Vol. 384, p. 263-281.

13. Contreras, A. L., Kuit, W., Siemerink, M. A. J., Kengen, S. W. M., Springer, J., & Claassen, P. A. M., *Production of longer-chain alcohols from lignocellulosic biomass: butanol, isopropanol and 2, 3-butanediol.* In Bioalcohol production, Woodhead Publishing, 2010. p. 415-460.

14. Saleema, N., Sarkar, D.K., Paynter, R.W., Gallant, D. and Eskandarian, M,. *A simple surface treatment and characterization of AA 6061 aluminum alloy surface for adhesive bonding applications.* Applied Surface Science, 2012. 261, p.742-748.

15. Sulka, G. D., Zaraska, L., & Stepniowski, W. J., *Anodic porous alumina as a template for nanofabrication.* In Encyclopedia of nanoscience and nanotechnology, American Scientific Publishers. 2011.11(349): p. 261-349.

16. Lee, W., Schwirn, K., Steinhart, M., Pippel, E., Scholz, R., & Gösele, U., *Structural engineering of nanoporous anodic aluminium oxide by pulse anodization of aluminium.* Nature nanotechnology, 2008. 3(4), 234-239.

17. Mínguez-Bacho, I., Rodríguez-López, S., Climent, A., Fichou, D., Vázquez, M., & Hernández-Vélez, M., *Influence of sulfur incorporation into nanoporous anodic alumina on the volume expansion and self-ordering degree.* The Journal of Physical Chemistry C, 2015. 119(49), 27392-27400.

18. Lohrengel, M.M., *Thin anodic oxide layers on aluminium and other valve metals: high field regime*. Materials Science and Engineering: R: Reports, 1993. 11(6): p.243-294.

19. Föll, H., Christophersen, M., Carstensen, J. and Hasse, G., *Formation and application of porous silicon*. Materials Science and Engineering: R: Reports, 2002. 39(4): p.93-141.

20. Diggle, J.W., Downie, T.C. and Goulding, C.W., Anodic oxide films on aluminum. Chemical Reviews, 1969. 69(3), pp.365-405.

21. Lee, W., *The anodization of aluminum for nanotechnology applications.* JOM, 2010. 62(6): p. 57-63.

22. Nicewarner-Pena, S.R., Freeman, R.G., Reiss, B.D., He, L., Peña, D.J., Walton, I.D., Cromer, R., Keating, C.D. and Natan, M.J., *Submicrometer metallic barcodes*. Science, 2001. 294(5540): p.137-141.

23. Lee, W., Scholz, R., Nielsch, K. and Gösele, U., *A template-based electrochemical method for the synthesis of multisegmented metallic nanotubes.* Angewandte Chemie International Edition, 2005. 44(37): p.6050-6054.

24. Huang, Z., Zhang, X., Reiche, M., Liu, L., Lee, W., Shimizu, T., Senz, S. and Gösele, U., Extended arrays of vertically aligned sub-10 nm diameter [100] Si nanowires by metal-assisted chemical etching. Nano letters, 2008. 8(9): p.3046-3051.

25. Liu, L., Lee, W., Scholz, R., Pippel, E. and Gösele, U., *Tailor-Made Inorganic Nanopeapods: Structural Design of Linear Noble Metal Nanoparticle Chains*. Angewandte Chemie International Edition, 2008. 47(37): p.7004-7008.

26. Huang, Z., Zhang, W., Yu, J. and Gao, D., Nanoporous alumina membranes for enhancing hemodialysis. 2007.

27. Ding, D., Chen, Z., Rajaputra, S. and Singh, V., *Hydrogen sensors based on aligned carbon nanotubes in an anodic aluminum oxide template with palladium as a top electrode.* Sensors and Actuators B: Chemical, 2007. 124(1): p.12-17.

28. Gong, D., Yadavalli, V., Paulose, M., Pishko, M. and Grimes, C.A., *Controlled molecular release using nanoporous alumina capsules*. Biomedical Microdevices, 2003. 5(1), pp.75-80.

29. Fan, Z., Razavi, H., Do, J.W., Moriwaki, A., Ergen, O., Chueh, Y.L., Leu, P.W., Ho, J.C., Takahashi, T., Reichertz, L.A. and Neale, S., *Three-dimensional nanopillar-array photovoltaics on low-cost and flexible substrates.* Nature materials, 2009. 8(8): p.648-653.

30. Asoh, H., Nishio, K., Nakao, M., Tamamura, T. and Masuda, H., *Conditions for fabrication of ideally ordered anodic porous alumina using pretextured Al*. Journal of the Electrochemical Society, 2001. 148(4): p. B152-B156.

31. Kwolek, P., *Hard anodic coatings on aluminum alloys*. Advances in Manufacturing Science and Technology, 2017. 41(3), pp.35-46.

32. Lee, W., Schwirn, K., Steinhart, M., Pippel, E., Scholz, R. and Gösele, U., *Structural engineering of nanoporous anodic aluminium oxide by pulse anodization of aluminium.* Nature nanotechnology, 2008. 3(4): p.234-239.

33. Makhlouf, A. S. H., *Protective coatings for automotive, aerospace and military applications: current prospects and future trends*. In Handbook of Smart Coatings for Materials Protection, Woodhead Publishing. 2014.: p. 121-131.

34. Vermeşan, H., Coroziune şi protecţie anticorozivă. Risoprint, 2008.

35. Chatterjee, A.K., *X-ray diffraction*. Handbook of analytical techniques in concrete science and technology, 200: p.275-332.

36. Araoyinbo, A.O., Noor, A.F.M., Sreekantan, S. and Aziz, A., *Voltage Effect on Electrochemical Anodization of Aluminum at Ambient Temperature*. International Journal of Mechanical and Materials Engineering, 2010. 5(1): p.53-58.

37. Fay, F., Linossier, I., Langlois, V., Haras, D. and Vallee-Rehel, K., *SEM and EDX analysis: two powerful techniques for the study of antifouling paints.* Progress in Organic Coatings, 2005. 54(3): p.216-223.

38. Wang, H.W., Skeldon, P., Thompson, G.E. and Stevens, K., *Hard anodising of aluminium alloys.* In ASST 2000: aluminium surface science and technology 2000: p. 588-593.

39. Nakajima, D., Kikuchi, T., Yoshioka, T., Matsushima, H., Ueda, M., Suzuki, R.O. and Natsui, S., *A Superhydrophilic Aluminum Surface with Fast Water Evaporation Based on Anodic Alumina Bundle Structures via Anodizing in Pyrophosphoric Acid.* Materials, 2019. 12(21): p.3497.

40. https://www.nanoscience.com/techniques/optical-profilometry/

41. https://www.ukessays.com/essays/engineering/theory-of-tensile-test-engineering-essay.php

42. Thrall, E. W., & Shannon, R. W., *Adhesive bonding of aluminum alloys*, 1985.

43. Zhang, J. S., Zhao, X. H., Zuo, Y., & Xiong, J. P., *The bonding strength and corrosion resistance of aluminum alloy by anodizing treatment in a phosphoric acid modified boric acid/sulfuric acid bath.* Surface and Coatings Technology, 2008. 202(14): p. 3149-3156.

44. Mullins, W. M., & Averbach, B. L., *The electronic structure of anodized and etched aluminum alloy surfaces.* Surface Science, 1988. 206(1-2), 52-60.

45. Chen, Y., Xin, X., Zhang, N., & Xu, Y. J., *Aluminum-Based Plasmonic Photocatalysis.* Particle & Particle Systems Characterization, 2017. 34(8): p. 1600357.

46. Smith, T., *Surface Treatment for Aluminum Bonding (STAB).* The Journal of Adhesion, 1977. 8(4), 313-320.

47. Cohn, C. C., U.S. Patent No. 2,729,551. Washington, DC: U.S. Patent and Trademark Office, 1956.

48. Carroll, J.A. and Newhard, J.N.J., *Amchem Products Inc, Method of and solution for the surface treatment of aluminum*. U.S. Patent 2,825,697, 1958.

49. Golru, S.S., Attar, M.M. and Ramezanzadeh, B., *Effects of different surface cleaning procedures on the superficial morphology and the adhesive strength of epoxy coating on aluminium alloy 1050*. Progress in Organic Coatings, 2015. 87: p.52-60.

50. Abbey, K.J., *Advances in epoxy adhesives*. In Advances in structural adhesive bonding, Woodhead Publishing, 2010: p. 20-34.

51. Petrie, E.M., *Adhesive bonding of textiles: principles, types of adhesive and methods of use*. In Joining Textiles, Woodhead Publishing, 2013: pp. 225-274.

52. Burchardt, B., *Advances in polyurethane structural adhesives.* In Advances in structural adhesive bonding, Woodhead Publishing. 2010: pp. 35-65.

53. Web of Science Group, a Clarivate company. *Web of Science Master Journal List - Wos MJL by Clarivate*, mjl.clarivate.com/home. Accessed 20 Nov. 2023.

54. Brockmann, W., Geiß, P.L., Klingen, J. and Schröder, K.B., 2009. *Adhesive bonding: materials, applications and technology*. John Wiley & Sons.

55. Wake, W.C., 1978. Theories of adhesion and uses of adhesives: a review. *Polymer*, *19*(3), pp.291-308.

56. Skeist, I. and Miron, J., 1981. History of adhesives. *Journal of Macromolecular Science—Chemistry*, *15*(6), pp.1151-1163.

57. Allen, K.W., 1993. Some reflections on contemporary views of theories of adhesion. *International journal of adhesion and adhesives*, *13*(2), pp.67-72.

58. Packham, D.E., 2003. The mechanical theory of adhesion. *Handbook of adhesive technology*, pp.69-93.

59. Voyutskiĭ, S.S., 1960. The diffusion theory of adhesion. *Rubber Chemistry and Technology*, *33*(3), pp.748-756.

60. Derjaguin, B.V. and Smilga, V.P., 1967. Electronic theory of adhesion. *Journal of applied Physics*, *38*(12), pp.4609-4616.

61. Packham, D.E., 2011. Theories of fundamental adhesion. *Handbook of adhesion technology*, pp.9-38.

62. Liang, Y., Hilal, N., Langston, P. and Starov, V., 2007. Interaction forces between colloidal particles in liquid: Theory and experiment. *Advances in colloid and interface science*, *134*, pp.151-166.

63. Bormashenko, E.Y., 2018. *Wetting of real surfaces* (Vol. 19). Walter de Gruyter GmbH & Co KG.

64. Ebnesajjad, S. and Ebnesajjad, C., 2013. *Surface treatment of materials for adhesive bonding*. William Andrew.

65. Bishopp, J., 2005. Aerospace: a pioneer in structural adhesive bonding. In *Handbook of adhesives and sealants* (Vol. 1, pp. 215-347). Elsevier Science Ltd.

66. Shanahan, M. and Spivak, M., 2021. Resin use by stingless bees: A review. *Insects*, *12*(8), p.719.

67. Song, Y., Wang, Z., Li, Y. and Dai, Z., 2022. Electrostatic attraction caused by triboelectrification in climbing geckos. *Friction*, *10*, pp.44-53.

68. Ditsche, P., Michels, J., Kovalev, A., Koop, J. and Gorb, S., 2014. More than just slippery: the impact of biofilm on the attachment of non-sessile freshwater mayfly larvae. *Journal of the Royal Society Interface*, *11*(92), p.20130989.

69. Davies, R.G. and Davies, R.G., 1988. Insect structure and function. *Outlines of Entomology*, pp.7-96.

70. Fang, Z., Cao, J., Guan, Y., Fang, Z., Cao, J. and Guan, Y., 2020. Anticorrosion Structural Design for Aluminum Alloy Vessel. *Corrosion Control Technologies for Aluminum Alloy Vessel*, pp.343-357.

71. Saile, V., Manufacturing Technologies for Polymer Microsystem.

72. Vernengo, A.J., 2016. Adhesive materials for biomedical applications. *Adhesives-Applications and Properties*, *6*, pp.111-133.

73. Wu, H., Huang, B. and Zare, R.N., 2005. Construction of microfluidic chips using polydimethylsiloxane for adhesive bonding. *Lab on a Chip*, *5*(12), pp.1393-1398.

74. Jeevi, G., Nayak, S.K. and Abdul Kader, M., 2019. Review on adhesive joints and their application in hybrid composite structures. *Journal of Adhesion Science and Technology*, *33*(14), pp.1497-1520.

75. Park, S.Y., Choi, W.J., Choi, H.S., Kwon, H. and Kim, S.H., 2010. Recent trends in surface treatment technologies for airframe adhesive bonding processing: a review (1995–2008). *The Journal of Adhesion*, *86*(2), pp.192-221.

76. Zhang, J.S., Zhao, X.H., Zuo, Y. and Xiong, J.P., 2008. The bonding strength and corrosion resistance of aluminum alloy by anodizing treatment in a phosphoric acid modified boric acid/sulfuric acid bath. *Surface and Coatings Technology*, *202*(14), pp.3149-3156.

77. Rudawska A (2015) Adhesive Properties of Metals and Metal Alloys. Surface Energy. InTech. Available at: http://dx.doi.org/10.5772/60599.

78. Lim, J.D., Lee, P.M., Rhee, D.M.W., Leong, K.C. and Chen, Z., Effect of surface treatment on adhesion strength between magnetron sputtered copper thin films and alumina substrate. Applied Surface Science, 2015. 355: p.509-515.

79. Boutar, Y., Naïmi, S., Mezlini, S. and Ali, M.B.S., Effect of surface treatment on the shear strength of aluminium adhesive single-lap joints for automotive applications. International Journal of Adhesion and Adhesives, 2016. 67: p.38-43.

80. Hu, Y., Yuan, B., Cheng, F. and Hu, X., NaOH etching and resin pre-coating treatments for stronger adhesive bonding between CFRP and aluminium alloy. Composites Part B: Engineering, 2019. 178: p.107478.

81. Abel, M.L., Allington, R.D., Digby, R.P., Porritt, N., Shaw, S.J. and Watts, J.F., 2006. Understanding the relationship between silane application conditions, bond durability and locus of failure. *International journal of adhesion and adhesives*, *26*(1-2), pp.2-15.

82. Qiu, J., Sakai, E., Lei, L., Takarada, Y. and Murakami, S., 2012. Improving the shear strength by silane treatments of aluminum for direct joining of phenolic resin. *Journal of Materials Processing Technology*, *212*(11), pp.2406-2412.

83. Muhammad Zain, N., Ahmad, S.H. and Ernie, S.A., Green polyurethane adhesive bonding of aluminum: Effect of surface treatments. In Applied Mechanics and Materials, 2013. 393: p. 51-56

84. Zhang, D. and Huang, Y., 2021. Influence of surface roughness and bondline thickness on the bonding performance of epoxy adhesive joints on mild steel substrates. *Progress in Organic Coatings*, *153*, p.106135.

85. Shemtov-Yona, K., Rittel, D. and Dorogoy, A., 2014. Mechanical assessment of grit blasting surface treatments of dental implants. *journal of the mechanical behavior of biomedical materials*, *39*, pp.375-390.

86. Demir, H., Gullu, A., Ciftci, I. and Seker, U., 2010. An investigation into the influences of grain size and grinding parameters on surface roughness and grinding forces when grinding. *Journal of mechanical engineering*, *56*(7-8), pp.447-54.

87. Medvedev, A.E., Ng, H.P., Lapovok, R., Estrin, Y., Lowe, T.C. and Anumalasetty, V.N., 2016. Effect of bulk microstructure of commercially pure titanium on surface characteristics and fatigue properties after surface modification by sand blasting and acid-etching. *Journal of the mechanical behavior of biomedical materials*, *57*, pp.55-68.

88. Ghumatkar, A.K.S.H.A.Y., Budhe, S.A.N.D.I.P., Sekhar, R.A.V.I., Banea, M.D. and Barros, S.D., 2016. Influence of adherend surface roughness on the adhesive bond strength. *Latin American Journal of Solids and Structures*, *13*, pp.2356-2370.

89. Shafiei, F., Behroozibakhsh, M., Abbasian, A. and Shahnavazi, S., Bond strength of self-adhesive resin cement to base metal alloys having different surface treatments. Dental research journal, 2018. 15(1): p.63.

90. Zhang, D. and Huang, Y., 2021. Influence of surface roughness and bondline thickness on the bonding performance of epoxy adhesive joints on mild steel substrates. *Progress in Organic Coatings*, *153*, p.106135.

91. Wang, B., Hu, X. and Lu, P., 2017. Improvement of adhesive bonding of grit-blasted steel substrates by using diluted resin as a primer. *International Journal of Adhesion and Adhesives*, *73*, pp.92-99.

92. Strobel, M., Jones, V., Lyons, C.S., Ulsh, M., Kushner, M.J., Dorai, R. and Branch, M.C., 2003. A comparison of corona-treated and flame-treated polypropylene films. *Plasmas and Polymers*, *8*, pp.61-95.

93. Kruse, A., Krüger, G., Baalmann, A. and Hennemann, O.D., 1995. Surface pretreatment of plastics for adhesive bonding. *Journal of adhesion science and technology*, *9*(12), pp.1611-1621.

94. Han, G., Tan, B., Cheng, F., Wang, B., Leong, Y.K. and Hu, X., 2022. CNT toughened aluminium and CFRP interface for strong adhesive bonding. *Nano Materials Science*, *4*(3), pp.266-275.)

95. Critchlow, G., 1997. *Pretreatments for metal-to-metal bonding* (Doctoral dissertation, Loughborough University).

96. Palmieri, F.L., Watson, K.A., Morales, G., Williams, T., Hicks, R., Wohl, C.J., Hopkins, J.W. and Connell, J.W., 2012. Laser Ablation Surface Preparation of Ti-6A1-4V for Adhesive Bonding (No. NF1676L-13483).

97. Akram, M., Jansen, K.M.B., Ernst, L.J. and Bhowmik, S., 2011. Atmospheric pressure plasma surface modification of titanium for high temperature adhesive bonding. *International journal of adhesion and adhesives*, *31*(7), pp.598-604.

98. Tandjung, D., 2004. *Mixed-mode loading analysis on the lap shear specimen test per ASTM D1002*. California State University, Long Beach.

99. Mikhaylov A., Moiseev N., Aleshin K., Burkhardt T., Global climate change and greenhouse effect, Entrepreneurship and Sustainability Issues, 7 (2020) 2897.

100. Lorenzoni I., Nicholson-Cole S., Whitmarsh L., Barriers perceived to engaging with climate change among the UK public and their policy implications, Global Environmental Change, 17 (2007) 445–59.

101. Kwakernaak A., Hofstede J., Poulis J., Benedictus R., Improvements in bonding metals (steel, aluminium), Advances in Structural Adhesive Bonding, Elsevier, 2010, pp. 185–236.

102. Adedeji O., Global climate change, Journal of Geoscience and Environment Protection, 2 (2014) 114.

103. Melentiev R., Yudhanto A., Tao R., Vuchkov T., Lubineau G., Metallization of polymers and composites: State-of-the-art approaches, Materials & Design, (2022) 110958.

104. Kwakernaak A., Hofstede J., Poulis J., Benedictus R., Improvements in bonding metals for aerospace and other applications, Welding and Joining of Aerospace Materials, Elsevier, 2012, pp. 229-75.

105. Djurišić A.B., Leung Y.H., Ng A.M., Xu X.Y., Lee P.K., Degger N., et al., Toxicity of metal oxide nanoparticles: mechanisms, characterization, and avoiding experimental artefacts, Small, 11 (2015) 26-44.

106. Shields J., Adhesives handbook, Elsevier, 2013.

107. Van Meerbeek B., Perdigao J., Lambrechts P., Vanherle G., The clinical performance of adhesives, Journal of dentistry, 26 (1998) 1-20.

108. Delzendehrooy F., Akhavan-Safar A., Barbosa A., Beygi R., Cardoso D., Carbas R., et al., A comprehensive review on structural joining techniques in the marine industry, Composite Structures, 289 (2022) 115490.

109. AL-Oqla F.M., Hayajneh M.T., Nawafleh N., Advanced synthetic and biobased composite materials in sustainable applications: a comprehensive review, Emergent Materials, (2023) 1-18.

110. Barnes T., Pashby I., Joining techniques for aluminium spaceframes used in automobiles: Part II—adhesive bonding and mechanical fasteners, Journal of materials processing technology, 99 (2000) 72-9.

111. Rodrigues D.D., Winfield P.H., Morrey D., Disbonding technology for adhesive reversible assembly in the automotive industry, Materials Science Forum, Trans Tech Publ, 2013, pp. 766-70.

112. Alderucci T., Borsellino C., Di Bella G., Effect of surface pattern on strength of structural lightweight bonded joints for marine applications, International Journal of Adhesion and Adhesives, 117 (2022) 103005.

113. Noury P., Hayman B., McGeorge D., Weitzenbock J., Lightweight construction for advanced shipbuilding-recent development, Proceedings of the 37th WEGEMT summer school, (2002) 11-5.

114. Braga D.F., Tavares S., Da Silva L.F., Moreira P., De Castro P.M., Advanced design for lightweight structures: Review and prospects, Progress in Aerospace Sciences, 69 (2014) 29-39.

115. Flegel H.A., The future of adhesive bonding as a joining technique, AutoTechnology, 2 (2002) 64-7.

116. Prolongo S., Ureña A., Effect of surface pre-treatment on the adhesive strength of epoxy–aluminium joints, International Journal of Adhesion and Adhesives, 29 (2009) 23-31.

117. Lunder O., Olsen B., Nisancioglu K., Pre-treatment of AA6060 aluminium alloy for adhesive bonding, International journal of adhesion and adhesives, 22 (2002) 143-50.

118. Cavezza F., Boehm M., Terryn H., Hauffman T., A review on adhesively bonded aluminium joints in the automotive industry, Metals, 10 (2020) 730.

119. Harris A., Beevers A., The effects of grit-blasting on surface properties for adhesion, International journal of adhesion and adhesives, 19 (1999) 445-52.

120. Shemtov-Yona K., Rittel D., Dorogoy A., Mechanical assessment of grit blasting surface treatments of dental implants, journal of the mechanical behavior of biomedical materials, 39 (2014) 375-90.

121. Ramaswamy K., O'Higgins R.M., Kadiyala A.K., McCarthy M.A., McCarthy C.T., Evaluation of grit-blasting as a pre-treatment for carbon-fibre thermoplastic composite to aluminium bonded joints tested at static and dynamic loading rates, Composites Part B: Engineering, 185 (2020) 107765.

122. Varacalle D.J., Guillen D.P., Deason D.M., Rhodaberger W., Sampson E., Effect of grit-blasting on substrate roughness and coating adhesion, Journal of thermal spray technology, 15 (2006) 348-55.

123. Teng J.-G., Fernando D., Yu T., Zhao X., Treatment of steel surfaces for effective adhesive bonding, Advances in FRP Composites in Civil Engineering: Proceedings of the 5th International Conference on FRP Composites in Civil Engineering (CICE 2010), Sep 27–29, 2010, Beijing, China, Springer, 2011, pp. 865-8.

124. Hu Y., Zhang J., Wang L., Jiang H., Cheng F., Hu X., A simple and effective resin pre-coating treatment on grinded, acid pickled and anodised substrates for stronger adhesive bonding between Ti-6Al-4V titanium alloy and CFRP, Surface and Coatings Technology, 432 (2022) 128072.

125. Müller M., Valášek P., Interaction of steel surface treatment by means of abrasive cloth and adhesive bond strength, Manufacturing technology, 10 (2010) 49-57.

126. Hu Y., Yuan B., Cheng F., Hu X., NaOH etching and resin pre-coating treatments for stronger adhesive bonding between CFRP and aluminium alloy, Composites Part B: Engineering, 178 (2019) 107478.

127. Fernando D., Teng J.-G., Yu T., Zhao X.-L., Preparation and characterization of steel surfaces for adhesive bonding, Journal of Composites for Construction, 17 (2013) 04013012.

128. Molitor P., Barron V., Young T., Surface treatment of titanium for adhesive bonding to polymer composites: a review, International Journal of Adhesion and Adhesives, 21 (2001) 129-36.

129. Wang B., Hu X., Lu P., Improvement of adhesive bonding of grit-blasted steel substrates by using diluted resin as a primer, International Journal of Adhesion and Adhesives, 73 (2017) 92-9.

130. Hamdan S., Evans J., The surface treatment and adhesive bonding of polyetheretherketone. Part I. Adhesive joint strength, Journal of Adhesion Science and Technology, 1 (1987) 281-9.

131. Slătineanu L., Potârniche Ş., Coteaţă M., Grigoraş I., Gherman L., Negoescu F., Surface roughness at aluminium parts sand blasting, Proceedings in Manufacturing Systems, 6 (2011) 69-74.

132. Abid J., Raza H., Akhtar A., Gohar G.A., Ullah S., Akram M., et al., Effect of surface roughness on shear strength of bonded joints of aluminum Al 6061 T6 substrate, VW Applied Sciences, 2 (2020) 87-91.

133. Ghumatkar A., Budhe S., Sekhar R., Banea M., Barros S.d., Influence of adherend surface roughness on the adhesive bond strength, Latin American Journal of Solids and Structures, 13 (2016) 2356-70.

134. Da Silva L.F., Carbas R., Critchlow G.W., Figueiredo M., Brown K., Effect of material, geometry, surface treatment and environment on the shear strength of single lap joints, International Journal of Adhesion and Adhesives, 29 (2009) 621-32.

135. Zielecfei W., Pawlus P., Perłowski R., Dzierwa A., Surface topography effect on strength of lap adhesive joints after mechanical pre-treatment, Archives of civil and mechanical engineering, 13 (2013) 175-85.

136. Watts J., Castle J., The application of X-ray photoelectron spectroscopy to the study of polymer-to-metal adhesion: Part 2 The cathodic disbondment of epoxy coated mild steel, Journal of materials science, 19 (1984) 2259-72.

137. Rudawska A., Adhesive properties of metals and metal alloys, InTech: Rijeka, Croatia, (2015) 85-121.

138. Yi J., Li X., Ding J., Seet H., Study of the grain size, particle size and roughness of substrate in relation to the magnetic properties of electroplated permalloy, Journal of alloys and compounds, 428 (2007) 230-6.

139. Mao L., Cooper J.R., Frostick L.E., Grain size and topographical differences between static and mobile armour layers, Earth Surface Processes and Landforms, 36 (2011) 1321-34.

140. Zhang J.-s., Zhao X.-h., Zuo Y., Xiong J.-p., The bonding strength and corrosion resistance of aluminum alloy by anodizing treatment in a phosphoric acid modified boric acid/sulfuric acid bath, Surface and Coatings Technology, 202 (2008) 3149-56.
141. Li Y.-d., Zhao P.-z., Feng Y.-j., Cao H.-l., Influence of anodic oxide film structure on adhesive bonding performance of 5754 aluminum alloy, Transactions of Nonferrous Metals Society of China, 29 (2019) 1836-41.

142. Ebnesajjad S., Adhesives for medical and dental applications, Handbook of Polymer Applications in Medicine and Medical Devices, Elsevier, 2011, pp. 103-29.

143. N'diaye M., Pascaretti-Grizon F., Massin P., Baslé M.F., Chappard D., Water absorption of poly (methyl methacrylate) measured by vertical interference microscopy, Langmuir, 28 (2012) 11609-14.

144. Ogawa T., Hasegawa A., Effect of curing environment on mechanical properties and polymerizing behaviour of methyl-methacrylate autopolymerizing resin, Journal of oral rehabilitation, 32 (2005) 221-6.

145. Alia C., Biezma M.V., Pinilla P., Arenas J.M., Suárez J.C., Degradation in seawater of structural adhesives for hybrid fibre-metal laminated materials, Advances in Materials Science and Engineering, 2013 (2013).

146. Farid R., Rajan K., Sarkar D.K., Enhanced corrosion protection of aluminum by ultrasonically dip coated sodium silicate thin films, Surface and Coatings Technology, 374 (2019) 355-61.

147. Mu W.-L., Xu Q.-H., Na J.-X., Wang H., Tan W., Li D.-F., Influence of temperature and humidity on the fatigue behaviour of adhesively bonded CFRP/aluminium alloy joints, The Journal of Adhesion, 98 (2022) 1358-76.

148. Hua D., Lin J., Zhang B., Effects of salt spray on the mechanical properties of aluminum-epoxy adhesive joints, Journal of adhesion science and technology, 27 (2013) 1580-9.

149. Zain NM, Ahmad SH, Ali ES (2014) Effect of surface treatments on the durability of green polyurethane adhesive bonded aluminium alloy. International Journal of Adhesion and Adhesives 55:43-55. doi: 10.1016/j.ijadhadh.2014.07.007

150. Saleema, N., Sarkar, D.K., Paynter, R.W., Gallant, D. and Eskandarian, M., 2012. A simple surface treatment and characterization of AA 6061 aluminum alloy surface for adhesive bonding applications. Applied Surface Science, 261, pp.742-748.

151. Sarkar, D.K., Brassard, D., El Khakani, M.A. and Ouellet, L., 2007. Dielectric properties of sol–gel derived high-k titanium silicate thin films. Thin Solid Films, 515(11), pp.4788-4793.

152. Luecken DJ, Waterland RL, Papasavva S, Taddonio KN, Hutzell WT, Rugh JP, Andersen, SO. Ozone and TFA impacts in North America from degradation of 2, 3, 3, 3-tetrafluoropropene (HFO-1234yf), a potential greenhouse gas replacement. Environ Sci Technol 2010;44:343-348.

153. Lamb WF, Wiedmann T, Pongratz J, Andrew R, Crippa M, Olivier JG, Wiedenhofer D, Mattioli G, Al Khourdajie A, House J. A review of trends and drivers of greenhouse gas emissions by sector from 1990 to 2018. Environ Res Lett 2021;16:073005.

154. Zheng X, Streimikiene D, Balezentis T, Mardani A, Cavallaro F, Liao H. A review of greenhouse gas emission profiles, dynamics, and climate change mitigation efforts across the key climate change players. J Clean Prod 2019;234:1113-1133.

155. Martin EW, Shaheen SA. Greenhouse gas emission impacts of carsharing in North America. IEEE Trans Intell Transp Syst 2011;12:1074-1086.

156. Cristea A, Hummels D, Puzzello L, Avetisyan M. Trade and the greenhouse gas emissions from international freight transport. JEEM 2013;65:153-173.

157. Pervaiz M, Panthapulakkal S, Sain M, Tjong J. Emerging trends in automotive lightweighting through novel composite materials. Mater sci appl 2016;7:26.

158. Ayalon O, Avnimelech Y, Shechter M. Alternative MSW treatment options to reduce global greenhouse gases emissions-the Israeli example. Waste Manag Res 2000;18:538-544.

159. Gadesman K, Kuhnert F. The automotive industry and climate change framework and dynamics of the CO2 revolution. Pricewaterhouse Coopers AG 2007;127.

160. Yoshitake S, Ito Y, Miyamoto N, Yoshizaki R, Sugita N. Ultrafast and large-gap microwelding of glass substrates by selective absorption of continuous-wave laser into transiently excited electrons. CIRP Annals 2022.

161. Mishra RS, Ma Z. Friction stir welding and processing. Mater Sci Eng R Rep 2005;50:1-78.

162. Kah P, Suoranta R, Martikainen J, Magnus C. TECHNIQUES FOR JOINING DISSIMILAR MATERIALS: METALS AND POLYMERS. Rev Adv Mater Sci 2014;36.

163. Ha D-W, Jeon G-W, Shin J-S, Jeong C-Y. Mechanical properties of steel-aluminum multi-materials using a structural adhesive. Mater Today Commun 2020;25:101552.

164. Christodoulou L, Venables J D. Multifunctional material systems: The first generation. Jom 2003;55:39-45.

165. Dumitrascu N, Balau T, Tasca M, Popa G. Corona discharge treatment of the plastified PVC films obtained by chemical grafting. Mater Chem Phys 2000;65:339-344.

166. Pizzi A. Handbook of Adhesive Technology ed A. Pizzi and KL Mittal Basel: Marcel Dekker;2003

167. Suganya A, Shanmugavelayutham G, Rodríguez CS. Study on structural, morphological and thermal properties of surface modified polyvinylchloride (PVC) film under air, argon and oxygen discharge plasma. MRX 2016;3:095302.

168. Amancio-Filho S, Dos Santos J. Joining of polymers and polymer–metal hybrid structures: recent developments and trends. Polym Eng Sci 2009;49:1461-1476.

169. Carradò A, Faerber J, Niemeyer S, Ziegmann G, Palkowski H. Metal/polymer/metal hybrid systems: Towards potential formability applications. Compos Struct 2011;93:715-721.

170. Aksit M, Altstädt V. Hybrid Materials-Historical Perspective and Current Trends. 2020.

171. Silva L, Marques E, da Silva LF. Polymer joining techniques state of the art review. Welding in the World 2021;65:2023-2045.

172. Reghunadhan A, Krishna A, Jose AJ. Polymers in robotics, in Polymer Science and Innovative Applications 2020; Elsevier:393-421.

173. Chen M-A, Li H-Z, Zhang X-M. Improvement of shear strength of aluminium-polypropylene lap joints by grafting maleic anhydride onto polypropylene. Int J Adhes Adhes 2007;27:175-187.

174. Ochoa-Putman C, Vaidya UK. Mechanisms of interfacial adhesion in metal–polymer composites–Effect of chemical treatment. Compos Part A Appl Sci 2011;42:906-915.

175. Wolf R. Improving Adhesion Performance Between Low-surface-tension Composites and Dissimular Substrates. 2008: Society of Plastics Engineers.

176. Taub A, De Moor E, Luo A, Matlock DK., Speer JG, Vaidya U. Materials for automotive lightweighting. Annu Rev Mater Res 2019;49.

177. Millet H, Vangheluwe P, Block C, Sevenster A, Garcia L, Antonopoulos R. The nature of plastics and their societal usage 2018.

178. Chiellini F, Ferri M, Morelli A, Dipaola L, Latini G. Perspectives on alternatives to phthalate plasticized poly (vinyl chloride) in medical devices applications. Prog Polym Sci 2013;38:1067-1088.

179. Machado J, Gamarra P-R, Marques E, da Silva LF. Improvement in impact strength of composite joints for the automotive industry. Compos B Eng 2018;138:243-255.

180. Atmakuri A, Palevicius A, Vilkauskas A, Janusas G. Review of hybrid fiber based composites with nano particles—material properties and applications. Polymers 2020;12:2088.

181. Endo K. Synthesis and structure of poly (vinyl chloride). Prog Polym Sci 2002;27:2021-2054.

182. Zhang H, Hackam R. Electrical surface resistance, hydrophobicity and diffusion phenomena in PVC. IEEE Trans Dielectr Electr Insul 1999;6:73-83.

183. Prestes SMD, Mancini SD, Rangel EC, da Cruz NC, Schreiner WH, Junior AR. Plasma Treatment to Improve the Surface Properties of Recycled Post-Consumer PVC. Plasma Process Polym 2015;12:456-465.

184. Schonhorn H, Hansen R. Surface treatment of polymers for adhesive bonding. J Appl Polym Sci 1967;11:1461-1474.

185. Sundriyal P, Pandey M, Bhattacharya S. Plasma-assisted surface alteration of industrial polymers for improved adhesive bonding. Int J Adhes Adhes 2020;101:102626.

186. Marques AC, Mocanu A, Tomić NZ, Balos S, Stammen E, Lundevall A, Abrahami ST, Günther R, de Kok JM, Teixeira de Freitas S. Review on adhesives and surface treatments for structural applications: Recent developments on sustainability and implementation for metal and composite substrates. Materials 2020;13:5590.

187. Molitor P, Barron V, Young T. Surface treatment of titanium for adhesive bonding to polymer composites: a review. Int J Adhes Adhes 2001;21:129-136.

188. Kruse A, Krüger G, Baalmann A, Hennemann O-D. Surface pretreatment of plastics for adhesive bonding. J Adhes Sci Technol 1995;9:1611-1621.

189. Chin JW, Wightman JP. Surface characterization and adhesive bonding of toughened bismaleimide composites. Compos Part A Appl Sci 1996;27:419-428.

190. Stewart I, Chambers A, Gordon T. The cohesive mechanical properties of a toughened epoxy adhesive as a function of cure level. Int J Adhes Adhes 2007;27:277-287.

191. Critchlow GW, Yendall KA, Bahrani D, Quinn A, Andrews F. Strategies for the replacement of chromic acid anodising for the structural bonding of aluminium alloys. Int J Adhes Adhes 2006;26:419-453.

192. Underhill P, Rider A, DuQuesnay D. The effect of warm water surface treatments on the fatigue life in shear of aluminum joints. Int J Adhes Adhes 2006;26:199-205.

193. Williams DF, Abel M-L, Grant E, Hrachova J, Watts JF. Flame treatment of polypropylene: A study by electron and ion spectroscopies. Int J Adhes Adhes 2015;63:26-33.

194. Chen S, Ono S, Teii S, Yoshino T. Improvement of the adhesion of the resin to the metal surface by using plasma jet. Surf Coat Technol 1997;97:378-384.

195. Bora MÖ, Akman E, Çoban O, Genc Oztoprak B, Demir A. The Effect of CO_2 Laser-Induced Microhole Formations on Adhesive Bonding Strength of CFRP/CFRP Joints. Polym Compos 2019;40:2891-2900.

196. Zou X, Sariyev B, Chen K, Jiang M, Wang M, Hua X, Zhang L, Shan A. Enhanced interfacial bonding strength between metal and polymer via synergistic effects of particle anchoring and chemical bonding. J. Manuf. Process. 2021;68:558-568.

197. Broad R, French J, Sauer J. CLP new, effective, ecological surface pretreatment for highly durable adhesively bonded metal joints. Int J Adhes Adhes 1999;19:193-198.

198. Critchlow G, Brewis D, Emmony D, Cottam C. Initial investigation into the effectiveness of CO2-laser treatment of aluminium for adhesive bonding. Int J Adhes Adhes 1995;15:233-236.

199. Quan D, Alderliesten R, Dransfeld C, Tsakoniatis I, Benedictus R. Co-cure joining of epoxy composites with rapidly UV-irradiated PEEK and PPS composites to achieve high structural integrity. Compos Struct 2020;251:112595.

200. Nemani SK, Annavarapu RK, Mohammadian B, Raiyan A, Heil J, Haque MA, Abdelaal A, Sojoudi H. Surface modification of polymers: methods and applications. Adv Mater Interfaces 2018;5:1801247.

201. Foerch R, Izawa J, Spears G. A comparative study of the effects of remote nitrogen plasma, remote oxygen plasma, and corona discharge treatments on the surface properties of polyethylene. J Adhes Sci Technol 1991;5:549-564.

202. Aydemir C, Altay BN, Akyol M. Surface analysis of polymer films for wettability and ink adhesion. Color Res Appl 2021;46:489-499.

203. Bashir M, Bashir S, Khan H. Deposition of polyacrylic acid films on PDMS substrate in dielectric barrier corona discharge at atmospheric pressure. Surf Interface Anal 2018;50:879-888.

204. Chan C-M. Surface treatment of polypropylene by corona discharge and flame, in Polypropylene. Springer 1999;800-805.

205. O'Hare LA, Leadley S, Parbhoo B. Surface physicochemistry of corona-discharge-treated polypropylene film. Surf Interface Anal 2002;33:335-342.

206. Narita S. S. Ichinohe u. S. Enomoto: J. Polymer Sci 1959;37:273.

207. Xu W, Rajan K, Chen XG, Sarkar DK. Facile electrodeposition of superhydrophobic aluminum stearate thin films on copper substrates for active corrosion protection. Surf Coat Int 2019;364:406-415.

208. Jussila P, Ali-Löytty H, Lahtonen K, Hirsimäki M, Valden M. Effect of surface hydroxyl concentration on the bonding and morphology of aminopropylsilane thin films on austenitic stainless steel. Surf Interface Anal 2010;42:157-164.

209. Stevens GC. Cure kinetics of a high epoxide/hydroxyl group-ratio bisphenol a epoxy resin—anhydride system by infrared absorption spectroscopy. J Appl Polym Sci 1981;26:4279-4297.

210. Wolf R, Sparavigna AC. Role of plasma surface treatments on wetting and adhesion. Engineering 2010;2:397.

211. Encinas N, Oakley B, Belcher M, Blohowiak K, Dillingham R, Abenojar J, Martínez M. Surface modification of aircraft used composites for adhesive bonding. Int J Adhes Adhes 2014;50:157-163.

212. Zain NM, Ahmad SH, Ali ES. Effect of surface treatments on the durability of green polyurethane adhesive bonded aluminium alloy. Int J Adhes Adhes 2014;55:43-55.

213. Schmidt DL, Brady RF, Lam K, Schmidt DC, Chaudhury MK. Contact angle hysteresis, adhesion, and marine biofouling. Langmuir 2004;20:2830-2836.

214. Louzi VC, de Carvalho Campos JS. Corona treatment applied to synthetic polymeric monofilaments (PP, PET, and PA-6). Surf Interfaces 2019;14:98-107.

215. Sellin N, Campos JSdC. Surface composition analysis of PP films treated by corona discharge. Mater Res 2003;6:163-166.

216. Pascoe R, O'Connell B. Flame treatment for the selective wetting and separation of PVC and PET. Waste Manag 2003;23:845-850.

217. Kusano Y, Mortensen H, Stenum B, Kingshott P, Andersen TL, Brøndsted P, Bilde-Sørensen JB, Sørensen BF, Bindslev H. Atmospheric pressure plasma treatment of glass fibre composite for adhesion improvement. Plasma Process Polym 2007;4:S455-S459.

218. Bormashenko E, Legchenkova I, Navon-Venezia S, Frenkel M, Bormashenko Y. Investigation of the impact of cold plasma treatment on the chemical composition and wettability of medical grade polyvinylchloride. Appl Sci 2020;11:300.

219. Bagiatis V, Critchlow G, Price D, Wang S. The effect of atmospheric pressure plasma treatment (APPT) on the adhesive bonding of poly (methyl methacrylate)(PMMA)-to-glass using a polydimethylsiloxane (PDMS)-based adhesive. Int J Adhes Adhes 2019;95:102405.

220. Carradò A, Sokolova O, Donnio B, Palkowski H. Influence of corona treatment on adhesion and mechanical properties in metal/polymer/metal systems. J Appl Polym Sci 2011;120(6):3709-3715.

221. Palkowski H, Carradò A. Metal-polymer-metal laminates for lightweight application. in Key Engineering Materials. 2016. Trans Tech Publ.

222. Rhee KY, Yang J-H. A study on the peel and shear strength of aluminum/CFRP composites surface-treated by plasma and ion assisted reaction method. Compos Sci Technol 2003;63:33-40.

223. Pantelakis, S.; Tserpes, K.I. Adhesive bonding of composite aircraft structures: Challenges and recent developments. Sci. China Phys. Mech. Astron. 2014, 57, 2–11.

224. Wang, S.; Shang, X.; Ju, S.; Jiang, D. Progress on research on composite-metal adhesive joints. Fiber Reinf. Plast./Compos. 2017, 44, 95–100.

225. Pitta, S.; Carles, V.M.; Roure, F.; Crespo, D.; Rojas, J.I. On the static strength of aluminium and carbon fibre aircraft lap joint repairs. Compos. Struct. 2018, 201, 276–290.

226. Zhang, Z.; Shan, J.G.; Tan, X.H.; Zhang, J. Effect of anodizing pretreatment on laser joining CFRP to aluminum alloy A6061. Int. J. Adhes. Adhes. 2016, 70, 142–151.

227. Xu, Y.W.; Li, H.G.; Shen, Y.Z.; Liu, S.Y.; Wang, W.T.; Tao, J. Improvement of adhesion performance between aluminum alloy sheet and epoxy based on anodizing technique. Int. J. Adhes. Adhes. 2016, 70, 74–80.

228. Chen, J.; Du, K.P.; Chen, X.M.; Li, Y.B.; Huang, J.; Wu, Y.T.; Yang, C.L.; Xia, X.C. Influence of surface microstructure on bonding strength of modified polypropylene/aluminum alloy direct adhesion. Appl. Surf. Sci. 2019, 489, 392–402.

229. Suganya, A.; Shanmugavelayutham, G.; Rodríguez, C.S. Study on structural, morphological and thermal properties of surface modified polyvinylchloride (PVC)

film under air, argon and oxygen discharge plasma. Mater. Res. Express. 2016, 3, 095302.

List of publications

Refereed Publications:

1. "Effect of roughness parameters on the single lap shear strength of AA 6061-T6 aluminum alloy for structural adhesive bonding applications", **M. M. Tiwari**, N. Saleema., D. K. Sarkar, X.-G. Chen, Journal of Adhesion Science and Technology (under review).
2. "Open Pore Effect on Structural Adhesive Joining Using an Epoxy Adhesive", **M. M. Tiwari**, N. Saleema., X.-G. Chen, D. K. Sarkar, Book chapter, COM 2022. Springer, Cham publisher, 2023.
3. "Simultaneous anodization and silanization for adhesive joining of AA 3031-T4 using an epoxy adhesive", **M. M. Tiwari**, N. Saleema., X.-G. Chen, D. K. Sarkar, Materialwissenschaft und Werkstofftechnik 54 (2023) 1092-1096.
4. "Surface treatment of PVC by corona discharge for adhesive joining with AA 6061 aluminum alloy" **M. M. Tiwari**, N. Saleema., D. K. Sarkar, X.-G. Chen. (under *internal review*).
5. "Polymer–Aluminum Lightweight Multi-Material Joints Bonded with Mixed Adhesive", **M. M. Tiwari**, N. Saleema., D. K. Sarkar, X.-G. Chen, Eng. Proc. 43 (2023) 29.

Conferences attended (oral and poster presentations):

1. "Mechanical polishing of AA6061-T6 alloy for the application of adhesive bonding", **M. M. Tiwari**, N. Saleema., X.-G. Chen, D. K. Sarkar

Poster presentation, Journée des étudiants du RÉGAL (JER 2020); 2020 November 5-6; Virtual Event.

2. "Mechanical abrasion of AA6061-T6 alloy for the application of structural adhesive bonding", **M. M. Tiwari**, X.-G. Chen, D. K. Sarkar

Oral presentation, 44th Annual meeting: The adhesion society; 2021, February 2-4; Virtual Event.

Oral presentation, International Conference on Material Characterization and Modelling (ICMCM 2021); 2021, December 13-14; Virtual Event.

3. "Facile mechanical abrasion surface treatment and its parametrical influences on adhesive bonding of AA6061-T6 aluminum alloy", **M. M. Tiwari**, N. Saleema., X.-G. Chen, D. K. Sarkar

Poster presentation, Journée des étudiants du RÉGAL (JER 2021); 2021 November 11-12; Centre des Congrès de Trois -Rivières, QC, Canada (acknowledged for best poster presentation award supported by HATCH)

4. "Simultaneous anodization and silanization for adhesive joining using epoxy adhesive", **M. M. Tiwari**, N. Saleema., X.-G. Chen, D. K. Sarkar

Oral presentation, International Conference on Material Characterization and Modelling (ICMCM 2021); 2021, December 13-14; Virtual Event.

5. "Open Pore Effect on Structural Adhesive Joining Using an Epoxy Adhesive", **M. M. Tiwari**, N. Saleema., X.-G. Chen, D. K. Sarkar

Oral presentation, 61st Conference of Metallurgists, COM 2022, 2022, August 21-24; Hotel Bonaventure, Montreal, QC, Canada.

6. "Surface preparation for structural adhesive bonding of aluminum with similar and dissimilar materials", **M. M. Tiwari**, N. Saleema., D. K. Sarkar, X.-G. Chen

Poster presentation, Journée des étudiants du RÉGAL (JER 2022); 2022, October 27-28; Hôtel Le Montagnais Chicoutimi, Canada

7. "Polymer–Aluminum Lightweight Multi-Material Joints Bonded with Mixed Adhesive", **M. M. Tiwari**, N. Saleema., D. K. Sarkar, X.-G. Chen

Oral presentation, 15th International Aluminium Conference, INALCO, 2023, October 11-13; Centre des congrès de Québec, Quebec city, QC, Canada.

Appendix I: Supporting information for Chapter 4

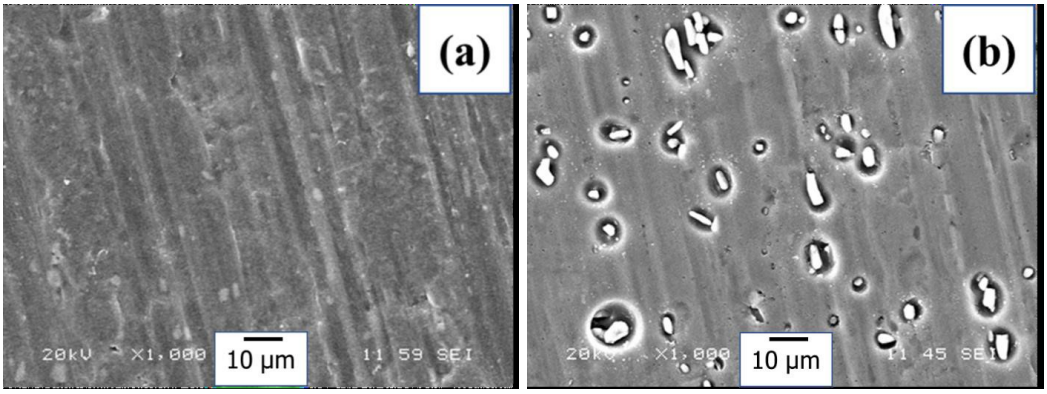

Figure I.1. SEM images of (a) as-received Al substrate. (b) Al substrate immersed in 0.1 M NaCl for 24 h [146]

Fig. I.1 (a) represents the SEM image of the as-received Al substrate and the lines appearing on the substrate surface are due to the rolling process. The SEM image of the Al substrate immersed in a 0.1 M NaCl aqueous solution for 24 h is shown in Fig. I.1 (b). The image exhibits corrosion-related features corresponding to the intermetallic phases. The potential difference between these intermetallic phases and the Al matrix causes the formation of galvanic corrosion cells and leads to localized corrosion of the Al matrix [146].

Appendix II: Supporting information for Chapter 6

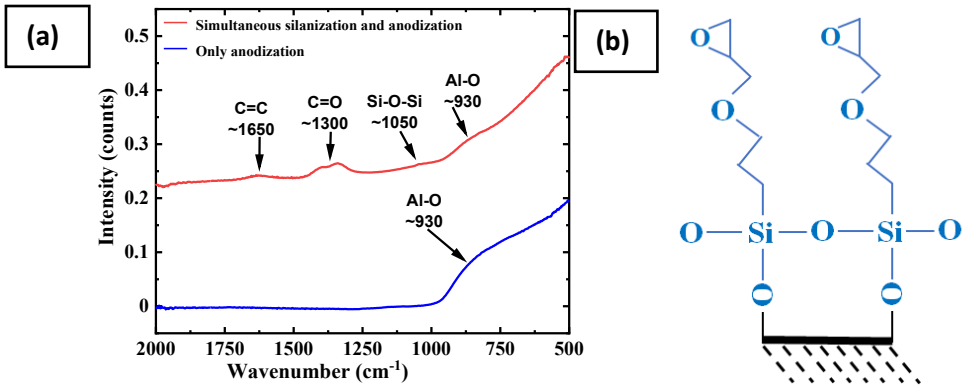

Figure II.1. (a) ATR-FTIR spectra of only anodized and in-situ silanization and anodization AA 3031-T4; (b) schematic model of glycidoxy propyl-trimethoxy silane (GPS)

Fig. II.1 (a) shows a comparative ATR-FTIR spectra of only anodized and in-situ silanization and anodized AA 3031-4. A broad band at 490–1000 cm^{-1}, is attributable to the Al-O vibrations confirming the presence of an oxide of aluminum on the surface of only anodized AA 3031-T4. On the other hand, the FTIR spectrum of in-situ silanization and anodization of AA 3031-T4 presents a broad peak at around 930 cm^{-1} attributable to the formation of anodic aluminum oxide. The Si-O-Si bonds at around 1050 cm^{-1} confirms the silane impregnation simultaneously during the anodization process. Additionally, 1650 and 1300 cm^{-1} can be assigned to the –C=C and –C=O stretching modes of glycidoxy propyl-trimethoxy silane. The Fig. II.1 (b) shows the schematic model of glycidoxy propyl-trimethoxy silane monolayer molecules. So, the stoichiometry of oxide layer associated with the FTIR spectrum band is given by Al_2O_3.

Table II.1. Elemental chemical composition of as-grown porous layer on AA 3031-T4

Current density ($m.A.cm^{-2}$)	Atomic %			
	C K	O K	Al K	Si K
j=120	13.62	49.88	35.60	0.90
j=150	25.66	38.65	34.45	1.24

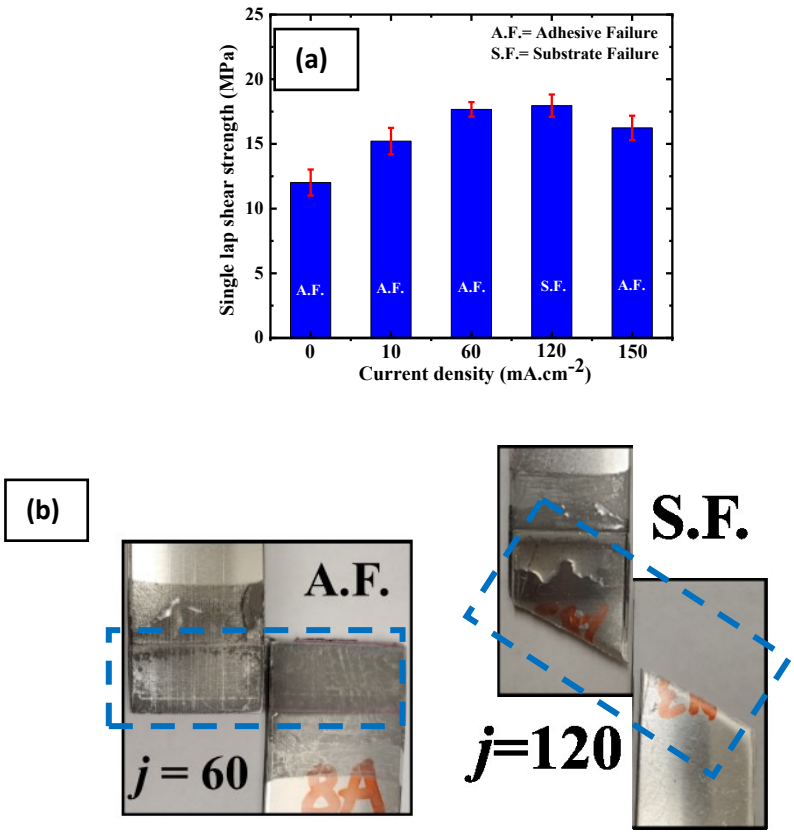

Figure II.2. (a) SLS strengths of adhesively bonded single lap shear specimens and (b) images of ruptured specimens *(A.F. – Adhesive Failure, S. F. – Substrate Failure).*

Though the lap shear strengths of samples anodized at j=60 mA.cm^{-2} and j=120 mA.cm^{-2} show similar result yet the nature of failures at the interface were completely different. At j = 60 mA.cm^{-2}, the rupture modes have been found to be adhesive as shown in Fig. II.2 (b). On the other hand, the samples anodized at j =120 mA.cm^{-2} failed at the AA 3031-T4 substrate for two SLS specimens out of three. Therefore, the lap shear strengths of adhesive joint is higher than the actual recorded value. The obtained lap shear strengths were in agreement with that of the rms surface roughness values as well as the morphological evolution.

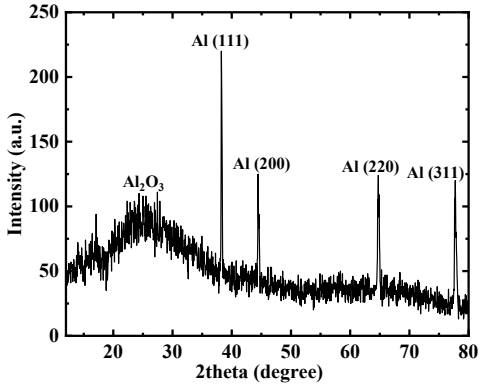

Figure II.3. XRD patterns of as-grown oxide layer on anodized AA 3031-T4 aluminum substrate.

The structural characteristics of porous oxide layer, synthesized by the silanization during anodization process are illustrated in Fig. II.3. The XRD patterns show a broad peak centered at 2theta ~ 25 degree. The broad peak is an indication of a highly disordered and/or amorphous aluminum oxide compound. Hence, the oxide layer is in amorphous phase.

Appendix III: Supporting information for Chapter 7

The detailed description of the water breaking test is summarized in Fig. III.1. The PVC substrates were kept on a flat surfaces and a drop of water with a constant volume were put on using a medical needles and syringe. The images were captures using a Samsung S10 cellular device, fixed at a distance from the PVC substrate using clamp rods. Later the captured images were analyzed in origin.10 software for water contact angle calculations.

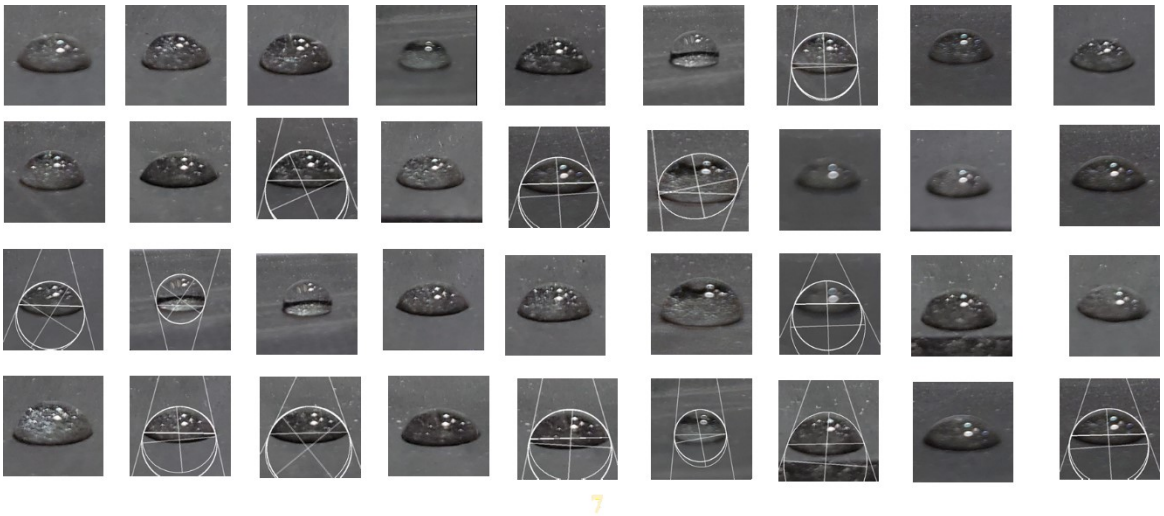

Figure III.1: Captured and analyzed images of water drops placed on the surface of PVC substrates for the contact angle calculation.